Catholic University of Leuven

Faculty of Bioscience Engineering

Simulation of Soil and Tillage-tool Interaction by the Discrete Element Method

Promoter: *Prof. Herman Ramon, KU Leuven*

Co-promoter: *Prof. Miguel Herrera, UCLV*

Elvis López Bravo

February 2013

Catholic University of Leuven

Faculty of Bioscience Engineering

Simulatie van de Interactie Tussen Bodem en Grondbewerkingswerktuig Door Middel van de Discrete Elementen Methode

Promoters: *Prof. Herman Ramon, KU Leuven*

Co-promoter: *Prof. Miguel Herrera, UCLV*

Examination committee:

Prof. Josse De Baerdemaeker, KU Leuven
Dr. Engelbert Tijskens, KU Leuven
Prof. Wouter Saeys, KU Leuven
Prof. Maurice De Proft, KU Leuven
Prof. Gerard Govers, KU Leuven
Prof. Miguel Rodriguez Orozco, UCLV, Cuba
Dr. Rafael Arturo Trujillo, UCI, Cuba

Elvis López Bravo

February 2013

Acknowledgment

I want to express my sincere appreciation and gratitude to my promoter Professor Herman Ramon, for his inspiration, guidance and support during this time.

At the same time I proclaim special thanks to my supervisor Dr. Engelbert Tijskens, for his unconditional support, patience, and for introducing me in the fascinating work of particle simulations.

I also bestow herein sincere gratefulness to my co-promoter Prof. Miguel Herrera, for all the work he did together with me, his precise orientations during all the time and confidence; and to Prof. Miguel Orozco and Osvaldo Fernandez coordinators of the project for their advises, confidence and support.

I express all my respects and deepest thanks to my co-promoter Prof. Josse De Baerdemaeker, for his encouraging orientations, opportune advice, and for opening the doors of the laboratory for me.

My acknowledgment for Prof. Wouter Saeys, for the time he devoted to me for planning, for his advice and recommendation during the thesis job and professor Gerard Govers for his recommendation and review.

I feel thankful for all the attention offered by the staff of the Department of Biosystems from KULeuven, especially to Bart De Ketelaere, Soner Akpinar, Paul Van Liedekerke, Bram Kamer, Kristof Mertens; at the same time, for the staff of the Central University of Las Villas: Yaidel Reyes, Ahmed Chacon, Prof. Ciro Iglesias and Omar Gonzales. Thanks to everyone else not mentioned, but not forgotten.

I should express my gratitude for the financial support received from the Belgium Council of Flemish Universities (VLIR) and Central University "Marta Abreu" from Cuba.

Finally, all my gratefulness for the scholarship granted to me by ANIMO "Chevere" from Granada University as part of the Erasmus Mundus project.

Dedication

This work is dedicated to my grandparents Emilio López and Asunción Hernández; and to my kids Adrián López and Arianny López.

Abstract

A frictional-cohesive model was implemented to simulate the interaction between soil and tillage tool using the Discrete Element Method. The model parameters are defined based on the mechanical properties of a clay soil obtained in a sugar cane plantation from Cuba. Soil characterization includes elements as liquid and plastic limits, plasticity index and content of sand, silt and clay at 15, 30 and 50 cm depth; as a result the soil was classified as Oxisol. Soil mechanical properties were experimentally determined by triaxial compression tests and modified shear tests. The experimental study was divided in different tests to determine properties related to the soil interface as Young's Modulus, Poisson's ratio, cohesion and internal friction, conducted by compression triaxial tests; and those properties related to the interface soil-metal, such as soil-metal adhesion and external friction, conducted by the direct modified shear tests. Soils, however, are in constant changes related mainly to climatic, natural and external factors. All these changes modify the soil mechanical response. To capture the soil strength at different conditions, the mechanical properties above defined were obtained at a different content of water and dry bulk density. A multilevel factorial experimental design was used to combine the soil gravimeter water content w ranging from 16 to 32% with a dry bulk density ρ_d between 1 and 1.4 g/cm^3. This led to a total of 15 experimental points tested for both mechanical tests. As a result, a set of statistical regression equations was obtained for predicting the magnitude of the mechanical properties as a function of soil moisture and compaction level.

The model, at the particle level, deals with normal forces, shear forces, cohesion forces and friction forces. The stiffnesses in normal and tangential direction are calculated based on the equation of best fit to relate soil elastic properties with geometric parameters of particles in contact. Inter-particles bonds keep the particles together formed by the action of cohesion and friction forces. The Mohr-Coulomb criterion of soil failure limits the shear force. Soil calibration was performed finding the macro-micro relationship of friction and cohesion. To this end, different values of micro-friction were tested in a direct shear test simulation. Micro-cohesion is also affected by the magnitude of micro-friction. To find out the corresponding relationship, the triaxial compression test was simulated. The effect of particle size over force prediction was

analysed using a narrow tool interacting with a block of soil which was generated in a hexagonal compacted array with radii 5, 7 and 9 mm. The result showed significant variation in force fluctuation on the tool and computational cost. Verification against analytical results from the Perumpral-Grisso-Desai model showed adequate results with respect to the simulated force.

To measure the soil reaction forces and loosening indicators a soil-bin experiment was executed. The water content and dry bulk density were combining according to a Central Composite experimental design resulting in nine experimental points. As a result, the draft and vertical forces increase with increasing soil compaction and dry condition. The final dry bulk density showed a proportional decreases with respect to the initial one, related also with the variation of the soil water content. The aggregates formation at the different conditions called *wet*, *medium* and *dry* soil showed that the amount of aggregates smaller than 10 mm in *medium* soil condition was larger than the other states.

To validate the model a soil-bin experiment was modelled following the same geometric and operational parameters as in the soil-bin experiment. Comparison of experimentally determined and simulated horizontal and vertical forces showed the model tendency of over-predicting horizontal forces for dry-compacted soils; however, the magnitude of the error made by the model did not overcome 10% of the nominal force obtained from the soil-bin test. Simulated forces on the tool during soil cultivation in *wet*, *medium* and *dry* conditions were lowest for soil *medium* condition with respect to the two others. The effects of the subsoiler shapes were evaluated under compacted and dry soil conditions showing clear variations in forces related to the tool geometry. The addition of lateral blades in the subsoiler tool was found advantageous in terms of force per area of disrupted soil. De-compaction soil operation was simulated introducing two different sections in the virtual block. The results showed the feasibility of modelling the forces demanded for the different parts of the tillage tool.

Table of Contents

Notation

τ = shear stress at failure [Pa]

c = soil cohesion [Pa]

c_a = soil adhesion [Pa]

σ_n = normal stress [Pa]

ϕ = internal friction angle [°]

δ = external friction angle [°]

w = gravimetric water content [%]

ρ_d = dry bulk density [g/cm^3]

m_{wet} = mass of the sample before drying in the oven [kg]

m_{dry} = mass of the sample after drying in the oven [kg]

$(\sigma_1 - \sigma_3)$ = deviator stress [Pa]

P = applied axial load [N]

A_c = corrected cross-sectional area of the specimen [m^2]

ε = axial strain [ ]

ΔL = change in length of specimen [m]

L_0 = initial length of specimen [m]

F_s = shear force [N]

$\Delta\varepsilon_v$ = incremental volumetric strain [ ]

ΔV = resultant soil volume after loading [m^3]

V_i = initial volume of soil specimen [m^3]

A = initial area of the specimen [m^2]

n = normal stress [Pa]

N = normal vertical force acting on the specimen [N]

$\sigma_{(50kPa)}$ = shear strength failure at 50kPa [kPa]

E = Young's modulus [MPa]

v = Poisson's ratio [ ]

d^{ab} = distance between disk centres [mm]

$\boldsymbol{n}^{ab}$ = normal vector [ ]

λ^{ab} = overlap [m]

$\varDelta t$ = time step [s]

$\varDelta u_n$ = relative displacement in normal directions [m]

$\varDelta u_s$ = relative displacement in tangential directions [m]

f_{lim} = shear force limit [N]

Fn = normal force [N]

$\mu\phi$ = micro-frictiom angle [°]

μc = micro-cohesion [N]

k_n = normal spring (N/m)

η_n = viscous damping [kg/s]

E_{ab} = equivalent Young's modulus of the materials in contact [Pa]

A_{int} = interior area of particles in contact [m^2]

D_{eq} = equivalent distance between the two particles [m]

α_k, = loading path [ ]

β_k, = softening factor [ ]

γ_k = interaction range [ ]

β = coefficient of viscous damping [ ]

m_a, m_b = mass of the objects in contact [kg]

D = draft force [N]

w_t = width of the tool [m]

γ = soil density [g/cm^3]

z = depth of the tool [mm]

Nγ, N$_c$, N$_a$ = coefficients of density, cohesion and adhesion [ ]

Chapter 1

Introduction

1.1 State of the art

Tillage tool geometry is a decisive factor in integrated soil conservation practices. The tools should have the quality of remaining the crop residues on the soil surface, holding the organic matter into the upper layer and causing limited soil disruption. In that way, tillage practices can prevent soil degradation by erosion, carbon release and soil compaction. Mulch tillage, ridge tillage, zone tillage and no-tillage are the principal types of conservation tillage techniques. The purpose of these procedures is to reduce tillage operation focused on economic and environmental advantages. As a consequence the soil quality is improved, less energy is used and time for tillage operations is saved (Carter and Daniel, 2005).

Soil physical and chemical degradation include soil compaction, losses in organic matter and nitrogen deficiencies. The evaluation of chisel tillage, no tillage and flexible tillage technologies showed an increment on soil quality indicators with respect to conventional inversion tillage. Unwanted effects as erosion and hard-pan formation were found more pronounced in conventional tillage than conservation one (Barber et al., 1996). Another study showed that the organic carbon activity was affected mainly by tillage disturbances. This conclusion was obtained from a long term soil preparation with ripping tools in sandy and clay soils. The research concluded that residue retention and reduction of tillage operations decrease the organic carbon decomposition, improving the soil agronomical quality (Chivenge et al., 2007). Runoff and erosion under conventional and conservation tillage were evaluated in a silty loam soil (Leys et al., 2010). The extrapolation's results from small to large field called scale effect was considered leading to an underestimation of the effectiveness of conservation tillage.

Conservation tillage was also considered as a viable option for European agriculture by Puttea *et al.* (2010). A meta-regression analysis that compares crop yields included factors as crop type, rotation, tillage depth, and climate. The results highlight the quality of conservation tillage to perform better under soil dry condition.

1.1.1 *Non inversion tillage tools*

The transition from the mouldboard plough to the current vertical non-inversion tools led to the development of many implements that have been tested in different soils and plantations. In order to introduce new shapes of tillage tools, the soil properties, and crops particularities need to be managed carefully (Morris et al., 2010). In this respect, the soil type is considered by the authors as the main factor for successful adoption of non-inversion tillage. As an example, in some cases clay soils have a lower risk of forming hard seedbed than sandy soils by applying non-inversion tillage, which was explained by the specific granular arrangement obstructing air and water movement. Tillage, in general, affects soil redistribution on arable land. However the action of a mouldboard plough on different slope gradients introduces an important amount of translocation and dispersion of soil constituents. This effect was modelled by Van Oost (2000), the model besides soil dispersion also considers the directionality of tillage and topography.

In agricultural practices a subsoiler is a tillage tool used for handling deep layers in the soil. This implement was designed to fight against compaction caused by high vertical pressures during horizontal ploughing, machinery traffic crossing the field and repeated conventional tillage. The non-inversion capacity of the subsoiler contributes to preventing erosion and soil degradation (Mouazen and Nemenyi, 1996).

The degree of soil disruption during tillage operation depends on the tool geometrical parameters and soil physical state. Geometrical modifications have been carried out on mouldboard ploughs, leading to a significant draft force reduction required to move the tool through different soil conditions (Shrestha et al., 2001, Godwin, 2007). Tillage-tool field performance and draft force requirements were evaluated in the nineties of the last century for management of the soil-ecosystem. In the experiments, several variations of tool shapes at different operation speeds were tested. The efficient designs were evaluated at farm level, correlating the energy supply and seedbed quality (Perdok and Kouwenhoven, 1994).

1.1.2 *Experimental studies on soil mechanical behaviour*

Studies about the variability of soil mechanical behaviour show the connection with soil properties as soil structure, texture, composition, moisture, organic matter and bulk density. In the present section some of the most relevant contributions related to soil tillage are presented.

Studying the mechanical behaviour of clay soils has a particular difficulty related to a cementation process. The water absorbed by mineral clay bonds the external and internal surface of the grain. The strength of the bond was found dependent on the clay chemical composition (Grim, 1988). On the other hand, in loose and compacted soils different deformation patterns were found when the soil was submitted to normal pressure during a triaxial compression test. Soils with lower bulk density showed a volume reduction, whereas lateral expansion and failure bands characterise the soil with large bulk density. The Poisson's ratio and Young's modulus measured with the triaxial apparatus also increase with the initial dry bulk density (Mouazen et al., 2002). In another study, the size of the aggregates was found to be related to specific soil moisture. Smaller fragmentations, under action of the stress, were observed in soils characterised by large amount of micro-cracks and linear net of pores. This relationship was called index of soil physical quality showing linear and positive correlation with soil friability (Dexter, 2004).

Several procedures to investigate the soil mechanical behaviour have been adapted from classic standard tests. The simple fracture test for metals was adapted to determine the brittle strength of agricultural soils. Specimens of sandy and cemented clay soils were tested, showing an increase in fracture strength at different soil densities (Aluko and Chandler, 2006). A torsion shear test was performed on a loam sandy soil. A statistical regression was performed on the data to predict cohesion and the friction angle as a function of water content and dry bulk density (Ayers, 1987b). A measurement of tensile strength on soil samples prepared in the laboratory using sandy loam soil was carried out at different moisture contents and bulk densities. It was found that drying the soil after densification can increase soil strength disregarding the compaction path (Ibarra et al., 2005). To predicting the soil penetration, a statistic model as a function of soil texture, bulk density, and water content was obtained by Dexter (2007). The equation showed good performance with respect to data from laboratory tests. The prediction results included also the degree of compactness and the contribution of pore water pressure over soil strength. On the other hand, a research about the impact of the mineral composition on soil geo-mechanical

properties highlights the importance of the plasticity index and shows a correlation with the normalised undrained shear strength (Dolinar, 2010).

1.1.3 *Numerical methods for soil dynamic simulation*

Predicting draft force, clod size distribution, and erosion damage by soil tillage are among the major motivations for modelling soil-tillage interaction. Faster and more precise prediction about soil-tool interaction now is possible though the combination of experimental data and theoretical knowledge in computational models. Techniques as finite element methods (FEM), discrete element methods (DEM), artificial neural network (ANN) and computational fluid dynamics (CFD) are used to simulate soil dynamical behaviour for different purposes. An important step towards the reproduction of the rheological soil behaviour by modelling was the transition from a quasi-static to a dynamic analysis (Karmakar and Kushwaha, 2006).

Soil-tillage simulation is becoming a powerful tool for increasing the quality of tool design. However, the behaviour of the soil during soil and tool interaction can become totally unpredictable due to inaccurate soil mechanical properties. Frictional, elastic-plastic, hypo-plastic and viscous-plastic models require soil parameters determined through laboratory tests as elastic modulus, poison's ratio, soil density, internal friction and soil cohesion. Correct values of these properties are essential for a reliable prediction of soil deformation and required draft forces.

For testing simple and complex tool shapes, several studies by FEM have been conducted in two and three dimensions, with the objective of determining the effect of cutting speed and blade angles in the draft force variation during soil-tool interaction (Abo-Elnor et al., 2004, Mootaz et al., 2003, Davoudi et al., 2008, Sahu and Raheman, 2006a, Mouazen and Neményi, 1999, Gebregziabher et al., 2007).

Prediction of draught requirements by ANN for three designs of mouldboard ploughs tested in sandy loam soil under different soil conditions, showed a good correlation in comparison with values calculated from prediction equations (Roul et al., 2009). Also considering the soil as a continuous medium the Cam-Clay Model was proposed for modelling the behaviour of clay soils. However, this approach was only suitable for soils with low cementation. Instead, the Modified Cam Clay Model introduced new parameters taking into account the effect of soil structure. It yields satisfactory results for compression and shearing tests (Liu and Carter, 2002).

This model included the time dependent effect, creep, and anisotropic soil behaviour. Von-Mises yield criterion for a perfectly plastic model was applied using the Lagrangian method, the model includes strain-softening and rate dependence. The authors present a numerical model for cone penetration into soft clay soil. The influence of the stiffness index, in-situ stress anisotropy and roughness were theoretically correlated and compared with the cavity expansion theory (Liyanapathirana, 2009).

Models of soil using the finite element method (Abbas et al., 2006, Abo-Elnor et al., 2004, Huang et al., 2004, Mootaz et al., 2003) and the discrete element method (Asaf et al., 2007, Shmulevich et al., 2007, Coetzee and Els, 2009a, Peron et al., 2009) were developed to reproduce laboratory and field experiments. All of these simulations showed good results in terms of force-displacement.

1.1.4 *Discontinuous method for soil and tillage applications*

Granular models are introduce in the seventh decade of the previous century by Cundall (1971). However, their capacity of reproducing complex dynamic processes opened a vast new field of applications in soil mechanics and soil physics. The interaction between particles as defined in DEM, shows a relative similitude with mechanical interactions that take place among grains of soil. A number of contact models determine the behaviour of the overall medium, depending on how each element interacts with the others. The model parameters called micro-properties are deduced from the soil mechanical properties in order to calculate the resultant contact forces (Cundall and Strack, 1979). Three dimensional models of complex mechanical interactions embody an important step for resolving contacts forces between bodies with arbitrary geometry. An algorithm to rapidly detect and categorize possible contact allows to use the DEM method in a personal computer (Cundall, 1988). A methodology for obtaining the micro-mechanical input parameters of the DEM model was based on in situ field tests, subjected to a statistical data optimization in order to minimize the differences between reality and simulation results. The deformation curve of numerical and experimental tests showed a good statistical correlation (Asaf et al., 2007). A contact bond model was developed considering the influence of friction and cohesive forces. Biaxial tests to validate and calibrate the parameters of stiffness and friction in the model were carried out in laboratory conditions. Using this model the soil movement was simulated for different weathering scenarios (Utili and Nova, 2008). Soil-tool interactions with a

high rate of plastic deformation was modelled using a cutting-blade and soil particles formed by two disk clumps joined by cohesion forces. Two-dimensional blades with different shapes were evaluated by a DEM model. Soil flow behaviour in front of the blades was found to be closely related with the horizontal and vertical force values (Shmulevich et al., 2007).

1.2 Problem statement

The introduction of a new tillage-tool requires several and expensive soil-bin and field tests including the manufacturing process and set up the measuring system. The dynamics of soil-tool interaction has been treated by several methods, from empirical approximation to numerical modelling. However, soil complexity goes beyond the scope of the predictions as soil behaves in different ways depending on its mineral composition and granulometry. In addition, soil moisture and compaction change the soil mechanical response affecting the tillage performance. Also the soil behaves in different ways in agreement with its mineral composition and granulometry.

The force needed for soil tillage depends on factors related to the shape of the tool, soil strength and operational parameters. By means of empirical models only an approximation could be obtained. This method is limited to a simple geometry of the tools. Several soil parameters related to soil adhesion, cohesion, density and friction have to be calculated from a diversity of soil mechanics tests.

FEM models have demonstrated the possibility to reproduce soil tillage by simulation. However, often it has been unable to find reliable dynamic solutions due to the soil natural discontinuities and the soil lack of homogeneity. Also, without changes in soil mechanical properties due to the variation in moisture and bulk density results in incomplete prediction of soil behaviour.

By a discontinuous method the soil natural structure can be simulated. The DEM model was developed to simulate the dynamic behaviour of granular material, showing encouraging results in dealing with soils as granular media. Nonetheless; elements like the number of particles, cohesion force, and the relationship between model parameters and soil properties need to be introduced in order to make useful prognostic in soil-tool interaction.

1.3 Objectives

The general objective of the present thesis is the development of a frictional-cohesive soil model by the Discrete Element Method for the phenomenological simulation of soil-tool interaction during tillage under different soil physical conditions.

The following sub-objectives are elaborated to achieve the general goal:

1. Obtain by experimental tests a mechanical characterization of a clay soil to estimate the behaviour of soil Young's Modulus, Poisson's coefficient, cohesion, adhesion, internal friction and soil-metal friction as a function of gravimetric water content and dry bulk density.

2. Implement in *DEMeter++* a soil frictional-cohesive model based on the Mohr-Coulomb criterion of soil failure including the effect of cohesion and adhesion force, as well as internal and external friction.

3. Calibrate the model, based on the relationship existing between friction and cohesion properties at the particle scale with those obtained from the soil at bulk scale by means of the simulation of biaxial compression test and direct shear test.

4. In soil-bin controlled conditions measure the reaction forces and soil loosening indicators as a function of soil moisture and compaction levels during tillage operation by cultivator tool.

5. Validate the proposed soil frictional cohesive model through the simulation of soil-cultivator tillage using the same design of the tool and soil conditions in the model as the experimental test performed in the soil-bin.

6. Simulate soil tillage operations at different levels of soil compaction and moisture content with actual designs of tillage tools to predict the draft force requirements for soil loosening and the load distribution over the soil surface.

1.4 Outline

In Chapter 2 the Cuban clay soil, widely used in the sugar cane plantation is characterised by its physical parameters and mechanical properties. A triaxial compression test and modified direct shear test were carried out in laboratory conditions, A factorial multilevel experimental design was used to determine Young's Modulus, Poisson's coefficient, adhesion, cohesion, internal friction and soil-metal friction as a function of soil water content and dry bulk density. Statistical regression equations were found to predict the magnitude of soil mechanical properties under different physical conditions.

In Chapter 3 a frictional-cohesive 3D soil model was implemented on the DEMeter++ platform. Soil micro behaviour was governed by normal and tangential contact models of soil-soil and soil-tool interface. Soil mechanical properties obtained in the previous chapter were used as macro-parameters in the model. Based on the best fit hypothesis, soil macro-parameters were combined with particle geometrical elements to calculate the force at micro level following the classical DEM formulation. Cohesive soil behaviour was obtained by inter-particle bonds. By the combination of micro-cohesion and soil micro-friction, inter-particle bonds are formed to keep the particles together after the Cauchy strain was reached. The Mohr-Coulomb criterion of failure was used to limit the amount of force resisted by the bonds in tangential direction. The model was calibrated by simulating direct shear tests at different values of micro-friction resulting in an empirical equation to calculate particle micro-friction from soil internal friction. In the same way the relationship between soil cohesion and particle micro-cohesion was obtained from simulations of triaxial compression tests. Spherical particles arranged in a hexagonal compact array were used for all simulations. The virtual soil structure was obtained by submitting the particle set to a vertical compression and getting the predefined cohesion during the de-compression time. The effect of particle size was evaluated by running three different particle diameters on a simplified model using a flat tool. Results were compared with the analytical model to verify the model results.

Chapter 4 is dedicated to the analysis of the results of tillage operation under controlled conditions. A soil-bin was conditioned with the same clay soil used for soil mechanics experiments. The geometry of the experimental tool was designed by combining basic elements

of soil-tools for soil cultivation and subsoiling operations. A computer measuring system was set up to measure reaction forces on the tool and the speed of the tool. A central composite statistical design was used for planning the experimental tests to measure the effect of soil water content and compaction on horizontal and vertical reaction forces. Loosening indicators as density variability, soil profile and granulometric distribution were also measured for all experimental combinations.

Chapter 5 deals with the soil model validation and prediction forces in several tillage operations. The soil cultivation operation explained in the previous chapter was modelled using the same tool geometry and soil conditions. To achieve the variety of soil states, regression equations from Chapter 2 were used to calculate the actual values of soil macro parameters used in the model. The changes in bulk density during the simulation of soil-cultivator interaction was analysed from the variation of the particle index in seven transversal sections of the virtual block of soil. Also the load distribution on the soil surface below the tool was simulated in soil with different states of compaction. Predictions of force variation for actual soil operations were made from modelling the soil-tool interaction for different soil strength. Soil cultivation by a simple tool was simulated at different soil moisture contents. At the same soil conditions, tillage by the so called para-plough and mouldboard plough were carried out to evaluate the force requirements and particle flow pattern. Two designs of subsoilers working in compacted soil conditions were compared in terms of force demanded. A hard-pan was modelled by a block of soil made by two particle bulk densities. The force requirement for the main body of the tool and lateral blades were computed during the simulation.

Finally, in Chapter 6 general conclusions and recommendation for future research were made on the subject of the simulation of soil-tool interaction.

Chapter 2

Soil Mechanical Characterization

2.1 Introduction

Tillage operations should generate a favourable soil structure in terms of water, nutrients, oxygen, and temperature. However, soil behaviour changes according to factors such as soil type, moisture, bulk density, loading type, and loading rate (Ayers, 1987a). Consequently, the variability in soil mechanical response makes it a difficult task to determine adequate parameters for tillage tools.

Soil mechanical response is characterised, in the first place, by the stress-strain relationship during soil deformation. Many internal and external factors, however, affect the way the soil is deformed under pressure. These factors can be categorized in four groups (Lambe and Whitman, 1969):

1. Soil composition: This group includes the influence of soil mineralogy, granulometry, shape of particles and porosity structure.

2. Initial state: Defined by the initial void ratio, effective normal stress and shear stress. This state can be described by terms such as loose, dense, over-consolidated, normally consolidated, stiff, soft, contractive and dilative.

3. Soil structure: Refers to the arrangement of particles within the soil mass; the manner in which the particles are packed or distributed. Features such as layers, joints, fissures, slickensides, voids, pockets, cementation, are part of the structure. Structure of soils is described by terms such as undisturbed, disturbed, remoulded, compacted, cemented; flocculent, honey-combed, single-grained; flocculated, deflocculated; stratified, layered; laminated; isotropic and anisotropic.

4. External loading: Effective stress, drained or undrained path, static or dynamic loading, time history.

The stiffness and soil strength are the direct results of increasing parameters as cohesion, internal friction, Young's modulus and Poisson's ratio. All of these parameters are found to be dependent on the soil compaction (Mouazen et al., 2002). An increment in bulk density results in a higher draught force and energy requirement during tillage. At the soil-tool interface, particle sliding takes place at a certain velocity, the friction between coarse grains of soil and the tool steel surfaces cause, in a specific period of time, wear on the tool surface in contact with soil which reduces the quality of the tillage and consequently leads to increments in the traction force (Bayhan, 2006, Graff et al., 2007).

On the other hand, the soil water content does not have a clear relationship with the soil mechanical behaviour. However, most of the researchers found a reduction in soil cohesion as water content rises (Komándi, 1992, Porter and McMahon, 1990, McKyes et al., 1994). Meanwhile soil elastic parameters and friction drop with the increase in soil moisture (Rickman, 1971). Prediction equations to relate soil water content and bulk density have been found successful in predicting the mechanical properties of soil (Da Silva and Kay, 1997, Dexter et al., 2007, Sánchez-Girón et al., 2001).

On the other hand, soil mechanical properties have been used indistinctly for FEM and DEM models as soil parameters for soil-tool interaction (Abo-Elnor et al., 2004, Mouazen and Ramon, 2002, Cui et al., 2007, Shmulevich et al., 2007, Coetzee and Els, 2009b). In general, soil simulations have been implemented with constant soil properties, focusing, most of the time, on finding the effect of the model parameters, called micro-parameters, on the simulation results.

The soil responses to physical conditions change dramatically along different patterns known as elastic, elastic-plastic, plastic, and viscous. This behaviour is hard to reproduce by a single mathematical model. Additionally, it is difficult to think about soil deformation patterns, without a variation in moisture and bulk density.

2.2 Classical theories about soil failure

Soil mechanics for agricultural issues is supported by the same theories as used in civil engineering application commonly named classic soil mechanics. Small displacements up to soil failure caused by high pressures in soil foundation and stability distinguish civil engineering

activities (Shen and Kushwaha, 1998). Agricultural soils, however, are tilled only to a shallow depth. By the action of relatively low pressure, large soil deformation characterises tillage operation where the soil condition after failure is the target.

Earth pressure theories tend to explain the interaction of soil-structure dividing the stress into active and passive pressures. Active pressure is the condition in which the earth exerts a force on the retaining system, whereas passive pressure is a condition in which the retaining system exerts a force on the soil. Based on the earth pressures theories two methods are accepted for calculating soil strength known as the Coulomb and Rankine theories. The general equations developed for both theories are based on the fundamental assumptions that soil is cohesionless, homogeneous, isotropic, semi-infinite and well drained. The Rankine theory is intended for determining earth pressures on a vertical plane within a mass of soil without considering wall friction. The Coulomb theory, however, provides a method to obtain the resultant horizontal force on a retaining system for any slope of the wall. As common point, both theories are based on the assumption that soil yield on the failure plane defined by a straight line. Refinements of these theories resulted in a logarithmic spiral failure called log-spiral theory which provides realistic results (Hettaratchi et al., 1966).

To represent the state of the stress and strain at a certain point into the soil, the equilibrium limit state is commonly accepted. This method is only reliable for obtaining information about the maximum forces before the soil is deformed (Shen and Kushwaha, 1998). The basic assumptions for the limit equilibrium method take into consideration soil as a rigid material. Acknowledging that the failures occur in soil-soil or soil-wall interfaces, the patterns of the failure surface are predetermined and the forces interacting on the failure surface are governed by the Mohr-Coulomb equation described in Coulomb (1776) and cited by Lambe (1969) ,it is written as:

$$\tau = c + \sigma_n \tan \phi \qquad (2.1)$$

where:

τ = shear stress at failure [Pa],

c = soil cohesion [Pa],

σ_n = normal stress [Pa],

ϕ = friction angle [°].

The Mohr-Coulomb criterion is also used to determine the forces acting on the soil-tool interface. Using the parameters related to the contact area, the original equation is modified as follows:

$$\tau = c_a + \sigma_n \tan \delta \tag{2.2}$$

where:

c_a = soil adhesion [Pa],

δ = external friction angle [°].

For a graphical representation in the normal-shear space, the Mohr circle is used (Figure 2.1). The straight line obtained by the combination of principal stresses and shear strength is called the failure envelope. The angle of internal friction (ϕ) is measured between the failure envelope and the horizontal axis; the intersection with the ordinate axis defines the soil cohesion value (c). By means of the failure envelope the maximum shear strength (τ_f) is determined under a specific normal load (σ_n).
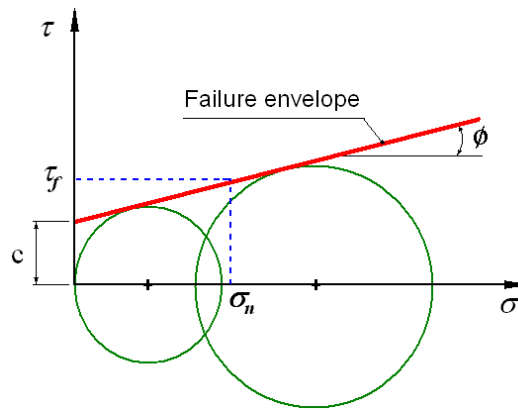
Figure 2.1 Mohr-Coulomb criterion of failure.

In the Mohr-Coulomb theory of failure, shear strength has two components: one for inherent strength due to bonds of attractive forces between particles, and another one produced by frictional resistance due to shear movement. The shear strength of cohesionless soils is limited to the frictional component and the failure envelope starts from the origin of normal-shear co-ordinates.

2.3 Physical properties and soil classification

Soil samples were collected in four diagonal points at three different depths of 15, 30 and 50 cm in a field of sugarcane with two-years of fallow, located in the central region of the Cuban island. Soil texture and physical properties were obtained by combination of soil sieve and hydrometer tests (Archer and Marks, 1985).The soil was classified as Oxisol according to the international classification based on soil taxonomy (ASTM D2487). In view of its granulometric composition according to the so-called soil textural triangle, the soil was considered as clay. Its physical properties are summarised in Table 2.1.

Table 2.1 Physical properties of clay soil.

Depth, cm	SG	PL, %	LL, %	PI, %	Sand, %	Silt, %	Clay, %
15	2.61	22.5	63.5	41	7	27	66
30	2.64	24.6	67.7	43.1	6	29	65
50	2.62	26.2	67.9	41.7	8	29	63

The soil plastic limit (*PL*) was determined by rolling out a thread of the fine portion of a soil on a flat surface. If the soil is plastic this thread will retain its shape down to a very narrow diameter. The sample can then be remoulded and the test repeated. As the moisture content falls due to evaporation, the thread will begin to break apart at larger diameters. Soil liquid limit (*LL*) was determined as the water content at which the soil changes from plastic to liquid behaviour. Finally, plasticity index (*PI*) was the size of the range of water contents where the soil exhibits a plastic behaviour. The procedure to measure the above parameters is defined in ASTM Standard D 4318.

The water content was determined according to the standard procedure (ASTM D2216). First the mass of the wet soil of the sample is measured, then the sample is dried in an oven for 12 hours at a temperature of 110°C, and finally the dry weight is taken. The value of the water content is expressed as a percentage of the sample's dry weight.

$$w = \frac{m_{wet} - m_{dry}}{m_{dry}} \cdot 100 \tag{2.3}$$

where:

w = gravimetric water content [%],

m_{wet} = mass of the sample before drying in the oven [kg],

m_{dry} = mass of the sample after drying in the oven [kg].

The economic importance of Oxisol soils is directly related to the main industry in Cuba where more than 40% of the sugar cane plantations is grown in clay soils. These tropical soils are characterised by close soil properties among different layers (Cairo, 1995). Their colour is generally red-grey, formed from hard calcareous rock. Heavy texture with high content of expansive clay makes this soil prone to forming deep cracks in drier seasons. In contrast, under irrigation regime these soils enhance their agronomic value with respect to friability, fertility and microbiological activity.

2.4 Experimental triaxial compression test setup

The soil mechanical properties related to soil-soil interaction, more specifically, the internal friction, soil cohesion, soil adhesion, Young's modulus, and Poisson's ratio were studied by means of the Standard Triaxial Compression Test (ASTM D2850). The compressive strength of cylindrical specimens of Oxisol is determined by using a strain-controlled application of the axial load while the specimen is subjected to a confining fluid pressure in a triaxial chamber. Widely used in civil and agricultural engineering the test provides data for determining strength properties and stress-strain relationship (Kézdi, 1980).

A multilevel full factorial experimental design was used to obtain the influence of the soil gravimetric water content (w) and dry bulk density (ρ_d) on the behaviour of the mentioned mechanical properties. The content of water was planned to vary in five levels: 16, 20, 24, 28 and 32%, and dry bulk density in three levels: 1, 1.2 and 1.4 g/cm^3; resulting in fifteen experimental points from the factorial combination as shown in Table 2.2. Four samples were prepared for each experimental point, tested by increasing the water pressures at 30, 50, 70 and 90 kPa. Only the extremes and the center experimental points (1, 5, 11, 15 and 8) were replicates, for the entire experiment a total of 80 soil samples were tested.

Table 2.2 Planning experimental points for soil test.

Test	1	2	3	4	5	6	7	8	9	10	11	12	13	14	15
w, %	16.3	19.8	24.1	27.6	31.7	15.8	21.1	25.4	28.1	30.9	16.2	19.8	23.4	26.7	31.1
$\rho_{d,}$ *g/cm^3*	1	1.01	1.02	0.99	1.01	1.19	1.16	1.16	1.23	1.18	1.36	1.38	1.3	1.36	1.37

In order to prepare the cylindrical samples for the triaxial compression test, the Oxisol soil from the first layer was mixed, and the specific content of water is added in accordance with the experimental points defined in Table 2.2. The dry bulk density for the test is obtained by pressing the soil within a cylindrical mould. The final shape of the sample is a cylindrical body of 50 mm diameter and 100 mm height as shown in   2.2a. Finally the samples are stored for 72 hours in a hermetic chamber until reaching the moisture homogenization and soil internal equilibrium required by the test.

To set up the sample in the triaxial apparatus, the soil specimen is covered by a rubber membrane and confined into a hermetic cylindrical chamber (Figure 2.2b) filled by distilled water, the axial pressure is controlled by the hydraulic system shown in Figure 2.2c. The changes in the volume of water with respect to the initial one, was also measured by the water drained from the cylinder. The corresponding volumetric change of the soil specimen was used to calculate the incremental volumetric strain of the soil.

(a)   (b)   (c)
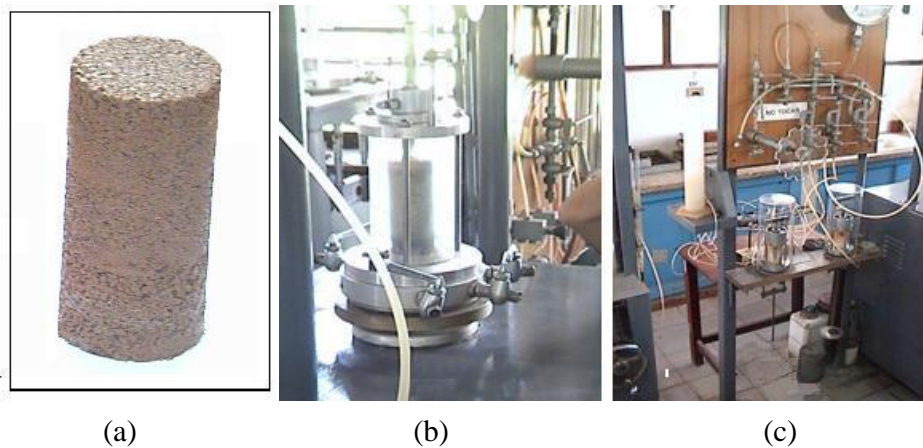
Figure 2.2 Soil specimen (a), chamber setup (b), and hydraulic system (c).

Soil strength is obtained by pressing on top of the soil a cylinder at constant velocity of 1.5 mm/s. Loading is stopped when the stress peaked and finally dropped.

Deviator stress is the difference between the major and minor principal stresses in a triaxial compression test (σ_1 - σ_3). The major principal stress σ_1 in the specimen is equal to the deviator stress plus the chamber pressure, and the minor principal stress σ_3 in the specimen is equal to the chamber pressure. The vertical load applied over the specimen is obtained directly from the force transducer; then the deviator stress is obtained by:

$$(\sigma_1 - \sigma_3) = P/A_c \tag{2.4}$$

where:

$(\sigma_1 - \sigma_3)$ = deviator stress [Pa],

P = applied axial load [N],

A_c = corrected cross-sectional area of the specimen [m^2].

The axial strain (ε) is determined by:

$$\varepsilon = \Delta L/L_0 \tag{2.5}$$

where:

ΔL = change in length of the specimen as read from the deformation indicator [m],

L_0 = initial length of the specimen minus any change in length prior to loading [m].

For each experimental point, maximum stress at failure $(\sigma_1 - \sigma_3)$ at the above mentioned confined pressures are plotted on the tension-shear plane define by the Mohr-Coulomb criterion (Figure 2.1), the straight line is drawn obtaining the values of internal friction angle and soil cohesion.

2.5 Direct shear test for external soil properties

The external properties of the soil called soil adhesion (c_a) and soil external friction (δ) were obtained by direct shear tests with respect to a steel surface (Figure 2.3a). Soil specimens were sized at 70 mm diameter and 16 mm height by means of the procedure of mixing and remoulding according to the standard (ASTM D3080). The modification proposed by Sánchez-Girón Renedo (1999) to evaluate the soil external behaviour is introduced in the test. This modification has to do with the substitution of half of the specimen by the steel body (Figure 2.3b), forcing in this way that the contact during sliding takes place on the soil-steel interface. The soil-metal shear test attempts to reproduce the interaction between the soil and steel surface of the implement during tillage operations. Figure 2.3b and 2.3c shows the final shape of the soil specimen and the steel plate. Both parts are placed in the cylindrical rings forming the main box of the shear apparatus shown in Figure 2.3a. During the test, the specimen was deformed at a controlled strain rate on a single shear plane determined by the configuration of the apparatus (Figure 2.3a).

In order to determine the influence of the water content and dry bulk density with respect to adhesion and external friction behaviour, in a way similar to the triaxial compression test, a multilevel experimental design was performed. The experimental points shown in Table 2.2 were tested in a direct shear test.
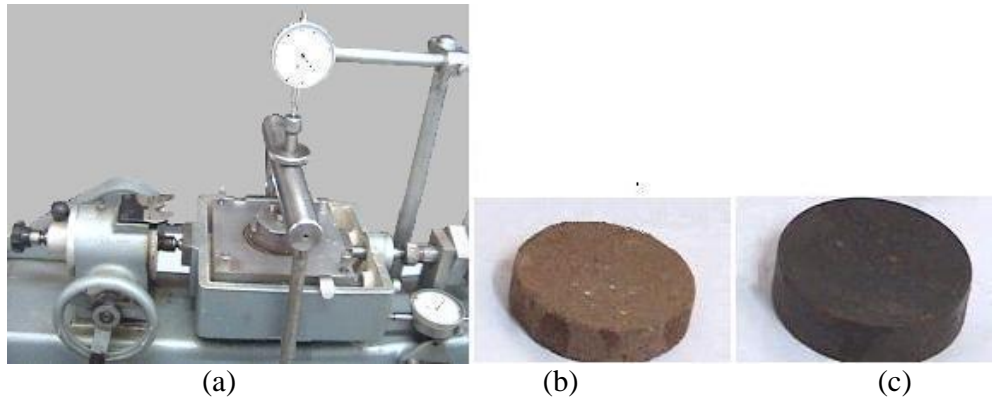
Figure 2.3 Shear box apparatus (a), soil samples (b) and steel disk (c).

Following the same procedure, four specimens of the soil for each experimental point under investigation (Table 2.2) have been tested at a different normal load of 30, 50, 70 and 90 kPa. A constant velocity of 1.5 mm/s was used to slide the bottom of the shear box making sure water is drained. Data of relative lateral displacement versus shear forces is recorded during the sliding time in order to draw the shear stress-displacement curve. The test is ended when the displacement covers 20% of the sample diameter.

Nominal shear stress (τ) acting on the specimen is calculated by the following expression:

$$\tau = F/A \tag{2.6}$$

where:

τ = nominal shear stress [Pa],

F = shear force [N],

A = initial area of the specimen [m^2].

Normal stress acting on the specimen is,

$$n = N/A \tag{2.7}$$

where:

n = normal stress [Pa],

N = Normal vertical force acting on the specimen [N].

Maximum values of nominal shear stress (τ) versus normal stress (n) are plotted for each experimental point under investigation. The Mohr-Coulomb criterion of failure (Equation 2.2) is used with a view to obtain the magnitude of soil adhesion and soil-metal friction angle.

2.6 Soil mechanical properties

The macro-behaviour of a clay soil as a function of water content and dry bulk density is analysed in the next sections. Using triaxial compression test and direct shear test, the soil-soil and soil-metal interface are characterised for different soil conditions. Each mechanical property under the study was submitted to a multiple regression analysis to obtain the statistical equations to predict the soil mechanical response. The statistical coefficients in the models were determined at 95% confidence intervals. The analysis also includes the adjusted coefficient of multiple determination *Adj. R^2* and standard deviation of the regression *RMSE*.

2.6.1 *Soil Shear Strength*

The stress-strain curve is a direct result of triaxial compression tests. From the variation of shear strength the soil deformation pattern is released. For all experimental points defined in Table 2.2, the stress-strain curves were drawn in order to use the data to calculate other soil mechanical parameters as the Young's modulus, cohesion and internal friction.

The stress-strain curve tested for dry bulk density at 1.37 g/cm^3 is shown in Figure 2.4. The pattern of soil failure undergoes a significant change, caused when soil water content increases. The maximum stress, selected as the inflection point on the curve, belongs to the minimum water content tested, i.e. for $w = 16\%$, what results in a typical curve of brittle material.

The lowest soil shear strength resulted from the higher soil water concentration tested, i.e. for $w = 32\%$ (Figure 2.4). Large plastic deformation characterises the stress-strain curve when the level of moisture increases, making it hard to define the failure shear points, as shown in the curve at 24, 28 and 32% of water content. The increase in soil shear strength also can be associated with the process of cementation taking place during soil specimen construction. During this process, the combination of large clay content in the soil with normal pressure applied for densification, and the final time of sample repose, lead to the creation of stronger inter-granular bonds in the specimen that yield a substantial increase in soil stiffness. This

behaviour was well explained by Dolinar (2010) considering the influence of water content and the mineralogical properties of clay.
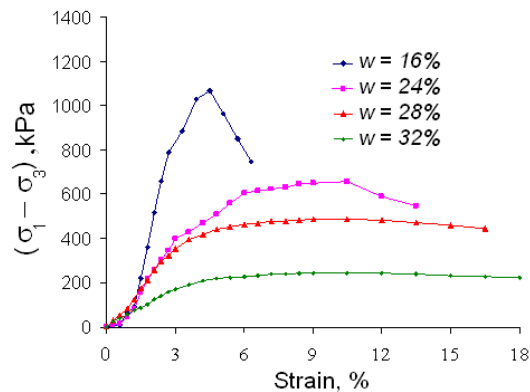
Figure 2.4 Stress-strain curves of clay soil at different soil water content.

As a measure of sample deformation the engineering strain also increases from a dry to a wet soil condition (Figure 2.4). In general, the soil under study showed larger values of shear failure than the loamy and sandy soils reported by McKyes and Maswaure (1997). However, studies carried out on Ferralsol soils with approximately the same concentration of clay, silt and sand (Herrera Suárez et al., 2008), report values of shear strength and pattern of failure close to the ones found in the present work. In addition, soil shear strength at failure was found to depend on the compaction level as shown in Figure 2.5. The statistical model was obtained with the values obtained from tests performed at constant lateral pressures of $\sigma_3 = 50$ kPa and called $\tau_{(50kPa)}$,the equation is used in the model to calculate the maximum overlap allowed by two elements in contact.
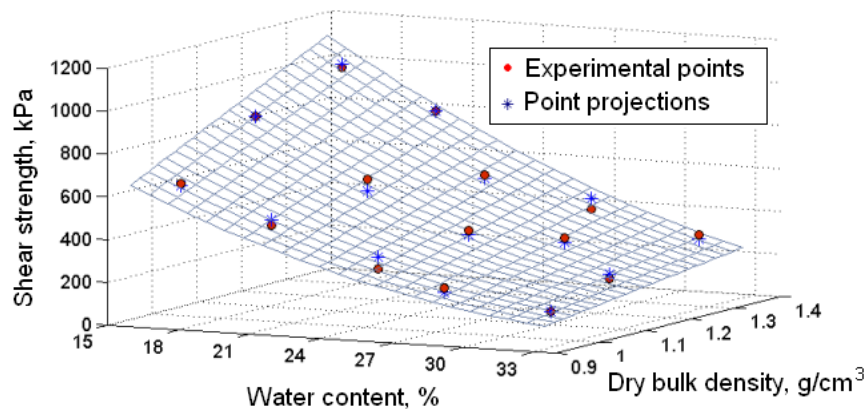
Figure 2.5 Variation of shear strength at failure as a function of water content and dry bulk density.

21

The general model for predicting the shear strength at failure as a function of water content and dry bulk density was fitted by the following regression equation:

$$\tau_{(50kPa)} = aw + b\rho_d + cw^2 + dw\rho_d \tag{2.8}$$

where:

$\quad\quad\tau_{(50kPa)}$ = shear strength at failure [kPa],

$\quad\quad a$ = -41.54 [kPa],

$\quad\quad b$ = 1706 [Nm/kg],

$\quad\quad c$ = 1.098 [kPa],

$\quad\quad d$ = -43.3 [kN·mm^4/g^2].

The shear strength at failure is also affected by the interaction between independent variables w and δ_d as written in Equation 2.8. The statistical goodness of fit of the model showed an *Adj. R^2 = 0.98* with a standard deviation of regression *RMSE* = 32.91 kPa. From the model surface response (Figure 2.5), the influence of the dry bulk density on the soil shear strength appears to be more pronounced toward the dry soil condition. At the maximum water content $w = 32\%$, the soil strength reached its minimum value as a consequence of a gradual weakening of intergranular bonds.

2.6.2 *Elastic Young's Modulus*

Young's modulus characterises the property of the soil to be elastic if it can return to its original size or shape after being stretched. It is an essential parameter in the model defining how rigid the medium is, independently of the computational method used (Roul et al., 2009, Coetzee and Els, 2009b, Gebregziabher et al., 2007). Also known as elastic modulus (E), it is defined as the ratio of stress to strain. However soils do not exhibit a linear stress strain curve, as shown in Figure 2.4, with the inconveniences that many elastic moduli can be obtained from the triaxial test results. The initial slope of the stress-strain curve was the criterion adopted to calculate the elastic modulus of each experimental point. The final Young's modulus was the average of those obtained at the four lateral pressures tested (30, 50, 70, 90 kPa).

Through the entire experimental region a strong linkage of soil elastic modulus with water content and dry bulk density was found. The obtained magnitude of Young's modulus ranged between 10 to 100 MPa (Figure 2.6).
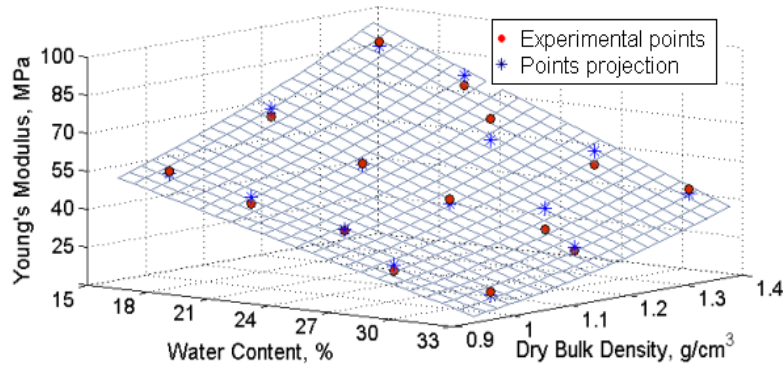
Figure 2.6 Variation of Young's modulus as a function of water content and dry bulk density.

The statistical model to predict Young's modulus *E* as a function of water content and dry bulk density is written as:

$$E = a + b\ w\rho_d + c\ \rho_d{}^2 \tag{2.9}$$

where:

    E = Young's modulus [MPa],

    a = 32.1 [MPa],

    b = -2.33 [Nm/g],

    c = 57.2 [Nm^4/kg^2].

The model was fitted with an adjusted coefficient of multiple determination, *Adj. R^2* = 0.95 and standard deviation of the regression was *RMSE* = 4.2 MPa. Young's modulus describes a quadratic relationship with respect to dry bulk density as is shown in Figure 2.6. The interaction between independent variables was also considered to be important in the model in accordance with Equation 2.9. On the other hand, an increasing in water content led to a linear reduction of Young's modulus. At low moisture the water binds the particles of clay, enhancing the effective soil strength. By this process, when the soil is drying out, the clay becomes very stiff. On the other hand, non-linear relation between soil elasticity and dry bulk density was found by Mouazen *et al.* (2002). The authors proposed a regression equation to involve the effect of moisture and dry bulk density for a sandy loam soil. However, although the soil showed a similar pattern of behavior, the values of Young's Modules found were considerable smaller than those found in the present study, ranging between 2 and 16 MPa. At the same time, a study carried out in a soil classify as Rhodic Ferrasol by Cueto (2011) showed close results with respect to Young's modulus magnitudes. As in the present one, the major effect was found by the action of

water content, between 22 to 34% the Young's modulus decreases from 52 to 12 MPa for a constant dry bulk density of 1 g/cm^3.

2.6.3 *Poisson's ratio*

When a soil specimen is compressed in axial direction, it tends to expand in the other two directions perpendicular to the direction of compression. This phenomenon is called the Poisson effect. Poisson's ratio is a measure of the Poisson effect; it is calculated as the ratio of the fraction of expansion divided by the fraction of compression.

On the other hand, volumetric soil changes take place during tillage operations. By the action of the tool the soil is compressed until failure. When the soil becomes incompressible the Poisson's ratio gets a value of 0.5. Values near zero indicate high soil compressibility (Mouazen et al., 2002). The values of the measured soil volume change, obtained from triaxial tests have been incorporated into the soil constitutive equation (Duncan and Chang, 1970). In general, numerical models to simulate soil-tool interactions include the Poisson effect.

To calculate the Poisson's ratio, the data corresponding with the soil volumetric strain from a triaxial compression test explained in section 2.4, is used in the following equation:

$$\Delta\varepsilon_v = \Delta V/V_i \tag{2.10}$$

where:

$\Delta\varepsilon_v$ = incremental volumetric strain of the soil specimen [ ],

ΔV = resultant soil volume after loading [m^3],

V_i = initial volume of soil specimen [m^3].

The other parameter needed to determine the natural Poisson's ratio is the incremental axial strain of the , which was obtained by using the following relationship:

$$\Delta\varepsilon_l = \Delta L/L_i \tag{2.11}$$

where:

$\Delta\varepsilon_l$ = incremental axial strain of the soil specimen [ ],

ΔL = incremental height change of the cylindrical specimen [m],

L_i = initial height of the specimen [m].

Eventually, the relationship to calculate the Poisson's ratio ν is written as:

$$\nu = (\Delta\varepsilon_l - \Delta\varepsilon_v) / (2 \cdot \Delta\varepsilon_l) \qquad (2.12)$$

Poisson's ratio is affected mainly by the dry bulk density as shown in Figure 2.7, a linear increase characterises its behaviour through the overall soil water content. The soil compressibility augments in loose soil, caused by large void spaces inside the structure. Accordingly, for a low dry bulk density, minimum values of Poison's ratio were obtained. Compacted soil, however, is characterised by low compressibility in agreement with maximum values of Poisson's ratio.
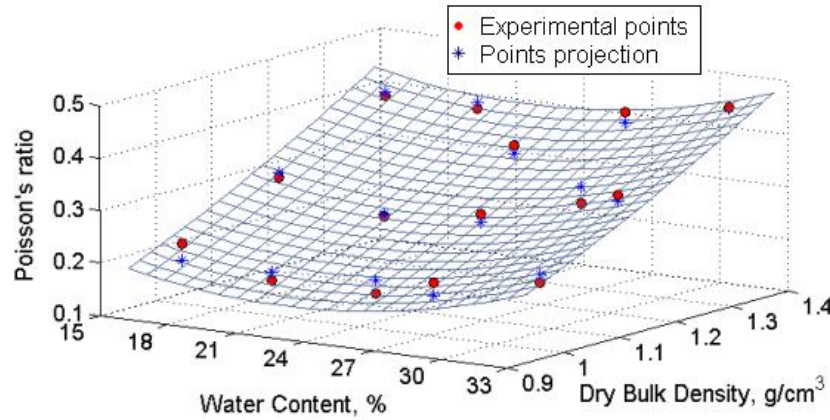
Figure 2.7 Variation of Poisson's ratio as a function of water content and dry bulk density.

The statistical model to estimate the Poisson's ratio as a function of water content and dry bulk density is written as:

$$\nu = a + bw + c\rho_d + dw^2 \qquad (2.13)$$

where:

ν = Soil Poisson's ratio[ ],

a = 0.25 [ ],

b = -0.03 [ ],

c = 0.25 [cm^3/gm],

d = 0.0007 [ ].

The model was fitted with an adjusted coefficient of multiple determination *Adj. R^2* = 0.94. The standard deviation of the regression was obtained at *RMSE* = 0.03.

A non-linear behaviour of Poisson's ratio under different water contents was found. Beyond 24% of water content, the value of Poisson's ratio grows slowly up to 0.3. The plastic limit *PL = 22.5* obviously is related with the position of the deflection point. Since the inter-granular

void spaces are progressively filled with water, the soil gradually loses its compressibility with a consequent increase in Poisson's ratio. The increase in water content from 15 up to 24% softens the soil, particles rearrange in the sample and the void pores are filled by water. The result is a slight decrease of Poisson's ratio in this interval. The variation of Poisson's ratio obtained in the present study is in agreement with those found in the same type of soil taken at different locations in Cuban island (Suárez et al., 2008, Cueto, 2011). These results also agree with those obtained by Mouazen (2002), the range of variation found by the author was in between 0.2 to 0.5 for values of dry bulk density between 1.2 to 1.8. Nonetheless, in the sandy soil tested during this experiment, the effect of the soil compaction was smaller in comparison with the effect found in the present study. To simulate the effect of the elastic properties over soil compaction, the Poisson's ratio was tested in the range between 0.13 to 0.38, these values were reported during experimental tests in loam soils (Raper and Erbach, 1990).

2.6.4 *Soil cohesion behaviour*

For a specific soil, the predominant factors that affecting soil cohesion are the index of compaction and soil moisture, as a result of chemical and physical phenomena taking place in the soil (McKyes, 1989). The internal soil cohesion was obtained by means of the Mohr-Coulomb theory of failure (section 2.2) at different soil physical conditions. The internal cohesion, obtained by triaxial compression tests, as function of the dry bulk density of the soil and soil moisture is shown in Figure 2.8.

Figure 2.8 Variation of soil cohesion as a function of water content and dry bulk density.

The statistical model to predict soil internal cohesion as a function of water content and dry bulk density is written as:

$$c = a + bw\rho_d + c\rho_d{}^2 + d\rho_d \qquad (2.14)$$

where:

c = soil cohesion [kPa],

a = 220.7 [Kpa],

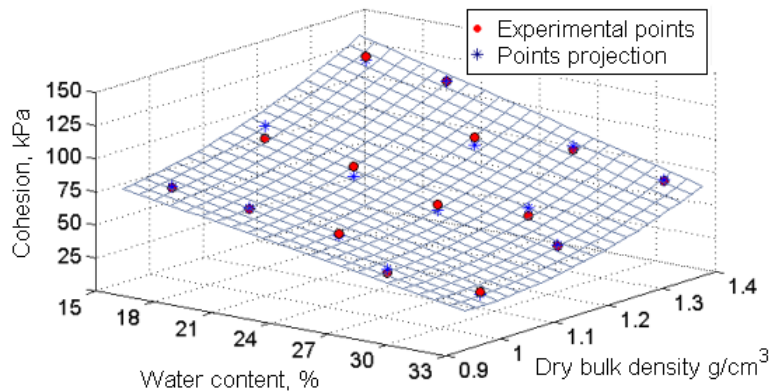b = -2.7 [Nm/kg],

c = 211 [kN·mm^4/g^2],

d = -317 [Nm/kg].

The model was fitted with an adjusted coefficient of multiple determination, *Adj. R^2* = 0.96. The standard deviation of the regression was *RMSE* = 4.6 kPa.

A quadratic increase with respect to dry bulk density characterises the cohesion for all values of soil moisture. At the same time, cohesion decreases linearly when soil water content increases as shown in Figure 2.8. In the range of soil moisture under study (w = 16 to 32%), the soil cohesion raises an average of 50 kPa for all values of dry bulk densities tested. This behaviour subjects the soil tendency to obtain higher values of cohesion in dry-compacted condition ($c > 120$ kPa) in contrast with the values found under wet-loose conditions ($c < 30$ kPa). These results coincide with the observation by McKyes *et al.*(1994), who reported that the pattern of behaviour of a Lixisol changes from hard to soft as the water content increases. Similar results have been reported by Horn and Fleige (2003). The authors linked the soil strength with soil suction, texture, structure, and applied stress. The moisture effect over soil cohesion was also reported by (García de la Figal, 1978, Suárez et al., 2001, Chancellor, 1994). On the other hand, González Cueto (2009) found values between 47 and 230 kPa of soil cohesion in a compacted Oxisol soil, the values were higher than those found in the present investigation.

2.6.5 *Soil adhesion behaviour*

The soil propensity of adhere to the tool surface is called soil adhesion. Its magnitude changes according to different soil physical conditions. During tillage in adhesive soil the cutting surfaces of the tool are partially or totally surrounded by a soil layer. This is the reason why a soil is force to slide over itself causing an increase in the friction angle. Specifically for clay soils the adhesion increases, affecting tillage quality and increasing draught requirement (Shrestha et al., 2001, Soni et al., 2007).

The modified direct shear test was used to derive the soil adhesion at the soil-metal interface as a function of dry bulk density and water content following the factorial experiment explained in section 2.4.

As shown in Figure 2.9, a small linear increase was found in soil adhesion with respect to dry bulk density with an average variation of 2.1 kPa for specific water content. This result suggests a weak dependence of soil adhesion on soil compaction. The predominant factor is the water content in a quadratic relation. Beyond 23% of water content the adhesion rapidly increases.
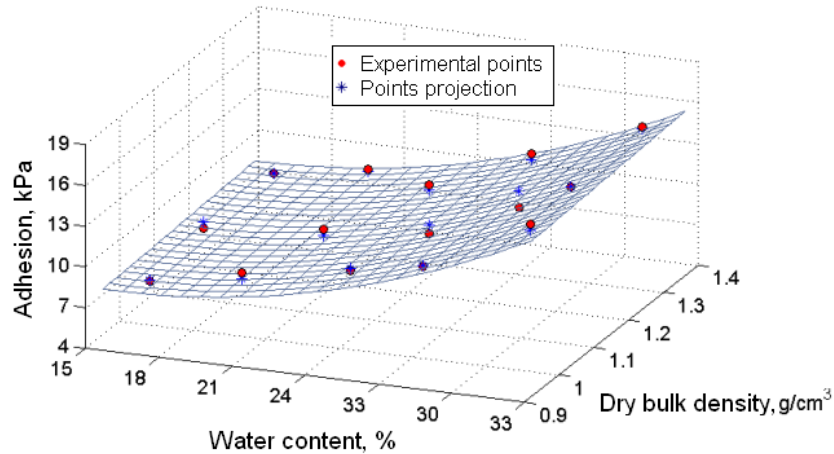
Figure 2.9 Variation of soil adhesion as a function of water content and dry bulk density.

The statistical model resulting from multiple regression analysis is written as:

$$c_a = a + bw + c\rho_d + dw^2 \tag{2.15}$$

where:

$c_a =$ Soil-metal adhesion [kPa],

a = 12.12 [kPa],

b = -0.7807 [kPa],

c = 1.28 [Nm/kg],

d = 0.02537 [kPa].

The model was fitted with an adjusted coefficient of multiple determination, *Adj. R^2* = 0.96. A standard deviation of regression *RMSE = 0.*4 kPa was obtained.

The role of water in the augmentation of soil-metal adhesion can be explained by the suction force acting on the metal surface. Also, a viscous mixture formed by the dissolution of silt, clay and organic matter acts as glue that sticks soil particles on the steel surface of the blades. This

condition makes the soil sliding over its own irregular layers instead of over the tool surface, causing an increment in the traction force. The relationship between soil adhesion and moisture content in several Cuban soil was studied by García de la Figal (1978), the author reported the quality of clay soils to acquire high values of adhesion in contact with plastic and steel at a specific water content, that behaviour was found weak for sandy soils. The values obtained in the present study corroborate the results reported by Rodríguez (1999) in a Vertisol soil with 50% of clay. The author reports values of adhesion between 5 to 18 MPa. However in extremes wet conditions ($w > 45\%$), the adhesion reached values of 22 MPa.

2.6.6 *Soil internal friction behaviour*

In the Mohr-Coulomb theory of failure, shear strength has two components: one for inherent strength due to the bonds or attractive forces between particles called cohesion, and the other produced by the frictional force as described in section 2.2. When the triaxial compression test is used to investigate the soil mechanics properties, successive tests with increasing normal stress, describe a straight line inclined at a specific angle defining the internal friction as is shown in Figure 2.1. The variation of internal friction angle with respect to water content and dry bulk density is shown in Figure 2.10.

Figure 2.10 Variation of internal friction angle as a function of water content and dry bulk density.

The statistical model to predict internal friction as a function of water content and dry bulk density is written as:

$$\phi = a\rho_d + bw^2 + c \tag{2.16}$$

where:

ϕ = internal friction angle [°],
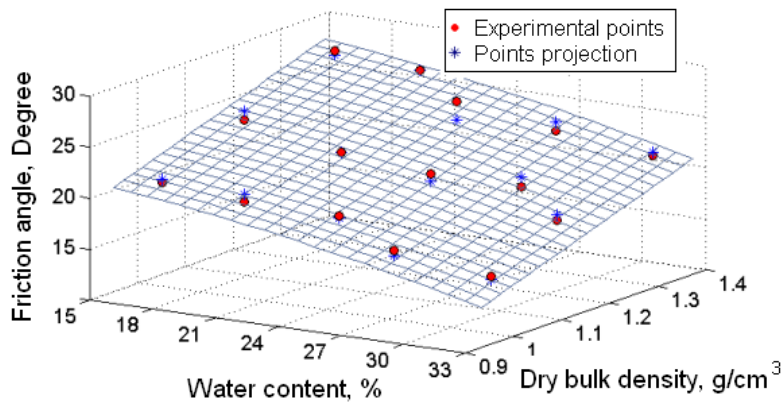
a = 16.6 [cm^3/g],
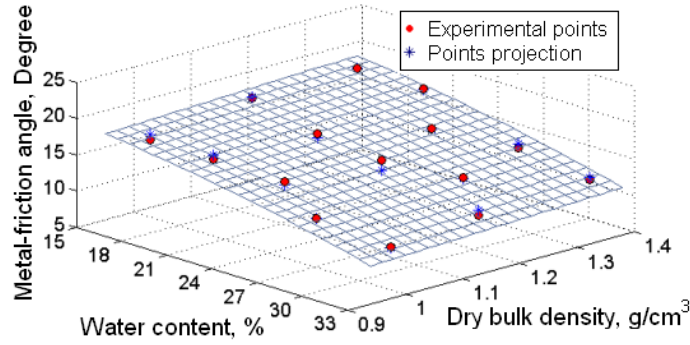
b = - 0.008 [°],

c = 6.2 [°].

The model was fitted with an adjusted coefficient of multiple determination *Adj. R^2* = 0.94, the standard deviation of the regression was obtained at *RMSE* = 0.82°.

Soil moisture and compaction level change the internal friction response as shown in Figure 2.10. With increasing soil water content friction was reduced until it reached a minimum value for lower dry bulk density, describing a non-linear behaviour. As previously discussed, soil softening and bond dissolution rise with water increase. Inversely, with increasing soil compaction the internal friction also linearly rises, probably due to the augmentation of the actual contact area and the number of contact points. During sliding, the soil grains are fragmented into new smaller grains affecting the soil internal friction. The increase in moisture content is accompanied by a decrease in the solid fraction in the soil. According to McKyes (1989),as the solid fraction decreases and moisture content increases, the interlocking and long-range forces between small particles, and the strength parameters i.e. friction and cohesion also decrease.

The same pattern in the variation of soil internal friction, with respect to water content and soil compaction, was found by Suárez (2008). In this study, carried out in an Oxisol soil placed at the central portion of the Cuban Island, the internal friction reached values of 10 to 38°, slightly higher than those presented here. In a loam soil, the internal friction was reported to increase with an increment in dry bulk density only for low content of water (Mouazen, 2002). On the other hand, the variation of internal friction was found dependent of soil moisture in a compacted Oxisol (Cueto, 2011), the values found were in between 10 to 62° for a range of moisture of 20 to 40%.

2.6.7 *External friction behaviour*

Soil external friction related to the soil-steel interface was determined from the modified direct shear tests. According to the Equation 2.2 the Morh-Coulomb criterion was used to obtain the failure envelope in the normal-shear plane (Figure 2.1). The variation of the soil-steel angle of friction to respect of moisture and compaction is shown in Figure 2.11.

Figure 2.11 Surface response of soil-metal friction.

The statistical model to predict the angle of soil external friction as a function of water content and dry bulk density can be written as:

$$\delta = a + b\rho_d + cw^2 \tag{2.17}$$

where:

δ = Soil-steel angle of friction [°],

$a = 15.8$ [°],

$b = 3.03$ [cm^3/g],

$c = -0.009$ [°].

The model was fitted with an adjusted coefficient of multiple determination, *Adj. R^2* = 0.94 and standard deviation of the regression was *RMSE* = 0.21°.

The soil external friction was mainly affected by the water content as shown in Figure 2.11. Starting from dry conditions, the soil-steel friction diminishes in a quadratic way (Equation 2.17) as water content increases. During the soil-tool interaction a water film emerges between the soil and the tool, playing the role of lubricant during soil sliding. These results are in agreement with the study carried out in fine-grain soil by Yao and Zeng (1988) where soil moisture modified the angle of soil-metal friction. Dry bulk density was found as a secondary factor in the behaviour of the soil-steel friction. From loose to compacted soil only 2.1° of average variation was observed. The results of metal-friction variation obtained in the present study elucidate the main effect of the water content as was reported by Suarez (2006). In this study however, the value of the angle changes between 10 and 32°. On the other hand, the secondary and in some cases negligible effect of the soil dry bulk density on the variation of soil-metal friction was obtained by Zhang (1986).

2.7 General behaviour of soil parameters

In general, the soil mechanical properties under study were influenced by the variation in water content and dry bulk density. As was shown, for high levels of compaction in dry conditions the parameters related to soil strength increase. Inversely, the soil strength was considerably reduced as the soil moisture increases under low levels of soil compaction.

The significance of the predictors in the model is shown in Table 2.3 for all the properties under study. Since the *P-value* is less than 0.05, there is a statistically significant relationship between the variables at the 95.0% confidence level. The coefficient *P-value* greater than or equal to 0.05 (since significance level operating at 5%) were removed from the model.

As shown in Table 2.3 the dry bulk density ρ_d shows a linear relationship with all soil mechanical properties except for Young's modulus, which increases quadratically as the soil becomes more compacted.

Table 2.3 Statistical parameters in the models of soil mechanical properties

Soil Properties	*P-values*					
	w	ρ_d	w^2	$\rho_d{}^2$	$w\rho_d$	R^2
t_{50}	0.0004	0.0001	0.0034	-	0.0000	0.9800
E	-	-	-	0.0000	0.0001	0.9500
v	0.0164	0.0002	0.0104	-	-	0.9400
c	-	0.0482	-	0.0195	0.0015	0.9600
c_a	-	0.0361	0.0000	-	-	0.9700
ϕ	-	0.0009	0.0012	-	-	0.9400
δ	-	0.0135	0.0001	-	-	0.9400

At the same time the water content only demonstrates a linear relationship with the shear strength and Poisson's ratio. The other properties increase in a quadratic way with respect to soil moisture. The statistical prediction models show values of the adjusted determination coefficients *Adj. R^2* > 0.94, also reaching more than 0.97 for soil cohesion and shear strength models.

2.8 Conclusions

Soil specimen collected from an agricultural field in Cuban island showed an average of 7% of sand, 28.3% of silt, and 64.6% of clay, which means that this soil belongs to the group of the

clays characterised by a large index of plasticity and plastic limit. Classified also as Oxisol according to the soil taxonomy classification, this kind of soil is one of the most economically important for agriculture in the country as more than 40% of the area of this soil is used for sugar cane production.

The properties of the soil which determine the soil mechanical behaviour during soil-tillage interaction at shallow depth were obtained by triaxial compression and direct shear tests as a function of water content and dry bulk density. The properties called Young's modulus, Poisson's ratio, cohesion, adhesion, internal friction, and soil-metal friction showed significant changes and predictable behaviour with respect to soil moistures variation $w = (16, 20, 24, 28, 32)\%$ and different levels of soil compaction $\rho_d = (1, 1.2, 1.4)$ g/cm^3.

Soil deformation changes from elastic to plastic behaviour as the water content increases. In case of a soil water content of $w = 16\%$, a fragile behaviour of the soil was demonstrated and the failure point was also well defined. However, at $w = 32\%$ large deformation with a plastic flow characterises a gradual decrease in soil strength.

The variation of Young's modulus showed a non-linear relationship with dry bulk density, increasing from 52 to 93 MPa at a minimum water content $w = 16\%$. The elastic property decreases with increasing water content until reaching a value of 18 MPa for $w = 32\%$.

The Poisson's ratio was described mainly by a linear relationship with the dry bulk density; with values ranging from 0.2 to 0.5 for all values of soil water content. The minimum value of Poisson's ratio was found near to the soil plastic limit (*PL = 22.5%*).

Soil internal cohesion increased linearly with the water content, and its response was quadratic with respect to dry bulk density. Both variables exert a significant influence on the rise in soil cohesion. Soil adhesion, however, shows a small linear increase with dry bulk density and was affected mainly by water content above 24%.

The soil internal friction ranged from 14° to 28° has a quadratic relationship with water content and a linear relationship with soil compaction. Different patterns of behaviour characterized soil external friction. This property is strongly influenced by the water content, decreasing quadratically for all levels of dry bulk density. A small linear increase is obtained by the action of soil compaction. In general, the soil-metal friction angle shows a variation from 16.1° to 19.9°.

In general terms, the mechanical properties of an Oxisol soil under study are in agreement with the results obtained by several studies. The mechanical properties of Cuban Oxisol soils from the literature show magnitudes and pattern of behaviour close to those obtained in the present study. These results are characterized by high values of Young's Modulus, cohesion and adhesion in comparison with loan and sandy soils. Soil internal friction and Poisson's ratio also show more dependence on dry bulk density and moisture than the other properties.

For each soil mechanical property under study a regression equation was obtained with an adjusted coefficient of multiple determination *Adj. R^2* from 0.94 to 0.97. These equations provide the data corresponding with the macro parameters of the soil needed for modelling soil-tillage interaction. The values of the soil mechanical properties at given soil moisture and compaction provide the soil data to simulate the soil-tool interaction during tillage at different soil conditions.

Chapter 3

Formulation of soil cohesive model

3.1 Introduction

Soil in a discontinuous model is commonly represented by an assembly of spherical particles with bonds that can break up and reform under external loading. Proposed by Cundall (1971), the method was developed for simulating rock slope stability and soil structures. The particles in the original model were represented by disks or spheres, and they are treated as rigid bodies. The contact between two elements occurs over a small area defined by the overlap between the two elements. The contact forces oriented in normal and tangential directions are related to the depth of the overlap. The magnitude of the contact force depends on material properties through micro-parameters appearing in the contact force model, such as contact stiffness and contact damping. The total force over the particles in contact is calculated each time step and a new spatial position is obtained by integrating the motion equation and Newton's second law, yielding a dynamical representation of the soil deformation. When suitable contact force models are used and microscopic model parameters are carefully selected, the DEM procedure can offer a realistic description of soil mechanical behaviour. However, as a real soil is composed of a huge number of small particles with complex shapes, it is inevitable to represent such a granular material as an assembly of larger idealized particles. Micro-macro parameter relationships resolve the difference in particles sizes and shapes, but introduce more complexity into the method. In the present chapter the state of the art on soil numerical simulation is presented, and a frictional-cohesive model is implemented and calibrated based on the Discrete Element Method.

3.2 Soil modelling by DEM, literature review

DEM was identified as a potential method to describe the soil rheological behaviour. Many studies have been carried out over the last fifteen years which involve topics as the influence of the parameters in the model, micro-macro relationship and methods for model calibration. To analyse the discontinuous deformation of a soil and discussing the applicability of the DEM model for soil simulation Tanaka *et al.* (2000) conducted a bar penetration test in which the soil is represented as an assembly of two dimensional circular elements. DEM parameters as stiffness, viscous damping and friction were used in the model to simulate the resistance of soil penetration. The movement described by the soil particles in the model was the same as described by real the soil in the experiment. As a tendency, penetration resistance increases with soil depth but in the simulation this value was considerably smaller than the results obtained from measurements. Moreover, large force fluctuations result from the simulation. The authors concluded that particles with adequate diameter and cohesive effect would be essential to settle the fluctuation of the force. The study aimed contributing to the establishment of a concrete method to determine the values of DEM parameters.

Inter-particle adhesion forces were introduced into a DEM model to evaluate the influence of suction forces in the collapse behaviour of unsaturated soil, as well as the effect of the initial void ratio (S. H. Liu, 2002). A constant value of adhesion was applied at each contact as initial condition, during the simulation the adhesion was reduced until collapse of the virtual unsaturated soil. The results agree qualitatively with the results of triaxial compression tests on unsaturated compacted clay. However, assigning a constant adhesion to all particles, results in a quite homogeneous medium. In addition, the reduction of soil adhesion without affecting the other soil parameters simplifies the changes taking places during soil sliding. Nonetheless, the addition of a tension force between particles was an important step towards the simulation of cohesive behaviour of soil.

Simulations of the isotropic mechanical test under drained and undrained stress of loose and dense spheres assemblies were carried out to explain the micro-mechanical material behaviour by Thallak.G. & Sitharam (2002). The study used the evolution of the coordination number, isotropy changes, and stress-strain curve to evaluate the capability of DEM to reproduce the mechanical granular test. The study showed a numerical simulation that clarifies the effect of inter-particle friction on the compression behaviour of granular media. Also the micro-mechanical analysis

indicated that the average coordination number is the same for loose and dense systems in drained tests under the same confining pressure.

Focused on geomechanics problems, a combination of DEM and FEM was investigated for modelling the dynamic behaviour of soil and rock materials (Oñate and Rojek, 2004). The combined model used a set of rigid spherical particles for the discretization of different parts of the system. Two theoretical algorithms of DEM and FEM were implemented in an explicit dynamic code. The model proposed involves the treatment of the contact between spherical elements and the boundary of the finite mesh. The model also included cohesion, damping, friction, wear, and heat exchange. Several examples were presented related to soil mechanical test and cutting operation denoting the wide applicability of the model, especially in the prediction of wear effect and energy requirement. Finally, the combined model was presented as a promising approach for simulation of geomechanical problems as fracture, penetration and wear evolution.

Finite Element Methods and Discrete Element Method were compared by modelling the behaviour of dynamic loads in soil-tyre interaction, tool penetration, shearing, and soil cutting (Tadesse, 2004). Mohr-Coulomb and Cam-Clay models were used to simulate the continuous medium. On the other hand, adhesion force between particles was introduced in the discrete model to reproduce the inter-particle tension. The study, for small soil deformation, showed consistent results using both numerical methods. However as the strain increases the FEM model was unable to simulate the soil deformation. As a limitation of the study, the model validation was made only by comparison with results from other authors and the simulation was reduced to a small quantity of particles with constant radii. Additionally, the adhesion was applied as an independent coefficient. Nevertheless, the study showed the advantages of the discontinuous method over the continuous one to simulate the dynamic force acting on the soil during tillage operation.

Based on field tests the parameters for a DEM model were obtained to model the soil penetration test (Asaf et al., 2007). The study was limited to quasi-static simulations, cohesionless soil, and a two-dimensional model. The forces measured during sinkage tests by different penetration tools were used to obtain the force-displacement curve. The model was calibrated by the inverse solution technique to simulate the effect of changing the micro-friction angle over the soil external friction and Young's modulus. In general, the results showed good correlation between real and virtual experiment, almost at 85% of confidence. Nevertheless, the predicted force tended

to be constant over depth while in real tests the force exponentially increased. In general, the proposed method proved the feasibility to use elastic and frictional soil parameters combined with interpolation techniques to calibrate the DEM models. Further study was suggested to extend the developed methodology to full dynamic cases including three-dimensional analysis.

The interaction of soil with a cutting-blade was simulated using four different shapes at the same speed of the tool (Shmulevich. et al., 2006). The soil was represented by clumps of disk connected by the cohesion force between them. Experimental validation was made by testing the tools in a soil box filled with sand. The force reaction on the tools named vertical blade, straight blade and two kinds of parabolic blades, were compared against the results of the DEM model. The simulation results were also compared with classical soil mechanics theories for straight blades, known as McKyes approach, and good correlation with respect to the draft force was obtained. Also the prediction of the curve of soil failure was in agreement with the results of experimental tests. The experiment showed the important effect of soil piling in front of the blade on the draft force results. However, a weak correlation was obtained between soil piling and vertical forces.

The intergranular friction angle and cohesive bond forces were the microscopic parameters at the core of a model for describing cohesive soils by Utili and Nova (2008). Based on several biaxial tests, a parametric analysis was performed to calibrate the micromechanical parameters and validate the DEM model. The model was used to minimize the parameters needed in the calibration process rather than attempting to reproduce the real grain interaction. In order to find adequate macroscopic variation in the friction angle, the rotation was inhibited in all simulations. The micromechanical parameters as coefficient of friction and cohesion were calibrated for the most common geomaterials. The evolution of natural cliff formation subject to different weather scenarios was simulated. However, the validation of the models was only possible against analytical predictions available from a limited analysis of the equations for which the results showed good agreement. The calibration procedure was only valid for a two dimensional model and the interaction took place between soil particles only.

Based on a coupling of FEM and DEM, a numerical model was proposed to describe the tensile behaviour under large displacement during interaction between soil and geosynthetic sheet by Villard et al. (2009). To reproduce the soil behaviour, a triaxial test was simulated representing the soil as a cluster made by three particles. Shear stress resulting from numerical simulation was

defined as a macro parameter for model calibration. The comparison between numerical and experimental results showed that the model reproduces the reinforced embankment in a satisfactory manner.

To investigate blade-granular material interaction, Coetzee and Els (2009b) used a box of corn grains in which a narrow tool placed at 90° rake angle was moved. The experimental setup was subsequently modelled with DEM using two spherical particles clumped together. The model parameters investigated were particle density, friction and contact stiffness. As a result, the predicted shape of the heap in front of the blade corresponded well to the experiment; However as the displacement increased the error became larger. The measured and simulated draft forces were satisfactory close up to 50% of the total travel. Beyond that, the predicted forces were systematically lower than the measured. The author recommended to model cohesive materials as sand and clay in a further study to evaluate the simulation results.

The travels of the pores into saturate granular soil, was simulated in a model which represented soil particles by discrete elements, and pore fluid by alternatively Lagrangian mass of water and Eulerian volume of space (Lamei and Mirghasemi, 2011). The pores of water in the model were surrounding soil particles applying a force according to some approximate assumptions. The shape of the pores was represented by cylinders and soil grains by ellipsoids. Macro-scale behaviour of the model was verified by simulating an undrained biaxial compression test and the micro-scale behaviour was compared with experiments described in literature. The study brought a more comprehensive knowledge about the behaviour of granular material at the scale of soil constituent elements. To avoid complexity, from the computational point of view, pore fluid flow was simplified in the model.

Predicting draft forces for simple tools was carried out on a cohesionless soil and the result was compared with a small-scale laboratory test (Obermayr et al., 2011). The study focused on the behaviour of granular material under quasi-static condition, for which a three-dimensional DEM was adopted to predict draft forces for a straight blade. For the experimental test steel balls and washed gravel were used as granular material. The influence of the model parameters as stiffness, local friction and density was tested by simulation of a triaxial compression test. From these results the calibration procedure was derived using the bulk internal friction parameter. The DEM model, applied to the simple case of a single blade, was successful in reproducing the variation of draft force for different cutting widths and depths.

Generally, in DEM modelling, the soil particles are treated as rigid elements without inter-particles cohesive force (Tanaka et al., 2000, Asaf et al., 2007, Liu et al., 2003, Lamei and Mirghasemi, 2011). In these studies the system was reduced to two dimensions. When some simulations were made in three dimensions the inter-particle bonds were not considered (Shmulevich et al., 2007, Obermayr et al., 2011). However, cohesion forces were explored by inter-particle bonds, combining the effect of friction force and cohesion (Utili and Nova, 2008). With the purpose to reproduce soil and tillage interaction, only elemental shapes of tillage tools were tested and the comparison of reaction forces between numerical models and experimental tests was performed with corn grain or steel balls as granular material instead of real soil (Shmulevich et al., 2007, Coetzee and Els, 2009b, Obermayr et al., 2011).

According to the actual development in soil modelling, the numerical method has been used mainly to reproduce soil mechanical tests, i.e. penetration tests, triaxial test, soil suction tests, and shear tests. These simulations have demonstrated the feasibility of the virtual test in predicting the soil mechanical response and calibrating the models. In the area of soil-tool interaction the studies have been focusing on the interaction of a simple tool with soil particles. The models used were implemented in two dimensions and a small number of particles, yielding results in a qualitative agreement with the experiment, which motivated further research in three dimensions with larger particle assemblies. The inter-particles interaction in the DEM model has been governed by parameters as stiffness, viscous damping, and friction. From these parameters the normal and tangential forces can be calculated in a relatively simple way. However, the action of the cohesion can be introduced using a more complex relationship to include the effect of the inter-particles bonds made up by the action of the frictional and cohesive forces. The soil was generally defined by its elastic properties, i.e., Young's modulus and Poisson's ration, and by the friction coefficient at the macro scale. These properties partially reproduce the nature of soil-tool interaction. By the addition of external properties as adhesion, soil-metal friction and Cauchy strain the DEM model performance can be improved.

The friction between particles in the model can be also obtained using the Mohr-Coulomb failure envelope by the simulation of triaxial compression test. This parameter is called micro-friction. A model calibration has been performed, in most of the cases, to obtain the relationship between macro and micro friction. This method is an effective way to fix the soil shear strength with the simulation results, but is only useful for cohesionless soils. To address the model toward real soil

behaviour also the micro-macro cohesion calibration together with the friction calibration is needed. Finally, the preferred procedure for model validation has been to reproduce in a physical medium the geometry of the particles used in the model. These kinds of experiments provide information about the model capacity to simulate the specific physical medium. Nonetheless, the amount and shape of particles in real soil is hard to reproduce in a simulated model. This particularly suggests a model with virtual particles focusing on the description of the soil macro behaviour validated by real experimental tests.

Considering the results obtained in Chapter 2, the soil macro behaviour can be related to the compaction level and soil moisture. By the statistical equations, the variation of soil mechanical properties provides enough information to implement a friction-cohesive model to simulate the soil-tool interaction at different soil conditions. In the present chapter the formulation of the DEM model, calibration and verification, again an empirical model is explained.

3.3 General formulation of the DEM model

Particles in DEM can be represented in two or three dimensions, they are considered as rigid bodies interacting at the contact points. Geometrically, two particles are in contact if an overlap results from the collision. Energy and momentum are dissipated due to the inelastic nature of the interaction. As was explained by Tijskens *et al.* (2003) the typical DEM algorithm can be organized as follows:

1. Initialize the system: the time step is initialized and for every particle the translational and rotational position and velocity are fixed.

2. Determine all contacts in the system at the current time: Construct a set of possible contacts by including only particle pairs which cannot be falsified immediately and determine the actual contacts testing every possible contact detected before.

3. Compute the contact force for every actual contact.

4. Introduce the forces and moments acting on each particle in the equation of motion.

5. Update positions and velocities by integration of Newton's equations over the time step and advance the time.

6. Back to step 2 until some criterion is met, that defines the end of the simulation.

The general DEM formulation is composed of a non-linear system of coupled ordinary differential equations. The force resulting from the interaction between two particles is governed by the contact model. Newton's equation of motion for each individual particle is written as

$$m_i \mathbf{a_i} = \mathbf{G}_i + \sum_c \mathbf{F}_{ci},$$

$$\mathbf{I}_i \boldsymbol{\alpha}_i = \mathbf{H}_i + \sum_c \mathbf{r}_{ci} \times \mathbf{F}_{ci}, \quad i = 1 \dots N. \tag{3.1}$$

In the equations, the vectors of translational and rotational acceleration of the *i*th particle are designated by $\mathbf{a}_i$ and $\boldsymbol{\alpha}_i$, respectively, its mass by m_i, its inertial tensor $\mathbf{I}_i$; and the body forces and moments acting on particle *i* by $\mathbf{G}_i$ and $\mathbf{H}_i$. The resultant contact force applied over particle *i* is calculated as the sum of the contact force $\mathbf{F}_{ci}$ from all particle interactions *c* in the same time step. The position vector of the contact, relative to the ith particle centre of mass $\mathbf{r}_{ci}$ is calculated by the contact position vector $\mathbf{r}_c$, and particle centre mass $\mathbf{r}_i$ as

$$\mathbf{r}_{ci} = \mathbf{r}_c - \mathbf{r}_i \tag{3.2}$$

In DEM models the contact force only acts between particles which are in contact causing non-linearity effect of the model:

$$\mathbf{F}_{ci} = k \, \xi_c, \qquad \xi \geq 0 \tag{3.3}$$

The above relationship shows the simple case of a normal force calculated by the spring coefficient *k* multiplied by the virtual overlap ξ. More specifically, the discrete model is decomposed into a normal and tangential force component with respect to the contact surface. A schematic representation of the contact with the general components used in a contact resolution is shown in Figure 3.1.
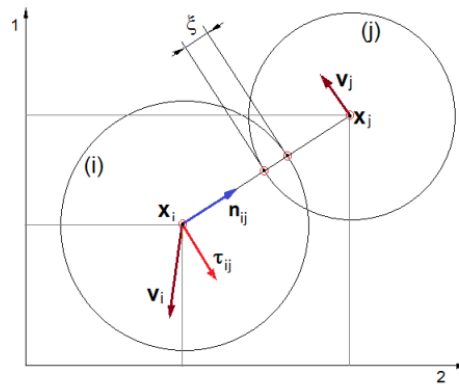
Figure 3.1 Two-dimensional scheme of the particle contact for DEM model.

To obtain the relative position between particles i and j (Figure 3.1), a normal unit vector $\mathbf{n}_{ij}$, and tangential vector $\boldsymbol{\tau}_{ij}$ are defined as

$$\mathbf{n}_{ij} = (\mathbf{x}_i\text{-}\mathbf{x}_j) \,/\, |\mathbf{x}_i\text{-}\mathbf{x}_j| \tag{3.4}$$

$$\boldsymbol{\tau}_{ij} = \mathbf{v}_{ij} \,/\, |\mathbf{v}_{ij}| \tag{3.5}$$

Where $\mathbf{x}_i$ and $\mathbf{x}_j$ are the position of the centres of the spheres in contact, $\mathbf{v}_{ij}$ is the relative translational velocity of the two particles in the contact plane perpendicular to $\mathbf{n}_{ij}$. This velocity is calculated by the relationship between independent velocities $\mathbf{v}_i$ and $\mathbf{v}_j$ with the normal vector in a system in which the particle rotation is neglected for reasons given in section 3.5.

$$\mathbf{v}_{ij} = \mathbf{v}_i - \mathbf{v}_j - [(\mathbf{v}_i - \mathbf{v}_j) \cdot \mathbf{n}_{ij}] \, \mathbf{n}_{ij} \tag{3.6}$$

The normal component of the contact force includes the contribution of the linear spring and viscous damper. The spring force and damping force are functions of the virtual overlap ξ and its time derivative $\dot{\xi}$ by which the resulting normal force is written as

$$F_n(\xi, \dot{\xi}\,) = k_n\, \xi + \gamma_n\, \dot{\xi} \tag{3.7}$$

The stiffness and damping constant k_n and γ_n are dependent on physics and geometrical parameters of the two particles in contact (Young's modulus, Poisson ratio, masses, radius, contact area). Meanwhile, for spherical and homogeneous particles the virtual overlap between two particles i and j during collision, is obtained as a function of the radius R of the particles and their spatial position at the current time:

$$\xi_{ij} = R_i + R_j - |\mathbf{x}_i - \mathbf{x}_j| \tag{3.8}$$

The magnitude of the overlap should fulfill specific conditions, which is also dependent on the nature of the medium:

$$\xi\,/\,R \lesssim 0.01 \tag{3.9}$$

On the other hand, the tangential component of the contact model considering only the action of Coulomb friction is written as

$$\mathbf{F}_\tau = -\,\mu\,|\,F_n\,|\boldsymbol{\tau} \tag{3.10}$$

The leap-frog scheme for time integration algorithms defines the new relative velocity and position:

$$\mathbf{v}_{t+\Delta t/2} = \mathbf{v}_{t-\Delta t/2} + \mathbf{a}_t \Delta t \, ,$$

$$\mathbf{x}_{t+\Delta t} = \mathbf{x}_t + \mathbf{v}_{t+\Delta t/2} \; \Delta t. \qquad (3.11)$$

Finally, spherical particles are selected, mainly because of the low computational cost of the contact tests between them. To verify the contact between two spheres only the radius r and its spatial position are required. The collision takes place when the virtual overlap is larger than zero:

$$\xi_{ij} \equiv (r_i - r_j) - || \mathbf{x}_i - \mathbf{x}_j || > 0 \qquad (3.12)$$

To represent complex elements as machine parts or irregular surfaces, polygonal models can be represented as a set of connected polygons for which contact verification is straightforward.

3.4 Model implementation

The soil-tillage tool interaction dynamics were implemented in the *DEMeter++* Software (Tijskens et al., 2003), developed by the DEM Research Group from the KULeuven in Belgium. This program provides tools for building and computing the interaction between simple and complex bodies, including contact detections, relative bodies' velocities, contact force calculation, time integration, etc. Written in C++ this software has the possibility to utilise open source libraries, compile own applications and create executable files. The output of the calculations can be saved according to the kind of application providing easy and comfortable management of the entire system. To post-process the results, data files can be exported to application software as MatLab or Excel. The newest version also has a python interface for pre and post-processing.

The general model described in the previous section was built in the algorithm for the DEM calculations. To describe the interaction between soil particles and tillage tool an explicit contact model was implemented. For the interaction between soil-soil and soil-tool the same scheme was used, only changing the data of soil macro properties. The soil mechanical properties Young's modulus, Poisson's ratio, internal and external friction angle, cohesion and adhesion were introduced as the model macro-parameters. The force system was composed of normal, shear, gravity, cohesion and friction forces at the particle scale (Figure 3.2).
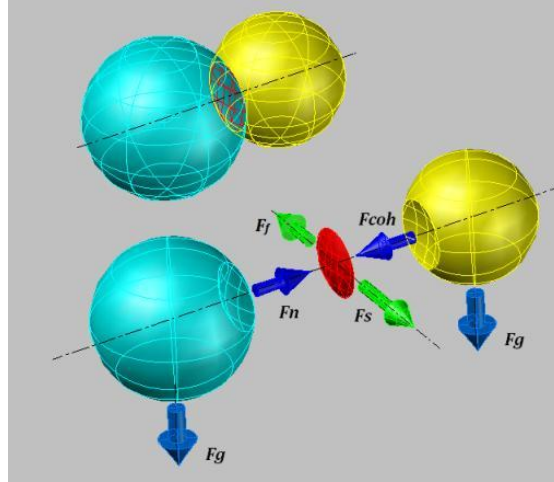
Figure 3.2 inter-particle forces acting at the contact point. F_f: Friction Force, F_{coh}: Cohesion Force, F_n: Normal Force, F_s: Shear Force, F_g: Gravity Force.

An inter-particle bond is created by the action of micro-cohesion in the normal direction and micro-friction force in the tangential direction. As shown in Figure 3.2, the cohesive force in the model is enabled beyond a specific overlap. Its action keeps the particles together by means of the equilibrium between the normal and cohesion forces conserving a constant certain overlap. The friction force is applied only during sliding reducing the magnitude of the tangential force. The Mohr-Coulomb criterion of shear failure is used to regulate the force in tangential direction:

$$F_t^{max} < F_n \cdot tan(\phi_\mu) + c_\mu, \qquad (3.13)$$

where:

F_t^{max} = tangential force limit [N],

F_n = normal force [N],

ϕ_μ = micro-friction angle [°],

c_μ = micro-cohesion [N].

The variation in normal force ΔF_n at the contact point has an elastic and a viscous component:

$$\Delta F_n = k_n \cdot u_n + \eta_n(u_n / \Delta t) \qquad (3.14)$$

where:

k_n = normal stiffness [N/m],

u_n = normal displacement [mm],

η_n = viscous damping coefficient [kg/s],

Δt = time step [s].

The stiffness parameter is calculated by the model proposed by Liao (1997) based on the stress-strain relationship. To obtain the values of the dimensionless parameters (α_k = 2.65, β_k = 0.65, γ_k = 1.0) in the Liao model, a set of compression tests was carried out by Hentz *et al.* (2004). The model was also verified in a mathematical study by Feng *et al.* (2007) with the purpose of validating the DEM prediction capacity. From this model the stiffness in normal direction was determined as:

$$k_n = \frac{E_{ab} \cdot A_{int}}{D_{eq}} \left[\frac{1 + \alpha_k}{\beta_k (1 + v) + \gamma_k (1 - \alpha_k)} \right] \tag{3.15}$$

where:

E_{ab} = equivalent Young's modulus of the materials in contact [Pa],

A_{int} = interaction surface [m^2],

D_{eq} = equivalent distance between the two particles [m],

v = Poison's ratio [ ],

α_k, = loading path [ ],

β_k, = softening factor [ ],

γ_k = interaction range [ ].

Similar to the normal force, the variation of the tangential force ΔF_s was calculated considering the elastic and plastic effects:

$$\Delta F_s = k_s \cdot \Delta u_s + \eta_s (\Delta u_s / \Delta t) \tag{3.16}$$

where:

k_s = tangential stiffness [N/m],

Δu_s = increment of tangential overlapping [m],

η_s = viscous damping coefficient in tangential direction [kg/s].

The magnitude of the tangential stiffness also depends on the value of the normal one (Hentz et al., 2004) and is calculated by the following equation :

$$k_s = k_n \left(\frac{1 - \alpha_k \cdot v}{1 + v} \right) \tag{3.17}$$

The viscous damping is obtained as:

$$\eta_i = \beta_i \cdot 2 \cdot \sqrt{\frac{m_a \cdot m_b}{m_a + m_b}} \tag{3.18}$$

where:

i = right subscript representing normal and tangential direction [ ],

β = coefficient of viscous damping [ ],

m_a, m_b = mass of the objects in contact [kg].

Finally, the equations to calculate the model parameters of micro-friction ϕ_μ and micro-cohesion c_μ are obtained by modeling the soil macro-behaviour during the simulation of the biaxial compression test and direct shear test. The procedure used is explained in detail in next sections.

3.5 Consideration of particle rotation

Particles in real soil are grains with a complex geometry and size distribution. The soil shear strength depends on the particle roughness and the consolidation state. This makes the soil a physical medium that is hard to reproduce by DEM.

The use of spherical particles to model soil has therefore a serious limitation. In an assembly of spheres the rotation is only counteracted by frictional forces because the particles can rotate without affecting the normal force. In realistic assemblies however, the rotation of the particles is primarily counteracted by the normal force that produce an irregular particle rotation. (Oda et al., 1982, Morgan, 1999). Testing typical values of soil internal friction in a DEM simulation, the rolling mechanism was found predominantly in the system, resulting in a significant reduction of shear stress. The experiment was carried out on a soil cut by a pendulum machine with the soil represented by spherical particles (Tadesse, 2004). To avoid the effect of excessive rolling, some authors introduced soil clods formed by a combination of spherical particles to study micro-mechanical interactions (Coetzee and Els, 2009b, Asaf et al., 2006). However, this kind of particle needed the introduction of new contact laws and geometric elements made up from several shapes which increased significantly the calculation time and limited the number of

particles that could be used in practice for the model. Fortunately, the comparison between non-rotation and rotation particle setups showed that non-rotation particles still allowed the reproduction of a realistic particles flow (Bierwisch C et al., 2009). Without particle rotations, the macroscopic soil behaviour was modelled, obtaining a good correlation between draft forces from simulation and experimental test (Obermayr et al., 2011). Following the above results the particles' rotational degree of freedom in the present study was suppressed for simulation of soil-tool interaction.

3.6 Model calibration

Simulations of soil mechanical behaviour generally showed good qualitative agreement with experimental tests, but accurate quantitative results were not yet obtained. The differences were related to the differences between the size and shape of the soil particles with those in the model. To find the proper values of soil resistance, some micro-parameters were used for calibration as stiffness, damping, friction, and bond strength (Asaf et al., 2006, Tanaka et al., 2007, Oida A, 1997, Ibuki T, 2000). However, the method used for obtaining the macro-micro relationship, changed according to the purposes of the different studies. A simple procedure was used in order to fix the value of the micro-friction coefficient in a simulation of soil strength distribution during bar penetration tests (Tanaka et al., 2000). The simulation test was repeated for a set of micro-frictions, and the final value of the micro-friction coefficient was selected according to the best reproduction of the pattern of particle movement in the experiment. A more complex procedure included the calibration of the micro-friction parameter for simulation of soil-track interaction (Asaf et al., 2006). Here, the model for soil deformation during the shear test was fitted using a semi-empirical model based on the shear stress–displacement curve. In the calibration procedure proposed by Coetzee and Els (2009b), particle stiffness and micro-friction angle were used to fit a model for blade-particles interaction. To do so, direct shear and confined compression tests were simulated using the macro-parameters from real experiments. The fit procedure started with a preselected particle stiffness parameter which was adjusted over the curve described by plotting the stress-strain curve. With the stiffness known new simulations were carried out to determine the final particle friction coefficient. Another calibration method was used in the simulation of runoff in a cohesive soil (Utili and Nova, 2008). The micro-macro relationship was obtained from the results of simulated biaxial tests. By the variation of particle friction and cohesion in the

model, different values of shear failure resulted from the shear simulation. Friction and cohesion at macro scale were drawn over the failure envelope in the shear-tension plane following the Morh-Coulomb criterion. Linear interpolation between macro and micro parameters allowed determining the corresponding particle friction and cohesion to satisfy the soil macro behaviour. Considering the characteristics of the soil under study, especially its considerable cohesion, the present section is focused on the virtual tests to calibrate the model following the procedure described by Asaf et al (2007) and Utili and Nova (2008). To obtain the soil micro-macro friction relationship the direct shear test was performed in the standard configuration. The micro-macro cohesion relationship however, came from the result of a biaxial compression test also performed in the standard geometric configuration. In both cases the soil macro-properties and soil sample dimension in the DEM model were the same as for the experiment. In the next sections the overall calibration procedure is explained.

3.6.1 *Geometrical model of direct shear test*

In order to reproduce the direct shear test with a DEM model a virtual reproduction of the direct shear test apparatus (Figure 2.3) was made. A set of samples for the simulation were also generated by spherical particles to test the micro-friction ϕ_μ effect over the macro-samples' strength. The geometrical setup for the simulation (Figure 3.3a) was divided in two main sections: an upper and lower box; each one with a cylindrical cavity at the centre. The other parts of the installation were called press and base, with the function of pressing the virtual sample of soil. Virtual cylinders and plane objects from the DEMeter++ Library are the elemental shapes used to build the shear apparatus.

The soil specimen is obtained by sequential steps, starting with spheres generated inside the cylindrical cavity of the shear apparatus following a hexagonal compacted spatial distribution. The centre of each particle is obtained by assigning an independent position in the (*x, y, z*) axes for an initial number of 4,000 particles. Dimensions of the particles were calculated by random distribution of the radii between 1.0 to 1.5 mm. In the next step the particles fell downward by gravity force. Then, the press was displaced in the downward direction, forcing the particles to move toward void spaces into the sample. Finally, the sample was decompressed until reach the internal equilibrium force.
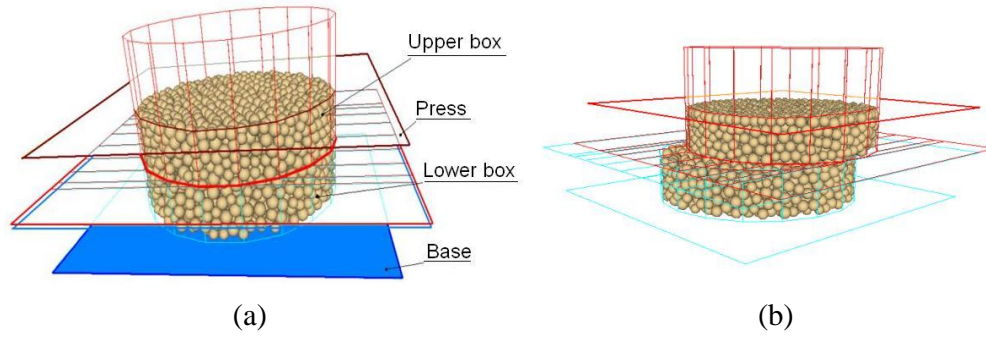
Figure 3.3 Virtual direct shear test. Geometric model (a), sample cutting simulation (b).

The particle number is fixed at 3,680 to obtain the desire height of the sample. The generated soil sample has a cylindrical shape of 70 mm diameter by 60 mm height. From this point, the geometrical model is ready for simulation of the direct shear test. The model macro-parameters (Table 3.1) were calculated by means of the regression equations defined in Chapter 2 at the soil intermediate physical condition according to soil moisture $w = 21.3\%$ and dry bulk density $\rho_d = 1.18$ g/cm^3.

Table 3.1 Model macro-parameters for soil at $w = 21.3\%$ and $\rho_d = 1.18$ g/cm^3.

Parameters	Values	Units
t_{50}	539.9	kPa
E	53.9	MPa
ν	0.28	
c	72.6	kPa
c_a	5.42	kPa
ϕ	22.2	°
δ	15.3	°

The goal of the sample compression is to obtain a solid structure by connecting all particles by the cohesion force. Between particles, the overlap remains constant forming inter-particles bonds. Internal tension and random distribution of empty spaces characterise the structure of the simulated sample, which is consistent with real soil features. During the simulation the sample is cut in the transversal direction as shown in Figure 3.3b. The shear operation takes place moving the upper box over a length of 20 mm at a constant velocity of 1.3 mm/s. The press surface ensures that shear take places at different normal load.

3.6.2 *Macro and micro-friction relationship*

The relationship between micro-friction and macro-friction was obtained by changing the value of the micro-friction angle in several tests computed with the same soil parameters. The empirical equation proposed by Utili and Nova (2008) was used to calculate an intermediate value for the range of the micro-friction angle to be used in the calibration:

$$\phi_\mu = \frac{\phi - k_1}{k_2} \tag{3.19}$$

In this equation, the micro-friction angle ϕ_μ shows a linear relationship with the soil macro-friction angle ϕ. The values of the statistical coefficients were $k_1 = 11.2$ and $k_2 = 1.9$. Accordingly, four values of ϕ_μ were tested (2, 4.2, 6.4 and 8.6°), each one at a normal pressure of 30, 50, 70 and 90 kPa resulting in a total of sixteen simulation tests. Figure 3.4 shows the tension-displacement curve obtained at 8.6° of micro-friction during direct shear test simulation. Shear strength at failure is selected as the maximum tension reached during the test. After this point the sample strength decreases.
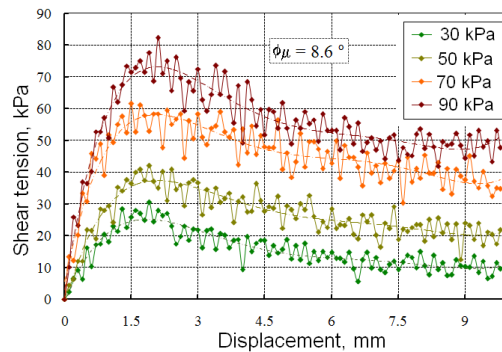
Figure 3.4 Force-displacement curves at of simulated shear test at different values of normal pressure.

When the normal pressure increases, a new value of shear strength is attained; the results for each combination are plotted in the shear-normal plane as shown in Figure 3.5. Shear strength at failure increases linearly with respect to normal pressure in agreement with the laboratory experiments. In addition, an increment in the micro-friction parameter enhances the values of shear tension.
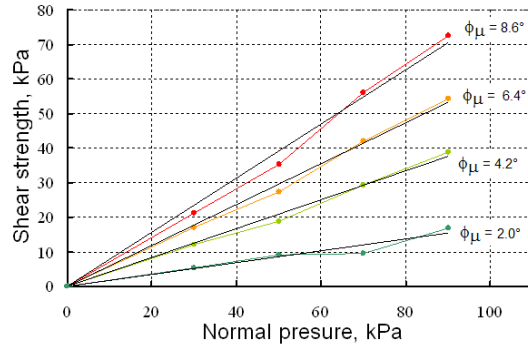
Figure 3.5 Friction angle envelopes from simulated test using different micro-friction angles.

The slope of the regression line of shear strengths provides the internal friction angle of the material corresponding with the micro-friction tested in the model. The relationship between macro and micro friction is obtained from the regression line describing the soil internal friction angle versus the micro-friction parameter (Figure 3.6).
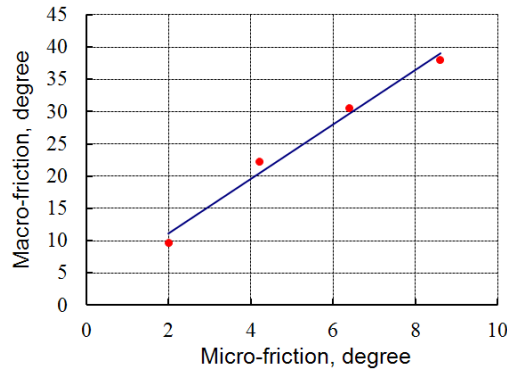
Figure 3.6 Macro-friction as a function of micro-friction angle from the model.

The linear regression equation characterises the particular condition tested, influenced mainly by the particle size distribution and sample porosity. The equation to define the relationship between internal friction ϕ and micro-friction ϕ_μ is written as:

$$\phi_\mu = 0.23\phi - 0.53 \tag{3.20}$$

By this equation the values of inter-particle friction ϕ_μ in the DEM model can be calculated as a function of the real soil internal friction angle ϕ. The model should be able to reproduce the soil shear strength according to the normal pressure applied. The differences with respect to equation 3.19 proposed by Utili and Nova (2008) are related to the range of particle radii used, the 2D and

3D model representation, and to the particle damping and particle stiffness. However, a linear model describes the micro-macro relationship in both models. But, since soil strength is also affected by cohesion, the calibration of soil micro-cohesion is needed.

3.6.3 *Geometrical model of biaxial compression test*

Soil by nature is a frictional and cohesive material; its strength is a result of both contributions. This behaviour is introduced in the model by the micro-friction and micro-cohesion parameters acting at the particle level. By means of the simulation of biaxial compression test the relationship between real soil cohesion and micro-cohesion for the model is obtained.

The virtual experiment is performed in accordance with the description of the laboratory test (Section 2.4). In order to find the variation of soil cohesion, the simulation is carried out in unconfined conditions, which means without lateral pressure. With the compression-displacement curve resulting from the test, the cohesion calibration procedure is made following the Mohr-Coulomb criterion of failure as discussed in section 2.2.

The procedure to form the virtual samples was the same as the one used for direct shear test, i.e. coordinates' generation, particles falling, compression, and decompression as was explained in section 3.6.1. An auxiliary cylinder of 50 mm diameter is used as a mould (Figure 3.7a) for a virtual sample made by 5,500 spherical particles. Before running the compression test the cylinder (mould) is removed from the installation and a total of 5,350 particles form the final sample after the height is fixed. The particles follow a random radius distribution between 1.5 to 2 mm. The test is sized at 50 mm diameter by 100 mm height.

(a)   (b)
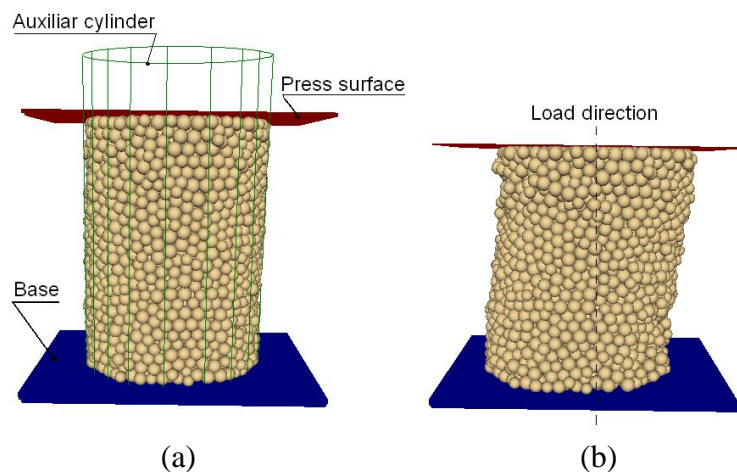
Figure 3.7 Compression test setup. Cylindrical specimen (a), deformation under load (b).

Finally, the geometrical model of the biaxial compression test is composed by the press surface, the base, and the soil sample (Figure 3.7a). In the experiment the press surface is moved at a constant velocity of 1 mm/min in a downward direction (Figure 3.7b). The reaction forces are computed until the sample reaches a deformation of 20% in vertical direction.

The micro-macro relationship for the cohesion parameter is obtained by testing the compression virtual model at three different values of micro-friction c_μ = 40, 80 and 120 kPa; the range was selected according to the equation proposed by Utili and Nova (2008) which also involves the effect of the inter-particle friction :

$$c_\mu = \frac{c(\tan \phi_\mu)^{k_4}}{k_3} \tag{3.21}$$

The statistical coefficients k_3 = 77.5 and k_4 = 0.6 were related to porosity and particles size distribution. To analyse the effect of particle friction over micro-cohesion the biaxial compression test was executed four times changing only the micro-friction angle at ϕ_μ = (2, 4.2, 6.4 and 8.6°) and keeping constant the inter-particle cohesion.

### 3.6.4 *Macro and micro cohesion relationship*

Shear strength at failure is localized in the compression-displacement curve as the maximum value achieved during the test. The pattern of soil deformation characterises the soil elastic-plastic behaviour shown in (Figure 3.8). Particle accommodation takes place at the start of the test without substantial increases in forces. After the first millimetre of deformation the sample strength increases until the maximum force is reached. After this point the tension gradually decreases.

From the micro-scale point of view, at the beginning all particles are connected with their neighbour by the micro-cohesion force forming a single solid structure. The inter-particle cohesion is used as a tension force acting on the particle interaction area resulting in a constant value for different sizes of the spheres. The bonds are broken when the force exceeds the Mohr-coulomb criterion (Equation 2.1). No new bonds are formed during the sample slide in diagonal direction.
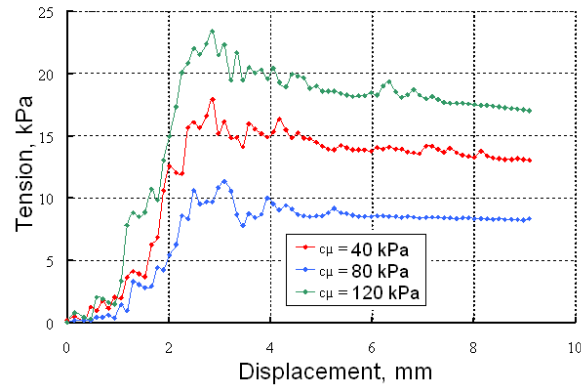
Figure 3.8 Pressure-displacement curves for different values of micro-cohesion.

The relationship between micro and macro cohesion for different incremental values of internal friction is shown in Figure 3.9.
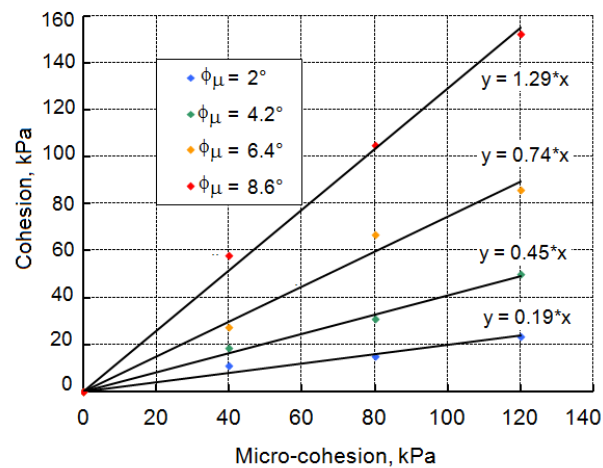
Figure 3.9 Specimens' cohesion obtained from incremental values of micro-cohesion.

Increasing soil micro-cohesion results in a linear increment of soil cohesion determined by the slope in the regression equation obtained for each value of micro-friction under test. In order to find an equation to involve both parameters of soil strength, the slope of c-c_μ versus the corresponding values of micro-friction are plotted. As shown in Figure 3.10, a non-linear behaviour distinguishes this relationship. As the slope of c-c_μ increases, the micro-friction angle increases too.
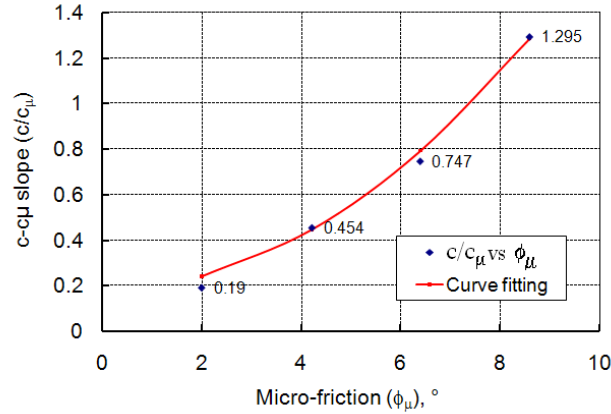
Figure 3.10 Regression curve for c-c_μ as a function of the micro-friction parameter.

The empirical equation to fit the model was obtained with an Adjusted $R^2 = 0.98$, standard error of RMSE = 0.05 and statistical coefficients at 95% confidence bounds. The regression equation is written as:

$$\frac{c}{c_\mu} = a \; \phi_\mu^{\,2} + b \tag{3.22}$$

where:

ϕ_μ = micro-friction [°],

a = 0.15[ ],

b = 0.18 [ ].

As shown in the equation 3.22, the magnitude of macro-cohesion resulting from the model increases proportionally with the increment of inter-particle cohesion and friction angle. Micro-friction angle ϕ_μ was found to increases quadratically in respect to macro-cohesion. These results agree with those obtained by Jean-Yves Delenne (2004) in a study of the influence of the friction parameter in cohesive bonds. However, the effect of this parameter over soil cohesion was found not to be the same as the one shown in equation 3.21 although in both cases they are in a power relationship. This can be caused by the different way the cohesive force into the model is applied.

3.7 Influence of particle size on soil-tool interaction

A virtual narrow tool with a simple geometry is used to simulate the effect of particle sizes over reaction forces. In the simulation the tool passes through the soil at constant soil conditions

defined by water content and dry bulk density. The virtual tests focus on evaluating the behaviour of draft and vertical forces acting on the tool for three different particle sizes.

Three prismatic soil samples are made by the procedure explained in section 3.6.2. The radii r of the spheres are defined at $r = 5$, 7 and 9 mm to form a block sized at 40x50x130 mm. In Figure 3.11 the virtual setup of the three blocks of soil during the contact with the narrow tool is illustrated.

$(r = 9$ mm) $(r = 7$ mm) $(r = 5$ mm)
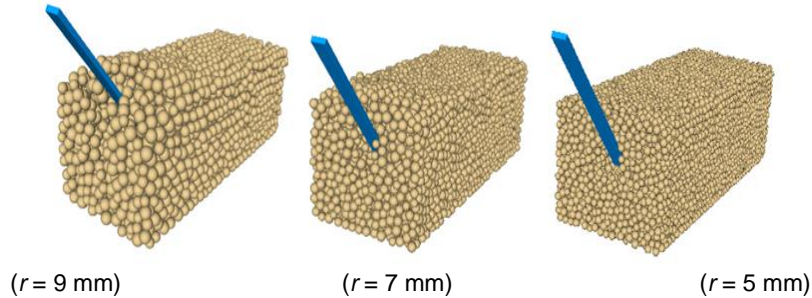
Figure 3.11 Soil and narrow tool interaction.

The narrow tool is dimensioned at 15x4x80 mm and ends up in a wedge of 22°. It is positioned in the centre of the block at a depth of 20 mm and an angle of 49° with respect to the trajectory. The soil macro parameters used are defined in Table 3.1.

Figure 3.12 shows the simulated draft and vertical forces exerted on the tool. The force-displacement curves at different particle radii experience more heavy fluctuations with increasing particle size. However, the magnitudes of the forces tend to be constant with an average of 96.9 N. For the three radii tested the draft and vertical forces (Table 3.2) show no significant variation with a coefficient of 0.48% and 2.6% respectively.
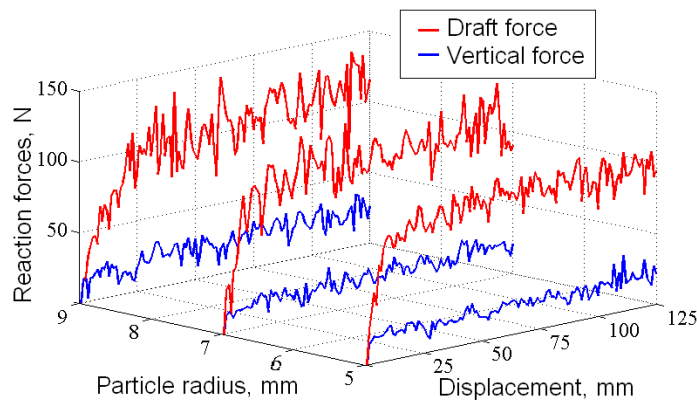
Figure 3.12 Simulated longitudinal and vertical soil forces acting on a narrow tool as a function of the particle radius.

57

The results of a quantitative analysis for the three cases are given in Table 3.2. The particle radii are not related to the slight variations of the average draft and vertical forces of 97.3 N and 19.3 N respectively. However, the standard deviation of the forces along the test increases in accordance with the particle size, amplifying the fluctuation effect.

Table 3.2 Results from soil-tool interaction with different particle sizes.

Spheres Radius , mm	Mean Fx, N	Std Fx, N	Mean Fy, N	Std Fy, N	Number of spheres	Time step, s
5	96.4	7.9	19.3	3.3	15,744	7.00E-05
7	97.3	12	18.7	4.7	8,320	1.00E-04
9	97.1	16.3	19.7	6.5	4,320	8.00E-03

As shown in Table 3.2, reducing the particle radius from 9 to 5 mm increases the number of particles by a factor of 3.6. This reduction also requires a time step decrease by two orders of magnitude at the expense of computation time. To select the appropriate particle dimension it is necessary to take into account the computational capacity and complexity of the model. The forces resulting from the simulation tend to be more precise as particle sizes are reduced which is in agreement with the oscillation pattern of horizontal forces obtained by Obermayr *et al.*(2011). The current value of the force in a given direction is calculated by the model as the sum of every particle contact force against the tool. The void spaces however, reduce the structural uniformity of the medium and introduce internal irregularities in the strength of the simulated soil that increase the force fluctuation.

3.8 Analytical verification

Semi-empirical models based on the theory of passive earth pressure have been widely used to calculate the maximum forces acting on the tool through Newton's equilibrium equations. This method only provides information about soil resistance without any detail about soil deformation. Several three dimensional models are based upon experimental observations and simplification of the number of variables that affect the soil-tool interaction.

On the Payne model (Payne, 1956) soil sections are identified as a triangular centre wedge, a centre crescent and two lateral blocks; The draft force is determined by the force contribution from each section. In the Hettiaratchi-Recee model however, the total force supported by the tool is divided into the force contribution from forward and transverse soil failure (Hettaratchi and

Reece, 1967). The McKyes-Ali model proposes a failure wedge divided by a centre wedge and two side crescents; The forces in each section are determined applying equilibrium mechanical equations (McKyes and Ali, 1977).

The model of Perumpral-Grisso-Desai includes only a centre wedge model of which the solution is simplified by replacing the side crescents by a set of two forces acting on the centre wedge. The horizontal force is calculated considering the contribution of the force of the soil along the blade, shear force from both sides, inertial force and friction force (Perumpral et al., 1983). Additionally, the effect of the speed and acceleration is subsequently modelled resulting in the Swick-Perumpral model (Swick and Perumpral, 1988).

The Perumpral-Grisso-Desai model was selected for the analytical verification against the numerical results from the simulation of soil soil-narrow tool interaction discussed in the previous section. This model was selected due to the parameter match with the soil properties obtained in Chapter 2, and its validity in three dimensions. To compare the results between the two methods, the shape of the central wedge defined on the analytical model is drawn in a longitudinal section of the soil-tool geometrical model as shown in Figure 3.13. The draft force in the equations including the effect of soil density, cohesion and adhesion, is written as:

$$D = w_t\left(\gamma z^2 N_\gamma + \; czN_c + c_a zN_a\right) \tag{3.23}$$

where:

D = Draft force [N],

w_t = width of the tool [mm],

γ = soil density [g/cm^3],

z = depth of the tool [mm],

c = soil cohesion [Pa],

c_a = soil adhesion [Pa],

$N\gamma,\ N_c,\ N_a$ = coefficients of density, cohesion and adhesion [ ].

The parameters of the failure zone defined in the Perumpral-Grisso-Desai model are wedge central angle β, failure surface angle α, height of the crescents h and those related to soil strength as metal-friction angle δ, and soil internal friction ϕ are introduced into the equations 3.25 to

calculate the draft force *D*. In this way, the empirical model is able to predict the soil reaction related to soil deformation and the input data of the DEM model.
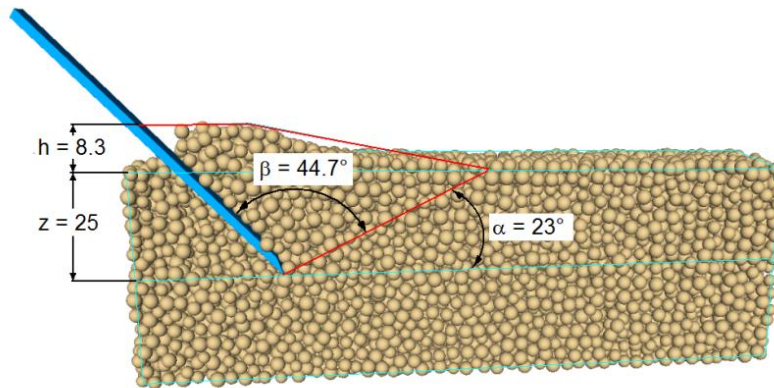
Figure 3.13 Failure wedge drawn on section of soil-tool simulation.

The draft force obtained from the Perumpral-Grisso-Desai model was smaller than the one from the DEM simulation. The draft force comparison of 88.2 N from the semi-empirical model against 97.3 N from the DEM simulations represents a negative error of 10.3% in simulated draft force with respect to the empirical model. However, the possible variation in the location of the surface failure angle α (Figure 3.13) and the height of the soil in front of the tool changes during the simulation. As the tool displacement increases, the resultant draft forces obtained by the empirical model also increases.

On the other hand, the results from equation 3.23 and the empirical models in general have an accuracy from 60 to 80% (Shen and Kushwaha, 1998). The same results were reported by Asaf *et al.* (2006) during comparison of the draft force obtained from a link-tract simulation with a curve fitted by the semi-empirical models of Bekker, Janosi and Wong. This fact, together with the tendency of DEM models to over-predict the draft force found by Obermayr *et al.* (2011) are subject to setup a real test to measure the reaction force during soil and tool interaction.

3.9 Conclusions

Soils are granular by nature, they are characterised by large discontinuities and a lack of homogeneity. To study the mechanical behaviour of soils granular models as the well-known Discrete Element Method (DEM), are more appropriate than continuum models. Applying discontinuous methods on soil-tool interaction have shown good agreement between draft forces and soil rheological behaviour obtained from laboratory experiments and numerical simulation.

The soil structure has been generally represented by spherical particles and assemblies of particles. Parameters as inter-particle bonds, micro-cohesion and micro-adhesion are introduced to modelling the mechanical behaviour of cohesive soils.

To calculate the mechanical response of a cohesive soil at particle level in the DEM model the system forces can be formed by normal force, shear force, friction force, cohesion force and gravity force. Shear force at failure is defined by the Mohr-Coulomb criterion. The contacts between particles are calculated based on soil mechanical properties. For soil-tool interaction the properties of soil-metal interface are used.

Using the geometrical elements from DEMeter++ software a virtual reproduction of the direct shear test and compression was made. The strength obtained in the virtual soil samples during the simulation are used to find the relationship between micro- and macro-parameters. Soil internal friction and cohesion are calibrated with respect to micro-friction and micro-cohesion. The statistical equations allow calculating the micro-values for the model from the macro-parameters of the soil which is valid for soil models with the same configuration of particle arrangement and force system.

Particle sizes as a model parameter are able to modify the magnitude of the force fluctuation during simulation. The fluctuation increases with increasing particle radius. However, no significant differences in the nominal forces are experienced. These results are coherent with the computed results from the DEM algorithms. However, as the particle sizes increase the scale difference between real and virtual soil also increases, providing less accurate soil deformation patterns. On the other hand, simulation time increases with a reduction in particle sizes, raising the model computational cost.

Several empirical models based on the pattern of soil deformation are used to calculate the reaction force on the tool. The parameters of Perumpral-Grisso-Desai model were drawn in a DEM representation of narrow tool and cohesive soil contact. The comparison between both models shows an error of 10.3% in terms of draft force results.

Chapter 4

Tillage in Experimental Conditions

4.1 Introduction

Tillage operation in a soil-bin condition plays an intermediate role between theoretical designs and field applications. Different soil-bin designs have been used for research on measuring dynamic forces during soil cutting. The determination of the critical speed related to soil deformation during high speed tillage was carried out using a soil-bin trolley (Kushwaha and Linke, 1996). To validate a FEM model based on the soil low rate of elasticity, the draft force was measured on a flat tool in soil-bin conditions. The experimental results were correlated with the dynamic parameters of the soil model (Rosa and Wulfsohn, 1999). To validate a continuous model, a monorail soil-bin system was designed using silt and compacted clay soil. They found an increment in power, tool draft and soil pulverisation with increase in speed (Rosa and Wulfsohn, 2008). Empirical equations to predict draft forces have been developed by Sahu and Raheman (2006b). The draft forces for these models were measured in a soil-bin during tillage using a simple tillage-tool in a loam soil, taken as reference condition. Generally, the experiments in the soil-bin lead to more consistent data, avoiding the variability of the soil structure, keeping control over operational parameters and reducing the effects of climatological factors.

The present chapter is focused on finding reliable data from tillage tool operations. The draft force calculated by the semi-empirical model and the simulated one in the section 3.8 provide only two kinds of predictions based on calculations and observation. For the soil-bin test the soil moisture and soil compaction can be managed to create different physical conditions. Draft and vertical forces measured for all these conditions, are used to compare the results with the model prediction. Also soil parameters related to the effect of the tool on soil loosening, can be controlled and related to the different soil conditions. Since the soil used in the soil-bin is the

same as the soil characterised in Chapter 2, and the experimental range for the tillage test are in the experimental region in which the regression equation were obtained, the condition of the tests are replicable in the DEM model giving a phenomenological simulation of the dynamic of soil-tillage interaction.

The objective is to investigate the force variations and soil loosening indicators during tillage. A multi-blade tool was designed for non-inversion tillage and tested at several soil conditions in the Oxisol soil described in section 2.3. The draft force resulting from soil-bin tests will be used to validate the proposed model.

4.2 Experimental design

Variation in soil mechanical response with respect to water content and dry bulk density modifies the input energy and tillage quality (Zadeh, 2006). Several researchers have found the relationship between tillage performance and physical factors as the state of compaction, soil moisture, tool geometry and operation speed (Mouazen et al., 2007, Mouazen and Ramon, 2002, McKyes and Maswaure, 1997).

Focusing on the effect of changing soil moisture content and compaction level, the experiment was organised using a Central Composite design for these two elements. Soil water content and dry bulk density were combined at nine levels and four centre point replications. Table 4.1 shows the planned experimental combinations.

Table 4.1 Experimental points from Central Composite design.

Points	w, %	$\rho_{d,}$ g/cm^3
1	17.5	1.4
2	12.2	1.3
3	22.8	1.3
4	10	1.1
5	17.5	1.1
6	25	1.1
7	12.2	0.9
8	22.8	0.9
9	17.5	0.8

During tillage tests at different soil conditions, the following response variables were measured: horizontal force on the tool, vertical forces on the tool, soil density changes after tillage, soil profiles after tillage, and soil particles sizes distribution.

4.3 Soil-bin and tool configuration

To measure the variation of tillage performance at different soil physical conditions, a longitudinal indoor soil-bin was used (Figure 4.1a). The effective working area was sized at 1.5 m width, 8.0 m length. The soil-bin was filled with Oxisol soil, obtained from the first layer at the same location as the one used for the soil mechanical test, presented in Chapter 2. A multi-blade tool called cultivator was manufactured for the experiment. This tool was designed for operation in the upper layer of the soil (Figure 4.1b).


| (a) | (b) | (c) |
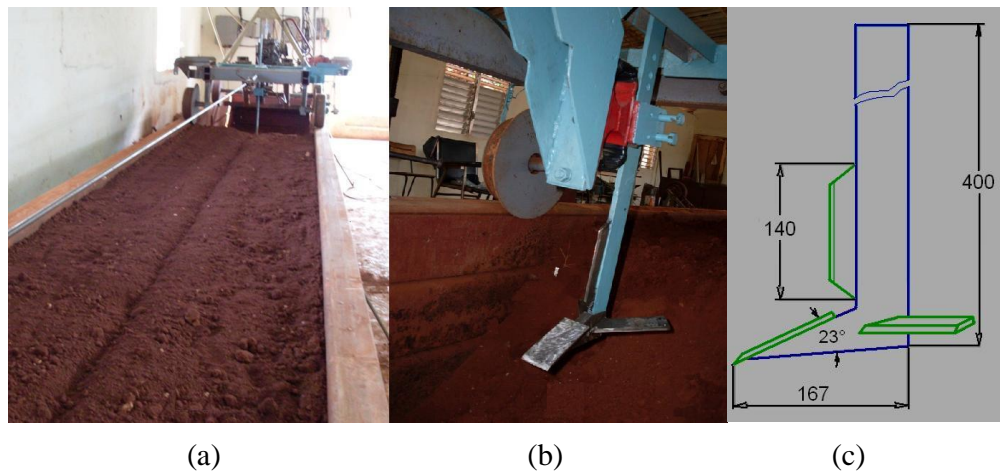
Figure 4.1 Trolley over railway (a), tool transducer (b) and tool dimensions (c).

Between the trolley and the tool the transducer ring was connected; the deformable device was placed at the central longitudinal line of the soil-bin. The system was mounted on steel wheels rolling over a steel railway. In addition, a steel cable was used to connect the trolley to the gear reducer, getting a constant velocity of 3.6 km/h.

4.4 Force measuring system

Draft and vertical forces were measured by the transducer designed for 5 kN capacity and non-linearity at 0.02%. The system was driven by an embedded controller Data logger NIcRIO-9012 from National instruments, Austin, TX, USA. For signal condition a module NI 9237 for full and half bridge connections was used. This module includes bridge excitation, signal amplification, multiplexing and signal filtering according to the data range. To manage the system a virtual instrument of Lab-View program was designed and installed in a Compact HP 6000 laptop (Figure 4.2).

<center>(a)   (b)   (c)</center>
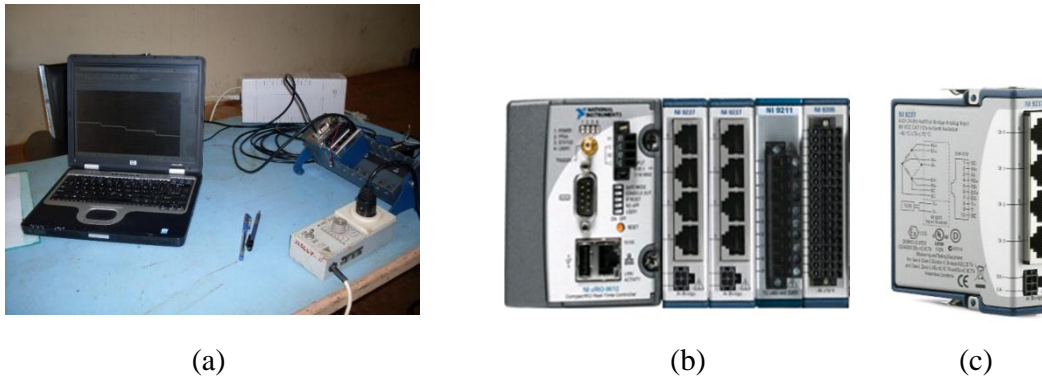
Figure 4.2 Measuring system (a). Data Logger (b), and signal condition module (c).

The sensor calibration was made conserving the tool work position on the trolley (Figure 4.3). The signal variation was saved at four different weights from 10 to 100 kg applied at the wedge centre of the tool. A similar process was followed in the vertical and longitudinal directions.
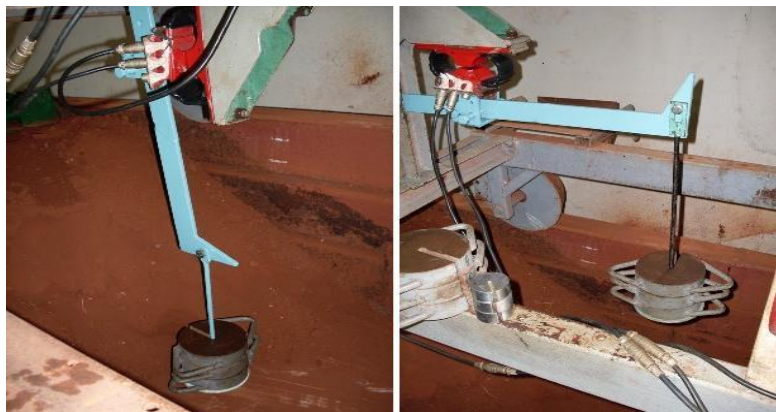
Figure 4.3 Sensor calibrations in vertical (a), and horizontal direction (b).

The adjusted line (Figure 4.4) obtained from the tool calibration in both directions shows the linearity of the transducer up to 1 kN. This condition proves the functionality of the transducer. Moreover, the arm section of the tool was dimensioned to support the forces below 4.5 kN without plastic deformation, maintaining the rigidity of the system. The regression equations obtained from the calibration procedure were used to calculate the magnitude of the nominal forces supported in the tool during the tillage test.

(a)   (b)
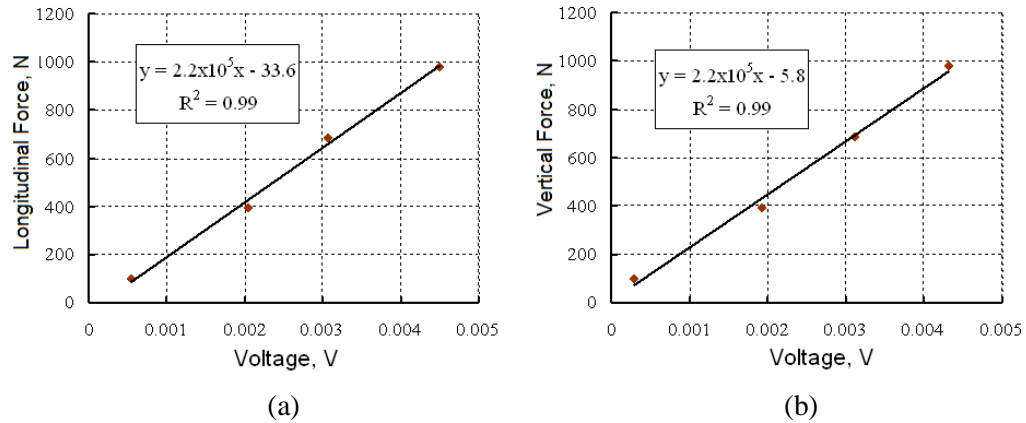
Figure 4.4 Sensor calibrations. Force in longitudinal direction (a), Force in vertical direction (b).

4.5 Soil conditioning for tillage test

To measure draft and vertical forces on the cultivator tool (Figure 4.1c) the soil-bin into the channel was submitted to a regime of moistened, compacted, dried and loosened soil according to the desire soil condition. The different soil physical states were obtained according to the experimental combination of water content and dry bulk density of the soil as defined in Table 4.1. The desired soil moisture was obtained by the addition of specific doses of water on the soil surface. The moisture homogenization was reached after a day of repose by the process of natural infiltration. The soil bulk density was modified by compressing the soil using a rolling cylinder (Figure 4.5).

Figure 4.5 Soil-bin compaction.

During the process of soil conditioning, for each experimental point the water content and dry bulk density were measured by taking seven soil samples along the channel at 50 and 80 mm depth. The soil is considered ready for the test when the values found, are close enough to those

defined in Table 4.2. However, between the proposed soil physical properties and the measured data, variations occur. The current water content and dry bulk density of each experimental point is shown in Table 4.2.

Table 4.2 Experimental points after soil condition in soil-bin.

Points	1	2	3	4	5	6	7	8	9	5.1	5.2	5.3	5.4
w, %	16.0	11.6	19.7	9.0	15.4	21.5	12.3	20.5	16.2	14.7	15.2	15.6	15.0
ρ_d, *g/cm³*	1.33	1.27	1.3	1.07	1.12	1.1	0.94	0.95	0.9	1.08	1.11	1.13	1.09

As is shown in Table 4.2 the distribution of the real experimental points was obtained according to the points previously defined in Table 4.1. The measured soil dry bulk density was between 0.9 to1.33 g/cm³. The water content varies between 9 to 21.5%, corresponding with a dry to slightly wet conditions, and from a loose to dense soil structure.

4.6 The force reaction behaviour

Vertical and draft forces were measured along the channel at 150 mm constant working depth for each soil condition (Table 4.2). The variation in reaction forces characterises the tension state of the soil as a function of moisture and compaction combination. These factors modify the soil mechanical response, resulting in a different soil failure pattern and force requirements.

4.6.1 *Draft force response*

The magnitude of the force in longitudinal direction or draft force defines the energy required for the tillage operation. Several studies show soil resistance correlated with the draft force through testing different tool geometries using the draft force magnitude as a soil strength indicator (Raper and Hall, 2003, Adamchuk et al., 2004, Miguel Herrera Suárez 2011).

The draft forces obtained from the tests at the soil conditions defined in Table 4.2 are shown in Figure 4.6a. The nominal force of each test was determined as the force average obtained from 150 to 450 cm in the tool trajectory.

The draft force variation was found to be between 350 and 390 N. The force standard deviation increases in dry soil conditions as shown in Figure 4.6b, revealing the stiffness of the soil. This pattern was well observed in test 4 carried out at the smallest soil water content *w* = 9.0%. In fact,

the magnitude of the forces characterises the general state of soil strength and was affected also by the soil compaction level.

(a)   (b)
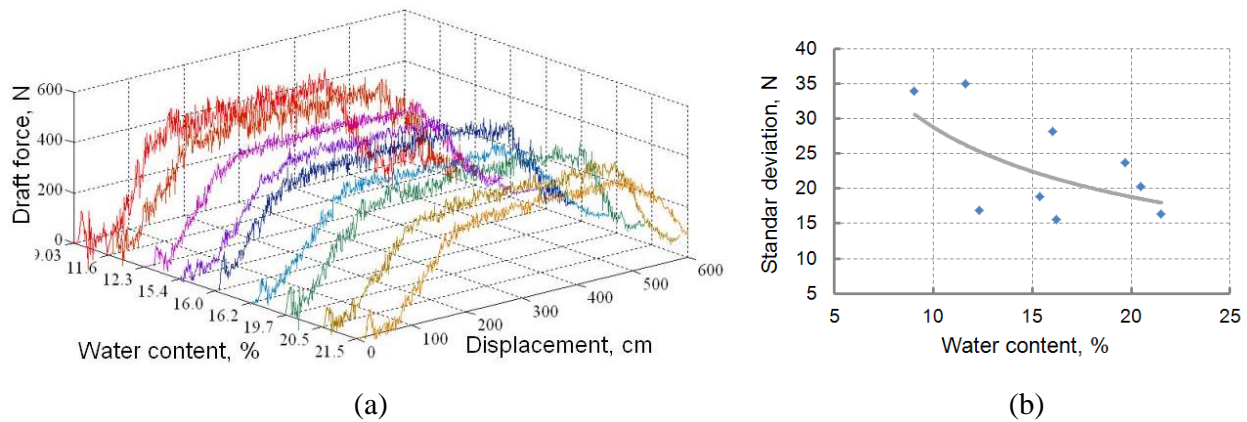
Figure 4.6 Horizontal forces from soil-bin tests (a) and standard error vs. soil water content (b).

The soil pattern of deformation has been found to be related with the intensity of force oscillations by Gupta and Rajput (1993). Other authors (Sharma et al., 1992, Makanga et al., 1997), had explained the gradual building up of the draft force and the attainment of the dynamic stability of the force as a function of the surcharge over the soil by the action of the tool, eventually defined by the general soil strength

The influence of water content and dry bulk density in draft force response is shown in Figure 4.7. For all values of soil moisture under study when the dry bulk density increases, the draft force increases too. However, this increase for higher soil moisture $w = 23\%$, is moderated in the range between 0.9 and 1.0 g/cm^3).

On the other hand, the influence of the soil water content is appreciable as the soil compaction increases ($\rho_d > 1.12$ g/cm^3). As the moisture increases the soil strength decreases. However, for smaller dry bulk densities, the influence of moisture is negligible.

This behaviour of the draft force at different soil conditions is in agreement with the variation found in the soil strength parameters discussed in Chapter 2.

As was found by Sahu and Raheman (2006b), soil compaction is the main factor that contributes to the increase in draft force. The authors, in spite of including parameters as tillage depth, operation speed, and tool shape decided to keep the water content constant. However, in several researches a significant effect of the moisture content was found for tillage forces.
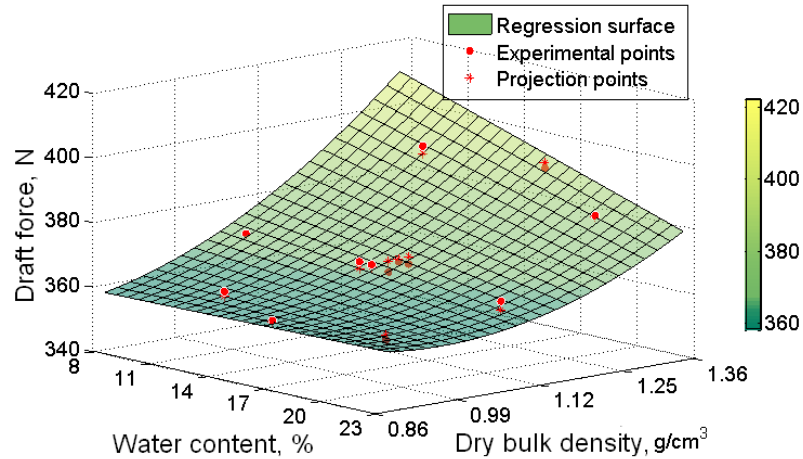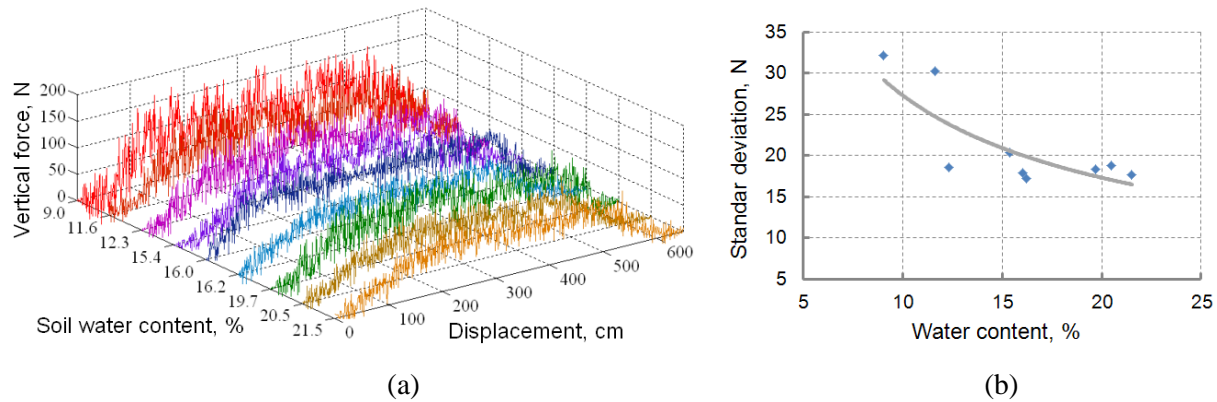
Figure 4.7 Drafts force response surface function of moisture and soil dry bulk density**.**

In general, the authors have focused on finding the optimum water content for tillage, defined as workability state (Mosaddeghi et al., 2009, Mueller et al., 2003, Barzegar et al., 2004). This condition is related with the minimal draft force needed to obtain the maximum soil loosening. The independent analysis of the draft force behaviour in the soil under study subject that the optimal water content can be placed between 14 to 23% and also beyond this point. To reduce the range of the optimum soil moisture, the loosening indicator discussed in next sections provides the entire information.

4.6.2 *Vertical force response*

The soil physical conditions defined by the different experimental tests (Table 4.2) also modify the reaction force measured in the vertical direction oriented downwards. This vertical component is related with the pressure applied by the tool over the soil foot surface and the compaction in the surface below the tool travel, usually called plough-pan.

As shown in Figure 4.8a, the reaction force magnitudes during the tests are found in the range of 76 to 97 N. The standard errors increase when the soil becomes drier, showing a similar pattern for the horizontal force in relation with the soil moisture (Figure 4.8b).

(a)   (b)

Figure 4.8 Vertical forces from soil-bin tests (a) and the standard deviation vs water content (b).

Vertical force response surfaces as a function of dry bulk density and moisture content are shown in Figure 4.9. As it was expected, the force increases when the soil becomes denser and decreases with increasing water content. These results are in accordance with the variation in soil strength parameters like cohesion, friction and soil elasticity. The susceptibility of the soil to compaction, however, is related to factors as content of clay and the critical water content (Saffih-Hdadi et al., 2009).
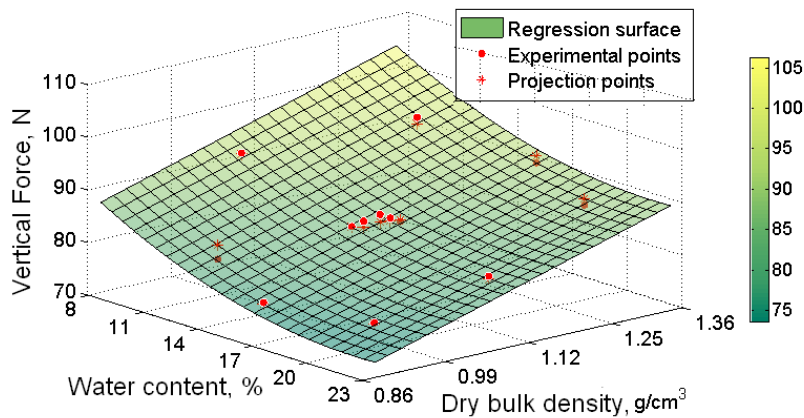
Figure 4.9 Vertical force functions of water content and dry bulk density.

4.7 Soil loosening indicators

As indicators of soil loosening variations in the initial dry bulk density, soil profile and particle size distribution by the tillage operation were measured during each different test in the soil-bin. The final dry bulk density was obtained from the disturbed soil (Figure 4.10a), according to the procedure explained in section 2.4.

71

<p align="center">(a)   (b)   (c)</p>
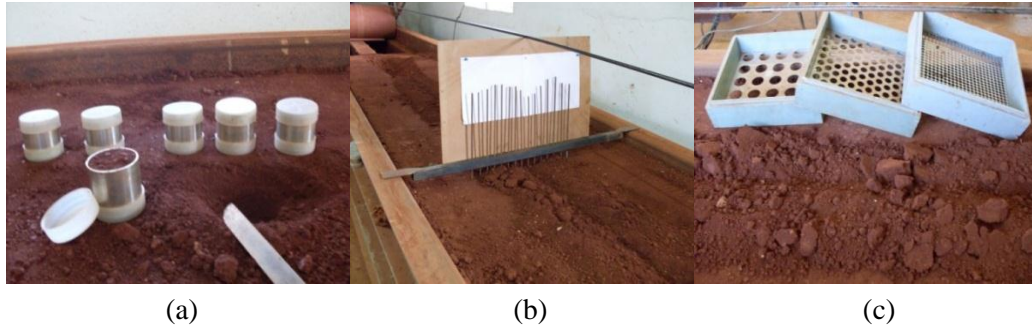
Figure 4.10 Parameters measured for all tests in soil bin.

The soil profile was measured after soil tillage by the profilometer method as shown in Figure 4.10b, and the soil texture classification was carried out by sieving using four different mesh sizes (Figure 4.10c). The variation of the dry bulk density through the different experimental points is showed versus water content in Figure 4.11a.
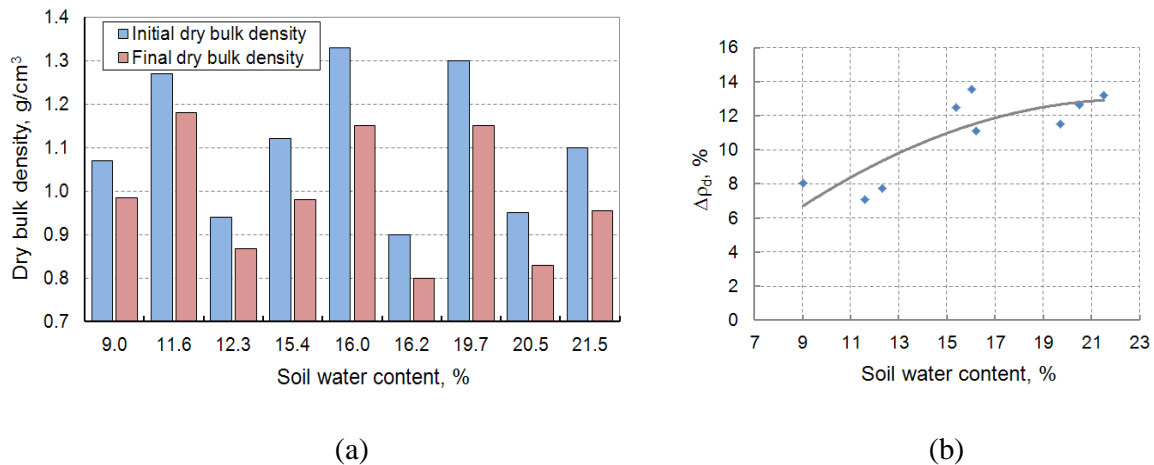

<p align="center">(a)   (b)</p>

Figure 4.11 Initial and final dry bulk density (a), and dry bulk density variation after tillage.

For all combination of water content and dry bulk density tested, the loosening effect during the tillage is denoted by smaller values of final dry bulk density (red bar). As the soil water content increases, the proportional variation of dry bulk density $\Delta\rho_d$ with respect to its initial value also increases as is shown in Figure 4.11b. However, for the experimental points with water content beyond 15% the variation tents to be constant. According to the results discussed in section 2.6.4, as the water content increases a reduction of inter-particle bond resistance take places, maximising the grain fragmentation during soil-tool interaction. The results are in line with those found by Arvidsson *et al.* (2004). The authors concluded that tillage operation at specific water

content before the soil plastic limit is reached, provides a large proportion of small aggregates, and also reduces the energy demanded for tillage.

The soil profile, measured after tillage (Figure 4.10b) was found strongly connected with the variation of dry bulk density as shown in Figure 4.12.
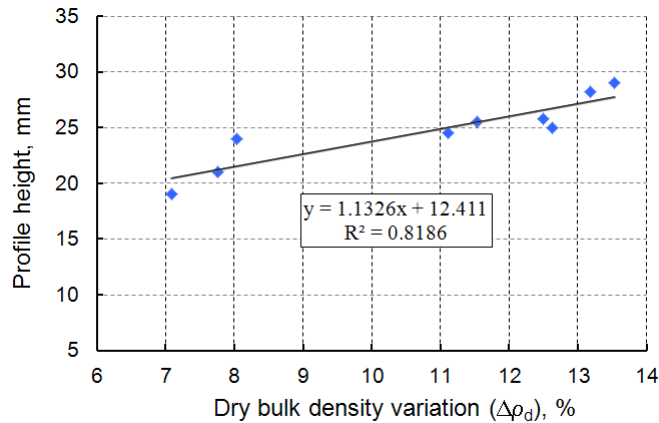
Figure 4.12 Soil profile behaviour concerning dry bulk density variation.

In the analysis, the variation of the profile height reached after each test was established as a function of the dry bulk density variation. The relationship shows a linear increase in the height of the soil profile with increasing $\Delta\rho_d$. The behaviour of the soil corresponds with the volumetric changes taking place in the soil granular structure during soil loosening.

4.8 Soil aggregates distribution

The analysis of the distribution of soil aggregate size a_s after tillage was carried out by the sieved process as shown in Figure 4.10c. The soil was classified in four groups of sizes to calculate their proportion in the soil disrupted by tillage. For the analysis three points were selected to represent the extremes and the centre of the experimental region called *dry-hard* ($w = 11.6$ %, $\rho_d = 1.27$ g/cm^3), *medium* ($w = 15.4$%, $\rho_d = 1.12$ g/cm^3) and *wet-loose* ($w = 20.5$ %, $\rho_d = 0.95$ g/cm^3). The particle distribution in the three conditions is shown in Figure 4.13.

An increase in the amount of aggregates size $a_s < 10$ mm is an indicator of better seed bed preparation. Inversely, the amount of aggregates with a size $a_s > 50$ mm shows an incomplete loosening of soil.
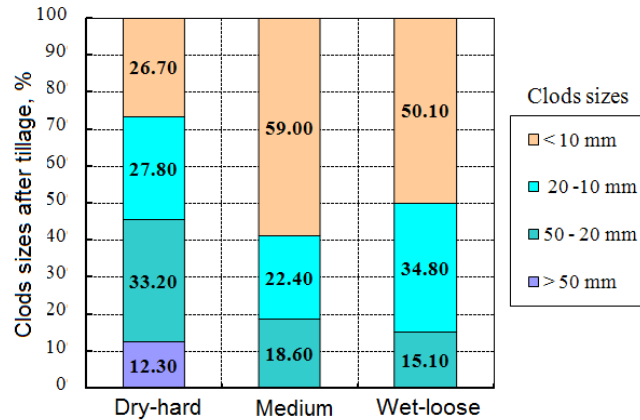
Figure 4.13 Clod sizes distribution at different soil state after tillage tests.

For the *medium* soil condition, the smaller grains of soil represent more than 50% of the sample. In contrast, *dry-hard* soil contains more than 10% aggregates bigger than 50 mm. Finally in a soil at *wet-loose* state the number of smaller particles is slightly lower than the *medium* one. As the soil becomes compacted, the aggregate size a_s between 20 mm and 50 mm increases. However for the *medium* moisture soil condition the maximum amount of clods with a size $a_s < 10$ mm is obtained. Then, considering that the draft forces obtained in section 4.6.1, slightly decrease as the moisture increase, the optimum water content for tillage of this kind of soil can be placed close to $w = 15.4$ %.

4.9 Conclusions

The indoor soil-bin installation to investigate the tillage operation process has been configured in several researches to control the effect of the environment and soil variability. Parameters as tool velocity, tool geometry, work depth, soil compaction and soil moisture can be controlled to measure the reaction forces on the tillage in safe and reliable conditions.

Draft forces measured along the tool trajectory in the soil-bin, for the nine defined soil conditions in an Oxisol soil, showed variations with respect to soil compaction and soil moisture. The magnitude of the force was found between 350 to 420 N. The draft force increased with an increment in soil compaction especially for dry bulk density beyond 1.1 g/cm^3. The effect of soil water content, was negligible for lower soil compaction. However, as the soil bulk density increases the draft force falls down under the effect of the water content.

The magnitude of the vertical force was found to vary between 76 and 97 N. The pressure exerted on the soil bottom increases with increasing dry bulk density. Inversely, for all levels of compaction, the water content reduces the magnitude of the force in the vertical direction.

By tillage operations, soil bulk density changes proportionally to the initial soil compaction. This variation also is affected by the water content. Soil loosening increases for low values of initial dry bulk density. However, the rate of variation is bigger for dense soil at 20% of water content.

The height of the soil profile measured in the transversal direction of the disturbed soil after tillage showed a linear correlation with the variation of dry bulk density. Profile height between 16 and 28 mm was an expression of the volumetric changes during soil-tool interaction.

The proportion of the aggregates with sizes less than 10 mm measured after tillage in three different soil conditions, called *dry-hard*, *medium* and *wet-loose,* vary with the soil state. As soil compaction increases the aggregate size after tillage also increases. However, more than 50% of the aggregates less than 10 mm in size were found in the *medium* soil condition. Considering that the draft force decreases as the moisture is becoming higher, the optimum water content for soil tillage can be placed close to $w = 15.4$ %.

Chapter 5

Model Validation

5.1 Introduction

A numerical model is only useful if it has been subjected to proper validation to investigate the model limitation, the range of validity, and the performance of the model for the different applications. For DEM models some authors have been used the comparison between their results with those obtained by other researchers in order to validate the model accuracy in a qualitative or quantitative sense as a way to validate the model results (Karmakar, 2005, Tadesse, 2004, Asaf et al., 2006). Validation of the soil-tool interaction DEM model, was made by using empirical models based on the Coulomb theory of earth passive and active pressure (Coetzee and Els, 2009b, Martin Obermayr, 2011, Shmulevich. et al., 2006, Mak et al., 2012). This method has shown to be suitable for validating a simple shape of the tool as used in the above simulations. However, for complex tool shapes, the empirical results of the equations have been shows to be inappropriate. Experiments in soil-bin and field are commonly performed to validate models for tillage simulation by continuum methods as FEM (Aluko, 2008, Gebregziabher et al., 2007, R. Jafari, 2004, Mouazen and Neményi, 1999). This approach brings more useful information about the model performance as well as soil behaviour. The different kinds of validation used for continuous and discrete models can be explained by the fact that DEM applications have been less developed than FEM models to make a realistic prediction of soil tillage requirements.

The objective of the present chapter is to validate the model performance with respect to draft and vertical forces by modelling soil-tool interaction with the same tool geometry and soil conditions tested in the soil-bin experiment.

5.2 Model setup for soil-bin simulation

With a view to reproduce the experimental results obtained from the soil-bin, a block of soil sized at 320x300x600 mm, was generated using 30,800 spherical particles (Figure 5.1b). This

dimension allows reducing the effect of the boundary condition. The block was made up by the same procedure used to generate the virtual soil samples explained in section 3.6.1. The particle radius was fixed between 6.5 to 7 mm according to the results obtained in section 3.7 related to the effect of particles size.

(a)   (b)
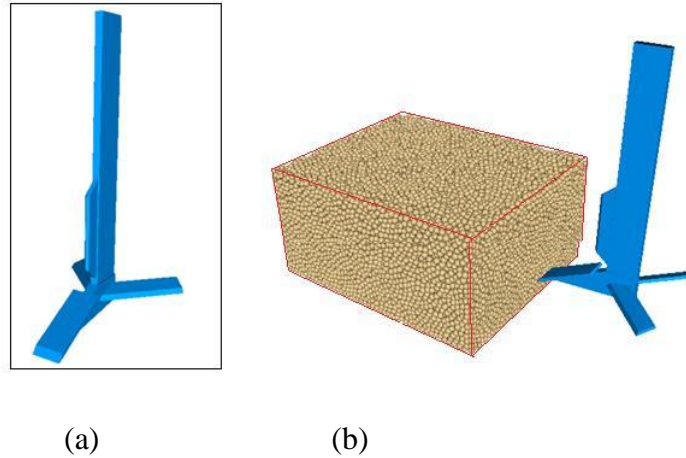
Figure 5.1 Virtual implement (a), and soil-tool simulation setup (b).

A virtual cultivator tool (Figure 5.1a) was also made with the dimensions showed in Figure 4.1c to reproduce the tool used in soil-bin tests. The operational parameters as tillage depth ($d = 15$ mm) and tool velocity ($v = 3.6$ km/h) were also the same as the experiment. The setup for the simulation shows the starting position of the tool with respect to the soil block, the boundary conditions are represented by the planes around the box (red lines), and they were defined with the soil micro-parameters.

Table 5.1 Soil macro-parameters for the DEM model of soil cultivation.

Parameters	Units	Simulation points								
		1	2	3	4	5	6	7	8	9
t_{50}	kPa	963.9	1195.3	718.2	1122	785.7	539.9	759	389	520.5
E	MPa	84.3	90.5	69.9	75.4	64.2	53.9	56	38.9	44.9
ν		0.4	0.4	0.4	0.3	0.3	0.3	0.2	0.2	0.2
c	kPa	114.8	118.7	96	97	83.8	72.6	77.9	57.4	66.9
c_a	kPa	3.6	2.3	4.9	1.6	3.2	5.4	2.2	4.9	3.3
ϕ	°	26.2	26.2	24.7	23.3	22.9	22.2	20.6	18.6	19
δ	°	17.5	18.4	16.2	18.3	17.1	15.3	17.3	14.9	16.2
ϕ_μ	°	5.5	5.5	5.2	4.8	4.7	4.6	4.2	3.7	3.8
c_μ	kPa	24.4	25.2	23.1	26.4	23.6	21.9	27.5	25.1	28.0

The properties to simulate the nine experimental points (Table 5.1) were calculated with the soil regression equations, and calibration equations obtained in Chapter 2 and Chapter 3 respectively.

5.3 Draft force prediction

The sum of the forces acting on the tool in the longitudinal direction caused by the contact between the tool surface and soil particles, was calculated by the model at each time step. The simulated draft forces from the soil-tool interaction model, with the parameters defined in Table 5.1 have been plotted against the tool displacement, as shown in Figure 5.2.
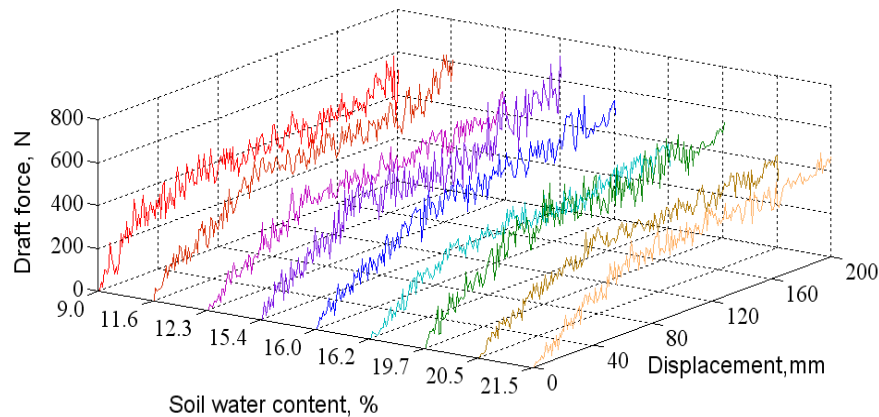
Figure 5.2 Simulated draft forces from the soil-tool setup.

The similar pattern of force oscillations obtained by the particle size described in section (3.7) is shown in the present simulation. As the general strength of the virtual block increases, the fluctuations tend to increase too. This behaviour was earlier observed during the implementation of a rotational soil-cutting tool in a cohesive model (Tadesse, 2004), explained by the action of the inter-particle tension. The variations in the geomaterial stiffness also have been explained from the variation of the cohesive bonds, yielding force and void ratio (Jiang et al., 2005).

The relationship between draft forces from simulation D_{sml} and those obtained from the soil-bin tests D_{msr} is shown in Figure 5.3a. The standard deviation of the regression was $RMSE = 11.5$ N, The mean absolute error MAE equals 8.2 N, while the p-value was found at 0.001, denoting the interrelation between both variables. The graph also shows the prediction and confidence limits according to the confidence bonds defined at 90 %.

From the difference between measured and simulated forces, the relative errors of each simulated point were obtained by $e_s = (\Delta D_f / D_{msr}) \cdot 100$. This error was found to be between -6 to 7% of the

measured force. Besides, the error distribution shows a certain correlation with the magnitude of the draft force from the soil-bin. As shown in Figure 5.3b the errors from the simulation tend to decrease as the measured draft force becomes lower. Negative errors characterize these forces which are in the range of 350 to 370 N. Instead, for values between 370 to 400 N, positive errors were found. That behaviour of the model tends to overestimate the draft force when the soil strength becomes higher.

(a)   (b)
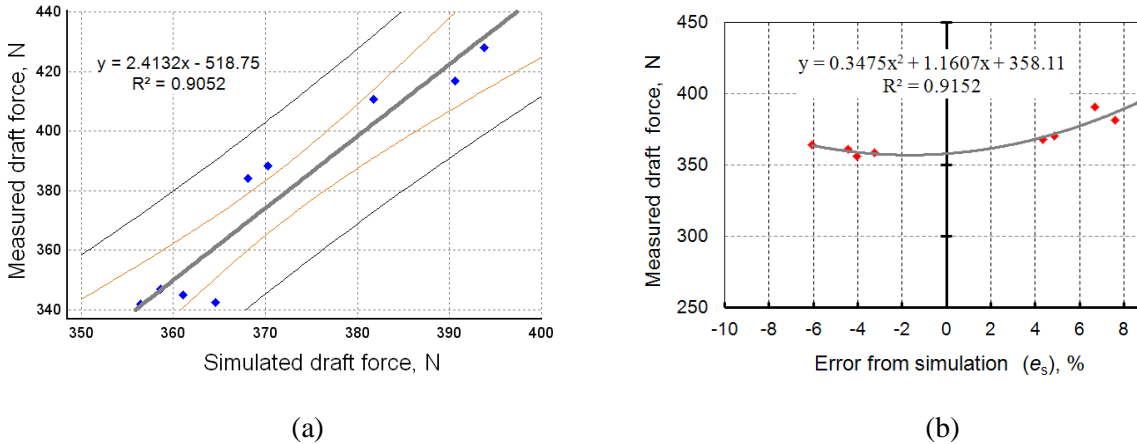
Figure 5.3 Draft forces from soil-bin and simulation (a), error of the model (b).

The reason for the over prediction tendency found in the model by increasing force magnitude can be associated with the differences between the soil macro-properties obtained during the mechanical tests and the current properties of the soil in the soil-bin experiment. The soil macro-parameters in the model are the factors that define the tensional state and consequently the reaction forces. As was discussed in Chapter 2 the parameters of soil strength in remoulded soil are affected by the process of cementation mainly in soil compacted conditions. However, the procedure for conditioning the soil in the soil-bin was in fact, quite different from the procedure used for soil compression and shear tests. As a result, the soil structural reinforcement, probably caused by mineral cementation, is lower in the soil used for the tillage tests in the soil-bin, causing overestimation on the draft force response by the DEM model.

On the other hand, taking an undisturbed sample directly from the soil-bin and testing it, so far, it is exposed to the same risk of hardening through the process of sample conformation. Additionally, to introduce no standard experiments to provide the specific data reduces the model applicability for the already knowing soil-properties. However, by an adequate relationship between soil penetration resistance measured by cone index in the soil-bin, and properties

obtained from soil mechanical tests, it should be possible to introduce a new model parameter that considers the soil hard structure forming during sample conformation.

The quality of the Oxisol soil to becomes hard during consolidation was also observed by Suárez *et al.* (2008) during the validation of a FEM model. In another study, the hard soil structure formed in clay Oxisol was associated with its mineralogical composition. The study showed high soil resistance to root penetration during non-inversion tillage (Tormena et al., 1999). Also the cohesive effect of Fe and Al oxides over an Oxisol micro-aggregates was found by Pinheiro-Dick and Schwertmann (1996).

5.4 Vertical force prediction

The magnitude of the vertical reaction force is computed by the sum of the contact force between soil particles and the tool surface in the vertical direction at each time step. From the soil-bin experiments this force was found depending on the soil physical conditions. The force displacement curve obtained from simulations of the nine experimental points defined in Table 5.1 shows a similar pattern in draft force behaviour. As the soil strength increases, the oscillation becomes higher. The frequency however, decreases with respect to the measurement force because this parameter depends on the quantity of force values saved along the tool displacement (Figure 5.4).
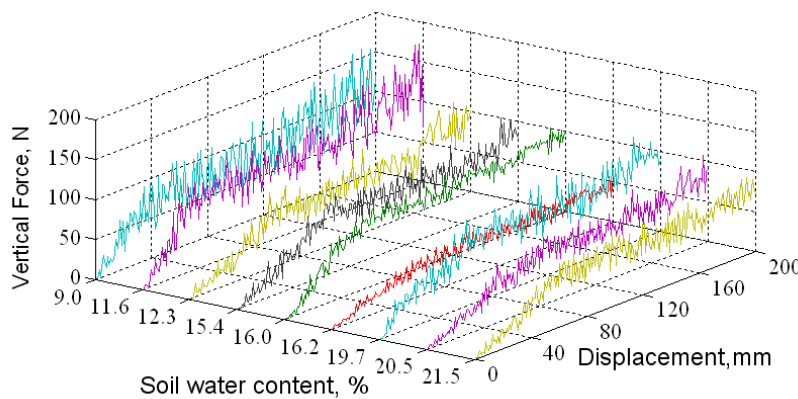

Figure 5.4 Vertical force reactions from simulation.

The model to describe the relationship between vertical forces from the simulations and the soil-bin tests is presented in Figure 5.5a. The model standard deviation of the regression was *RMSE* = 3.5 N, The mean absolute error *MAE* equal 2.1 N. Similar to the draft force, the p-value was

found at 0.001, denoting the interrelation between simulated and measure forces. The prediction and confidence limits according to the confidence bonds and defined at 95 % are also show in the figure.

The error of each simulated force e_s with respect to the experimental ones also shows a similar pattern as was observed in the draft forces, decreasing with the force magnitude (Figure 5.5b). The values of the error from the simulation are between -10 to 12%.
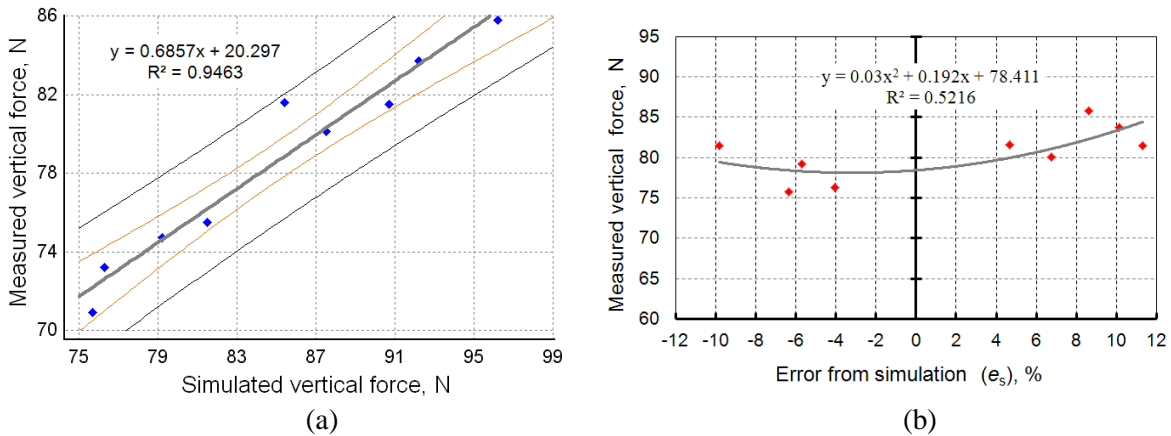
Figure 5.5 Vertical forces from soil-bin and simulation (a), error of the model (b).

The results of the simulated force in vertical direction are affected soil hardness during sample conformation in a similar way as for the draft force. Moreover, the results are also affected by the non-isotropic behaviour of the soil in the experimental tests caused by the irregular compaction in vertical direction during the rolling cylinder explained in section (4.5).

The importance of the vertical force prediction is related to avoid the hard-pan formation decreasing the pressure provided by the tool (Spoor et al., 2003). However, the prediction of soil vertical pressures is always associated to the soil compaction and modelled separately from the draft force, usually by pedotransfer functions (Saffih-Hdadi et al., 2009, Keller et al., 2007). From this point of view the DEM simulation brings a more versatile interpretation of the soil compaction related to the direct action of the tillage tool.

5.5 Conclusions

The soil physical conditions used for the experimental tests in the soil-bin are reproduced in a DEM model. For each experimental point a set of parameters was obtained from soil regression equations to simulate the strength state of the virtual block of soil. By the geometrical elements provided by the DEMeter++ software the exact shape of the tool was obtained.

The force-displacement curves described by the tool trajectory in the DEM simulation are in correspondence with soil strength variation introduced in the model by the different states of soil, defined by the level of compaction and soil moisture. The force oscillation pattern during the real test is also observed in the DEM simulation of draft and vertical forces. This behaviour of the model response is associated with the effect of void spaces into the virtual block of soil, reproducing the real porosity property of the soil.

The relationship between simulated and measured draft forces follows a linear model with R^2 = 90% and a standard deviation of *RMSE* = 11.5 N. The results from simulation were obtained in the frame of the prediction limits defined at 90% of confidence bounds according to the model. The independent error of each simulation of draft forces shows an error between -6 to 7% of the force measured, tending to increase for higher values of soil strength. This behaviour is related with the hardening capacity of the Oxisol soil at specific moisture content and pressure, introducing differences between mechanical properties used in the model and those attained during soil conditioning in the soil-bin. From this point of view, a model parameter related with the soil hardening capacity should fix the tendency of error to increase in more compacted soil.

The relationship between simulated and measured vertical force also is described by a linear model. The statistical goodness of fit of the model showed an R^2 = 95% with a standard deviation of regression *RMSE* = 3.5 N with a confidence bonds defined at 90%. The error from each simulation with respect to the measured vertical force shows ranges from -10 to 12%. The error increasing as vertical force becomes high can be related to the soil hardening, and to the non-isotropic behaviour of the soil.

The DEM simulation was made from loose to compacted soil at different values of soil water content according to tillage purposes in the limits of $w = 9.0$ to 21.5% and $\rho_d = 0.9$ to 1.33 g/cm^3. Based on the results from soil-bin tests, the dry compacted soil is the condition that more increases in draft and vertical force and, consequently, the error tendency found in the present chapter. Hence, the limit of the model prediction can be defined by the critical combination of water content with soil the dry bulk density $w > 11\%$ and $\rho_d > 1.25$.

Chapter 6

Simulation of Tillage Applications

6.1 Introduction

Several studies have focused on tillage force requirements. They are motivated by the need to reduce the energy consumed by the process where the soil physical state, the tool geometry, and the selected operational parameters play an important role. The performance of the tillage by two kinds of cultivator sweeps was tested in five different soils with different clay content (Sahu and Raheman, 2006b). In this study the draft force on a trailing sweep was 27% less than that measured on a leading sweep. The vertical force was also reported to increase with depth depending on the type of soil tested. In other experiments (El-Sayed, 1991) the effect of shank shape, shank material and shank cross-section on the draft requirement for chisel ploughs was tested at different levels of forward speed, ploughing depths, and rake angle. The results show that a curved shank chisel plough performed better compared to a straight shank chisel plough. In similar research, Al-Janobi *et al.* (2002), measured the influence of the shank shape of three common chisel ploughs operating on a sandy loam soil. The experiment was carried out at different levels of forward speed and ploughing depth. The curved shank was observed to demand a higher draft and vertical force compared to the other two shanks when operated at different forward speeds. However, no significant increase in vertical forces was observed for all three ploughs with an increase in the forward speed. A novel approach for predicting draft force requirements by primary tillage implements was proposed by Desbiolles J.M.A. *et al.*(1997). They developed a force prediction model which described the draft of a standard tine as the product of two factors: soil strength and tool geometry. The model was validated in two friable sandy loam soils i.e., compact clay and plastic clay soil. The average prediction errors for

mouldboard ploughs and the disc tool were 14.2 and 30% respectively. The influence of tool design and tillage system parameters was also studied by Gupta P.D (1985). In this approach the performance of wide cutting blades was determined for dry land farming. The results showed that specific draft increased with the radius of curvature of the cutting blades from 410 to 600 mm, whereas the draft decreased in a similar way with a further increase in the curvature from 700 to 1000 mm. The lead angle in shanks finally affected the soil tilling.

On the other hand, numerical models have been implemented taking account for the tool geometry, leading to numerical solutions for tillage applications. Using FEM models several authors reported satisfactory results related to the tool structural resistance and tillage force demanded (Gebregziabher et al., 2007, Mouazen and Ramon, 2002, Plouffe et al., 1999, Cui et al., 2007, R. Jafari, 2004, Fervers, 2004). This result showed the advantages of the FEM models with regard to analytical calculations based on earth passive pressure discussed in section 3.8, i.e., the possibility of defining an appropriate constitutive soil low and the potential to introduce a quite complex tool. FEM was found suitable for a continuum analysis under static conditions of soil and tool interaction (Upadhyaya et al., 2002, Tadesse, 2004), but not appropriate for modelling particle flows and crack formation which characterizes tillage operations. On the contrary, the DEM model was successfully used to simulate the flow of granular material as the interaction forces among the elements in contact, describing the discontinuous dynamical behaviour of the particles. However, only a few attempts were made when using DEM for tillage operations (Shmulevich et al., 2007, Martin Obermayr, 2011, Tanaka et al., 2007, Mak et al., 2012). Even though DEM models suppose the opportunity to introduce specific contact rules to reproduce the real soil behaviour, all of these approaches have the limitations that soil was considered as non-cohesive, and also the tool geometries are extremely simplified.

Considering the results from the validation explained in Chapter 5, and the state of the art in the DEM model in tillage applications, in the present chapter different tillage-tool applications are modelled with a view to simulate the force requirements and soil patterns of loosening at the reference soil condition.

6.2 Geometrical setup for tillage applications

Soil-tillage applications called soil cultivation, primary tillage, and subsoiling have been implemented using the proposed frictional-cohesive model. The tillage virtual tools were

constructed according to the original shape of those manufactured by Cuban Factory of Tillage Tool, following a 1:2 reduction scale. These tools are widely used for soil conditioning in sugar cane plantations for weed control, soil loosening and de-compaction under non inversion tillage criterion.

Soil virtual blocks were generated by the pre-simulation method. Particles are dropped (Figure 6.1a), compressed, and reloaded (Figure 6.1b) to provide the initial condition of the medium. The structure obtained, is characterised by the presence of inter-particles bonds proportional to the given soil macro-cohesion.

(a)   (b)
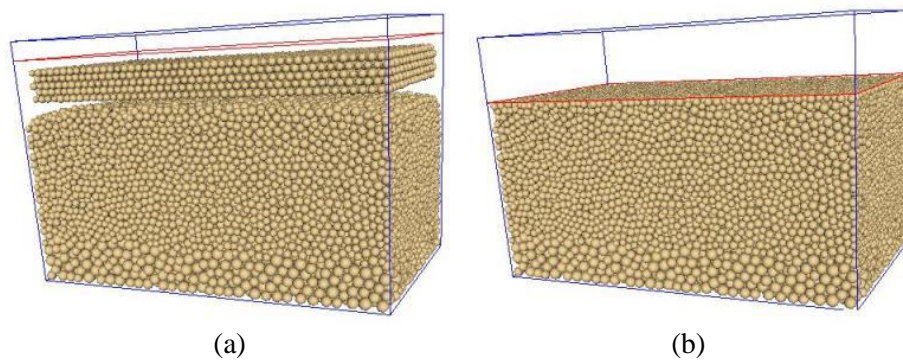
Figure 6.1 Virtual block of soil. Particles dropped (a), Block compression (b).

As in previous simulations (section 5.2), the blocks of soil were generated in a hexagonal-compacted spatial array of spherical particles. In correspondence with the dimension of the tillage tool and operational depth, three configurations of the block were carried out (Table 6.1). The macro-parameters used for modelling the different soil blocks were calculated according to the soil condition used for the tillage applications, the tillage travel speed of all operations was kept at 3.6 km/h, i.e. the same speed as for the tests in the soil-bin condition.

Table 6.1 Virtual blocks configuration used in simulation of tillage operations.

Blocks	Blocks sizes			Radius range			Particles	Operation
	Width	Height	Length	Layer A	Layer B	Layer C		
1	350	300	600	4..6			48,000	Cultivation
2	400	250	600	3..4	4..6	6..8	40,000	Tillage
3	350	350	600	3..4	4..6	6..8	45,000	Subsoiling

6.3 Simulation of soil cultivation

Field cultivation is a common tillage to provide air and nutrients by loosening the soil close to the plant root location, and to remove weed along the furrow. To model this operation a tool called cultivator was reproduced, the design includes a main ploughshare and two lateral blades as shown in Figure 6.2a. The block of soil selected was sized at 35x30x60 cm with the parameters defined in Table 6.1, and the cultivation depth was fixed at 15 cm.

(a)   (b)
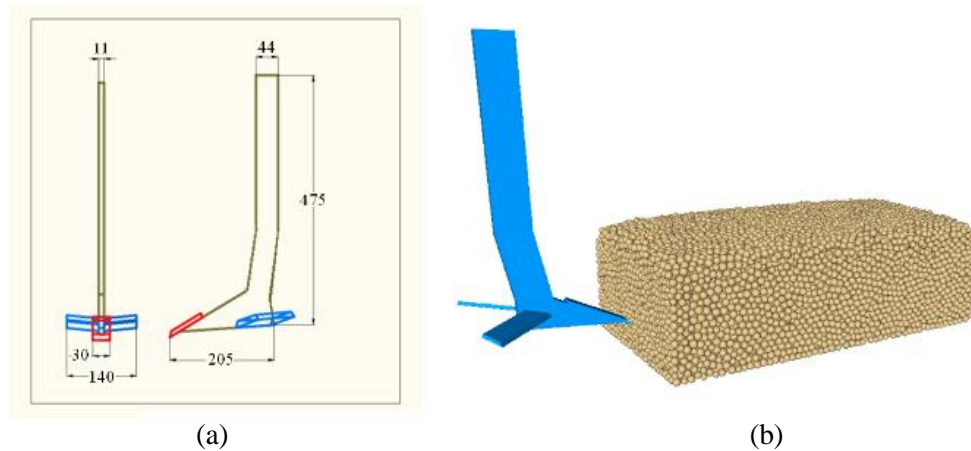
Figure 6.2 Cultivation setup. Tool general dimensions (a), model setup (b).

The geometrical model (Figure 6.2b) was subjected to three different combinations of soil macro-parameters, conditioned by the change in water content and defined as: *wet* ($w = 30$ %, $\rho_d = 1.15$ g/cm^3), *medium* ($w = 18$ %, $\rho_d = 1.15$ g/cm^3) and *dry* soil state ($w = 10$ %, $\rho_d = 1.15$ g/cm^3). To predict the reaction forces at three water states, the values for the soil macro-parameters were calculated by the soil regression equation, as shown in Table 6.2.

Table 6.2 Macro-parameters for modelling *wet*, *medium* and *dry* soil condition.

Parameters	Wet	Medium	Dry	Unit
t_{50}	331.8	675.0	1159.0	kPa
E	39.0	60.1	81.3	MPa
ν	0.3	0.3	0.4	
c	54.5	79.3	104.1	kPa
c_a	7.6	4.1	1.9	kPa
ϕ	19.9	22.7	24.5	°
δ	13.2	16.4	18.4	°

The draft force obtained from the simulations at the three conditions is plotted against the travel distance (Figure 6.3). The lower draft force was obtained in soil wet condition (green points) as it

was expected due to the weakness of the soil strength parameters. The average traction force measured 0.18 kN with a standard error of 36 N. The highest force was reached in dry soil condition (red points) as a consequence of the increment in soil resistance.
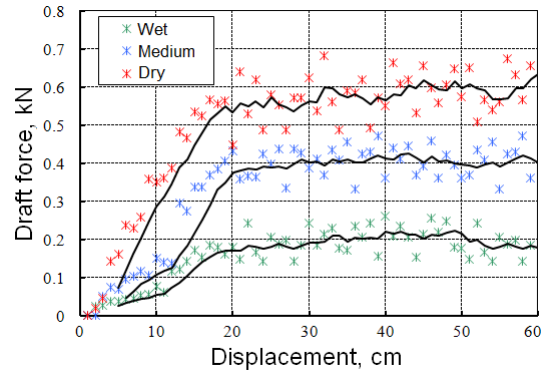
Figure 6.3 Simulation of draft forces at different soil water content.

As shown in Figure 6.3, the draft force in the dry condition of the soil is characterized by large oscillation in comparison with the other two conditions, showing a standard error of 58 N while the average force exceeds the value of 550 N. This behaviour agrees with the results discussed in section (5.3) with respect to force oscillation.

6.3.1 *Particle bulk density*

The macroscopic bulk density variation is calculated by the amount of particles per cubic centimeter after the simulation. This value was called particle index. The soil particles disturbed during soil cultivation (section 6.3) by the tool were divided into seven sections, as is shown in Figure 6.4a. For each section the value of particle index is calculated at *wet*, *medium* and *dry* soil conditions defined in Table (6.2).

As shown in Figure 6.4b the particle index decreases mainly in the central section of the block by the action of the main part of the tool. This effect decreases gradually toward the lateral direction, becoming nil at the boundary sections. In wet condition the particle index decreases as is described by the green line. This condition is characterised by small volumetric variation according to plastic particles flow.

(a)   (b)
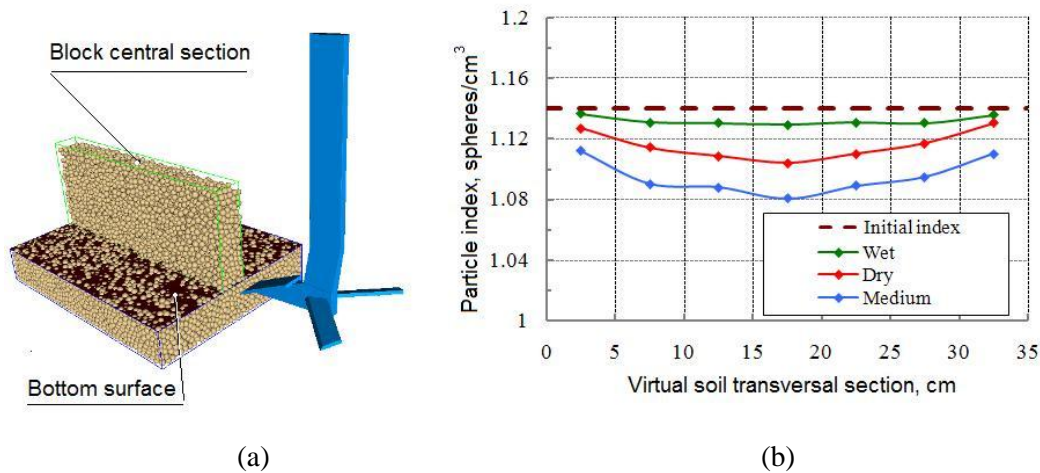
Figure 6.4 Block sections (a), particle index variation (b).

The minimum particle index is found at medium soil condition (blue line), which also remains more uniform through the section compared to *dry* condition. The decreases in particle index meaning an increase in virtual block porosity, that behavior found in *medium* soil condition defined at $w = 15.4\%$ is consistent with the result from soil-bin test related to soil density variation described in section 4.7. These results are in agreement with the study carried out in clay soil (Porter and McMahon, 1987), where it was found that maximum soil porosity during tillage operations takes place at the optimum water content where the soil has a friable condition.

6.3.2 *Particle force distribution*

The formation of hard pan through the direct action of the tool depends on the physical condition of the soil and the implement shape. Some surface layers are more susceptible to compaction than others but a ploughpan generally occurs at tillage depth (Saffih-Hdadi et al., 2009). A prediction of vertical force over this layer (Figure 6.4a) is graphically represented in Figure 6.5, showing the simulated forces on the particles placed below the cultivator path at 45 cm travel in *medium* and *dry* soil condition.

The results from simulations demonstrate a rise in vertical forces associated with the level of soil moisture. For the simulation in soil *dry* condition the amount of particles submitted to pressure also increase and some maximum values are obtained at the current tool position (Figure 6.5b). This result agrees with those obtained by Cui *et al.* (2007). The authors were focused on the simulation of soil and tire interaction by hypoplastic FEM model to predict the distribution of

vertical stress at the soil surface. As a result the investigation showed the influence on the magnitude of soil compaction associated with the soil physical state.

(a)   (b)
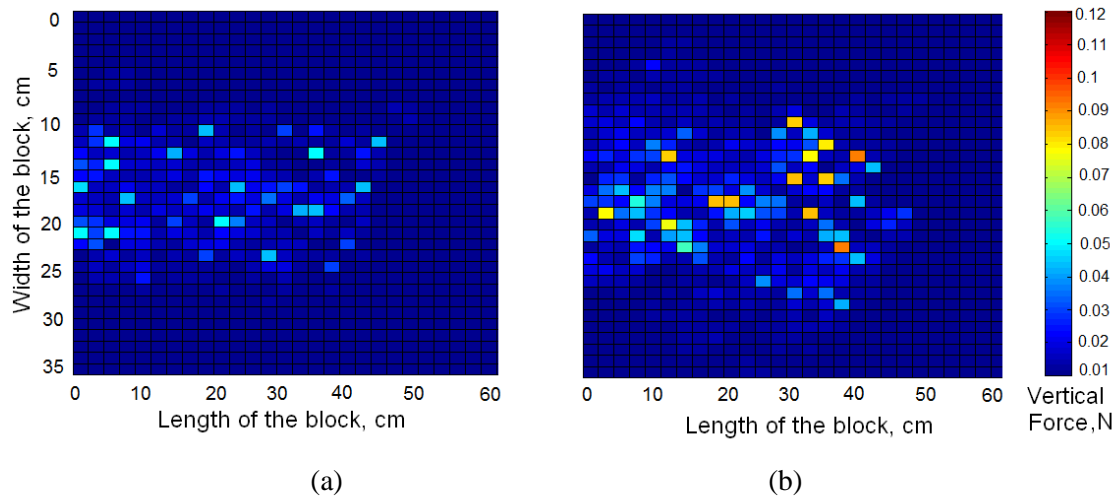
Figure 6.5 Vertical force distributions on the bottom layer at *medium* (a), and *dry* soil condition (b).

6.4 Tillage simulation by Para-plough and mouldboard

Designed for first tillage operations, the paraplough and mouldboard (plough) make use of different concepts of soil management. Conventional tillage by mouldboard is widely applied and based on soil inversion. Instead, the paraplough loosens the soil without turning the soil layers. To simulate the draft force in both cases the shape of the tillage tool has been sized such a way the tools cover the same working area (Figure 6.6).

(a)   (b)
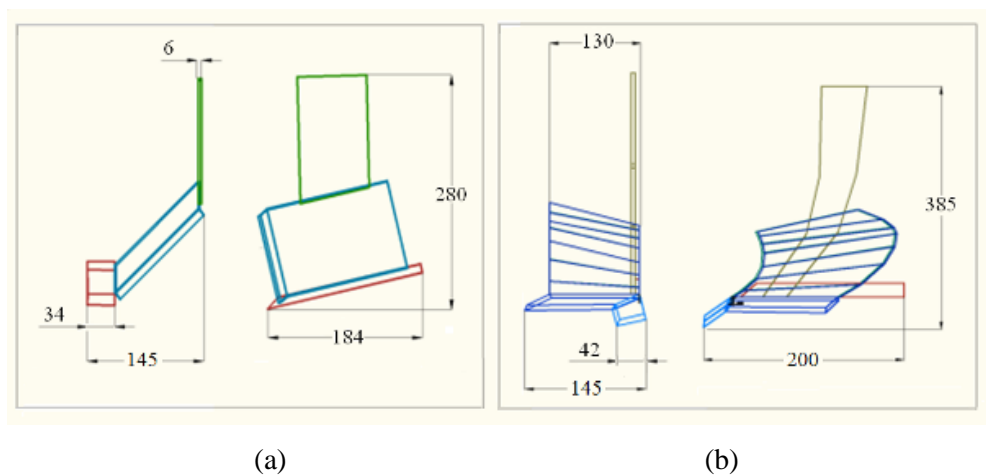
Figure 6.6 Tools designs of. Paraplough (a), and mouldboard (b).

The model setups for both operations are presented in Figure 6.7. The unique soil block was generated as a soil *medium* condition sized at 40x25x60 cm, details are shown in (Table 6.1). The working depth was fixed at 12 cm.

(a)   (b)
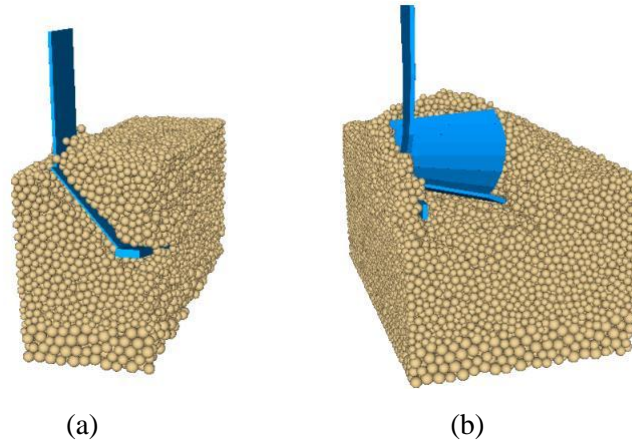
Figure 6.7 Primary tillage using paraplough (a), and mouldboard (b).

During the simulation, the soil disruption by mouldboard ploughing changes the position of soil particles, turning the top layers to down position. In addition, bigger sizes of clods characterise this operation (Figure. 5.10b). On the other hand, by paraplough tillage small aggregates are uniformly separated and deposited in their original relative position (Figure. 5.10a).
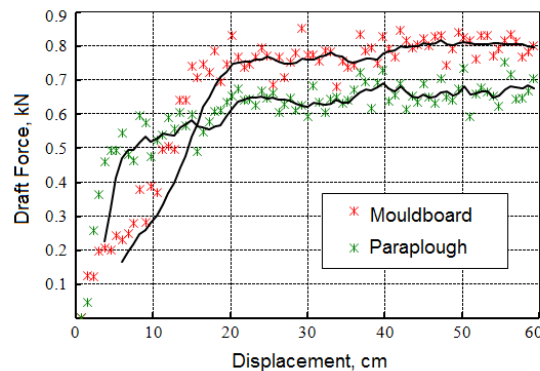
Figure 6.8 Draft force prediction for primary tillage.

The behaviour of draft forces in both cases is shown in Figure 6.8. The draft force exerted by the mouldboard was found to be bigger than the draft force by the paraplough with an average of 0.77 kN for the former compared to 0.64 kN for the latter, revealing an important difference between the two designs. As the data show, the inversion tillage increases the energy requirements. The results agree with those obtained by Shrestha *et al.* (2001) in a study focused

on improving the mouldboard plough. Similar results have been found by Desbiolles *et al.* (1997) during a series of measurement to obtain a model to predict the draft demanded in primary tillage.

6.5 Sub-soiling simulation by different tool

To reduce the undesired effects of soil compaction, deeper tillage is carried out by a tool known as subsoiler. It is characterised by a robust structure and being a large power consumer. To reproduce the high level of soil strength, lower water content was combined with high dry bulk density called *hard-dry* state ($w = 9$ %, $\rho_d = 1.3$ g/cm^3). The macro-parameters associated with this condition are shown in Table 6.3.

Table 6.3 Macro-parameters to modelling hard-dry soil condition.

Parameters	Hard-dry	Unit
t_{50}	1426.79	kPa
E	101.86	MPa
v	0.46	
c	133.60	kPa
c_a	1.79	kPa
ϕ	27.13	°
δ	19.01	°

Soil de-compaction simulations were performed by three tool designs called *simple*, *knife* and *Blade* subsoiler as shown in Figure 6.9.

(a) (b)
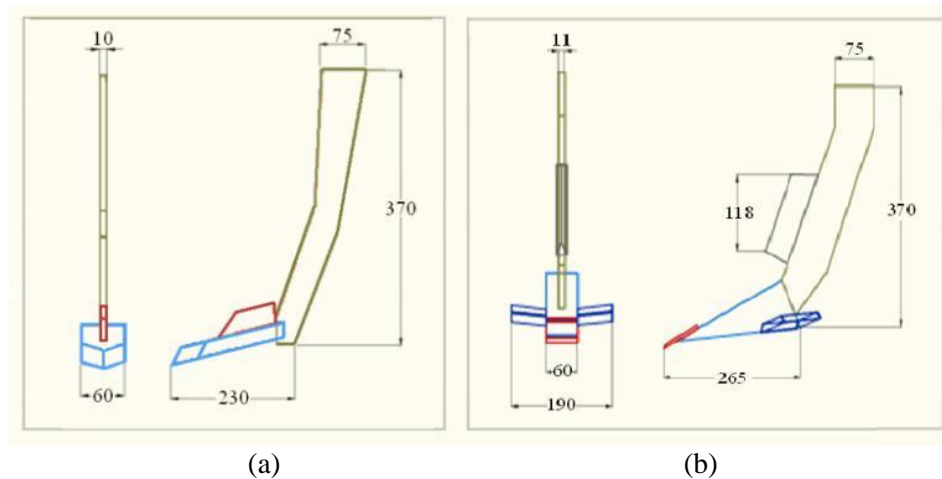
Figure 6.9 Simple subsoiler (a), and blade subsoiler (b).

93

The geometry of the tools was increased in complexity by adding different parts to the basic tool structure. Figure 6.9a shows the geometry of the *simple subsoiler* used, and the shape of the *knife* subsoiler having the same structure as the *blade* one, but without lateral blades (Figure 6.9b). To visualize the behaviour of the particle movement, longitudinal cross sections of the subsoiling simulation for the three tool designs are shown in Figure 6.10. The unique block of soil was sized at 35x35x60 cm as defined in Table 6.1. The working depth, according to common practice in subsoiling operation was fixed at 25 cm.

(a)   (b)   (c)
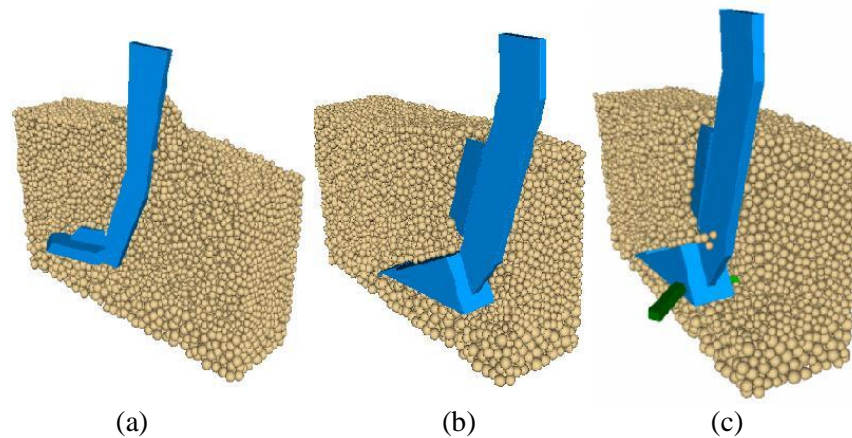
Figure 6.10 Longitudinal cross section of simulated of soil de-compaction. Simple subsoiler (a), knife subsoiler (b) and blade subsoiler (c).

The chart of draft forces for each simulation shows a small increment on the *knife* subsoiler with respect to the *simple* one (Figure 6.11). The difference is probably caused by the increase in rake angle of 12º for the *knife* subsoiler with respect to *simple* one.
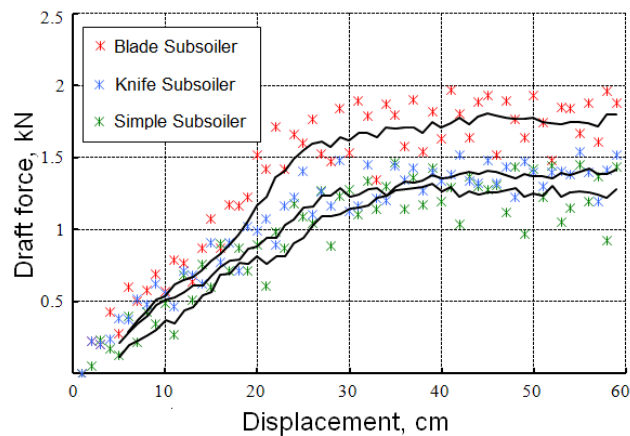
Figure 6.11 Horizontal forces form simulation of simple, knife, and blades subsoilers.

This result is in agreement with the findings of (McKyes and Maswaure, 1997); In their study, the authors describe the relation between the rake angle and draft force during tillage. The *blade* subsoiler however, demands around 450 N more than the *simple* one, suggesting that the force demanded during soil de-compaction increases also according to the subsoiler frontal scope defined by the width of the tool.

However, the work performed by the *blade* subsoiler, with respect to the soil disturbed area, is almost two times larger compared to the *simple* and *knife* subsoilers, while the draft force only grew around 25% . For this reason the *blade* subsoiler is more interesting from the energy point of view. The magnitudes of the forces obtained from the simulation are consistent with the results presented by Sahu and Raheman (2006b) predicted from empirical equations tillage draft for narrow tools in relation with the soil physical conditions.

6.6 Simulation of soil hardpan disruption

No homogenous bulk density distribution is generally found in the different soil layers. Several studies have been related to the degree of densification with the soil mineral composition, physical factors, and systematic loading by transporting and tillage operation. Although repeated tilling with the same tool and depth can cause the formation of a compacted layer (Trouse, 1985), the action of the mouldboard plough is commonly associated with this phenomenon (GueÂrif and Soane, 1994). To disrupt the hardpan layer a tillage operation of subsoiling is needed to restore the soil productivity by growing water infiltration, root development and soil aeration.

The soil block selected to simulate soil hardpan disruption was sized at 35x35x60 cm, which is detailed in Table 6.1.

The block is divided in two sections, each one generated with different particle densities resulting in a variation in the model macro-parameters by mean of soil regression equations (Table 6.4). The two conditions were selected considering the variation in dry bulk density found by Cueto (2011) in the same kind of soil. In the Figure 6.12 is shown the sectioned block and the layers called *soft* soil ($w = 12$ % and $\rho_d = 1.0$ g/cm^3) and *hard* soil ($w = 12$ %, $\rho_d = 1.35$ g/cm^3).

Table 6.4 Soil macro-parameters to model hardpan.

Parameters	Soft	Hard	Unit
t_{50}	331.8	1159.0	kPa
E	39.0	81.3	MPa
ν	0.3	0.4	
c	54.5	104.1	kPa
c_a	7.6	1.9	kPa
ϕ	19.9	24.5	°
δ	13.2	18.4	°

The *Blade* subsoiler is the tool used in the hardpan disruption model (Figure 6.12). To calculate the draft force variation with respect to the tool shape, the tool is divided in two main parts: the subsoiler body (blue) and the lateral blades (green).
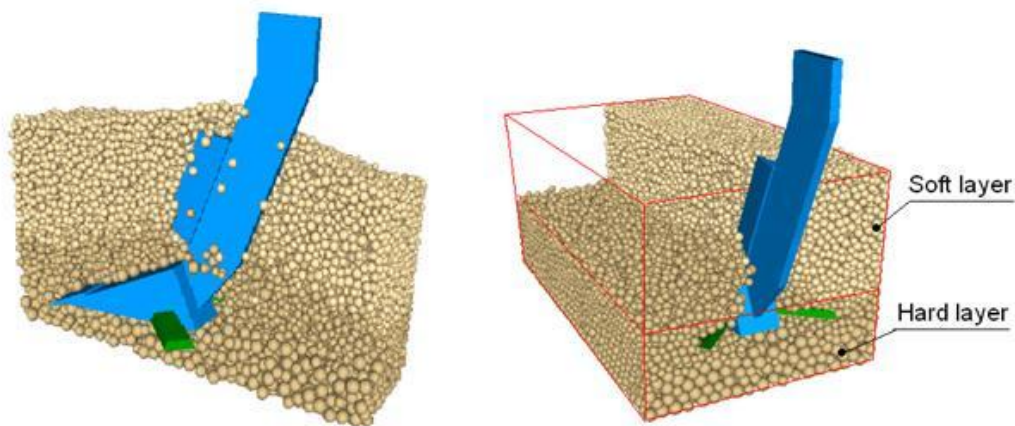
Figure 6.12 Soil hardpan disruption by blade subsoiler.

The draft force prediction from the subsoiler main body and the blades are shown in figure 6.13. A total force of 0.42 kN results from the addition of the blades to the original subsoiler geometry. The addition of the lateral blades increases almost three times the width of the tool increasing the disrupting action over the hardpan while the draft force rises only close to 30%. Nevertheless, the soil disruption caused by the lateral blades, should be lower than the area disrupted by the central wedge, in agreement with the results discussed in section (6.3.1).
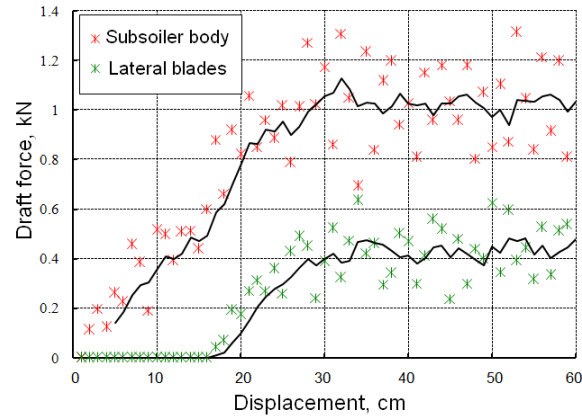
Figure 6.13 Force demanded by the tool main body and lateral blades during hardpan disruption.

A few investigations using numerical methods have been dedicated to modelling the soil-tool interaction considering the non-homogeneous nature of soil. Focused on that goal, Mouazen and Neményi (1999) presented a FEM model to simulate the force demanded for several subsoilers. They concluded that more accurate draft force predictions are obtained employing a non-homogeneous soil structure. Accordingly, the DEM draft force results presented in Figure 6.13 predict with more fidelity the required forces in real soil hardpan disruption.

6.7 Conclusions

The draft force prediction from the DEM model in soil cultivation tillage increases as the soil reaches the dry state. The draft forces for three soil moisture contents: $w = 30\%$ (*wet*), $w = 18\%$ (*medium*), and $w = 10\%$ (*dry*), resulted in the mean values of 184, 406 and 568 N respectively for a cultivator tool. The standard error increases according to the rise in draft force magnitudes revealing the increment in soil stiffness.

The bulk density variation in a virtual block of soil after simulating soil cultivation shows an adequate reduction in the particle index according to the simulated soil physical state. The least increment in bulk density variation was found in *wet* soil. As the soil water content decreases at 18%, according to the *medium* condition, the particle index variation reaches the maximum level showing a linear distribution in the block transversal section. For the *hard* soil however, the particle index decreases considerably, and the main variation is placed in the centre body of the tool.

The vertical force distribution on the layer below the tool path in the soil virtual block during the simulation of soil cultivation increases for the *dry* soil condition compared to the *medium* soil. The intensity of the force on particles and the area under pressure typify the loading condition by the tool shape and soil physical state.

The *medium* soil condition defined at 18% of moisture, among the three simulated conditions can be selected as the optimum water content for tillage, considering the particle density demanded draft force and the effect of the vertical force.

Non-inversion tillage by paraplough shows advantages in demanding draft force and soil loosening with respect to conventional tillage by mouldboard plough during simulation of primary tillage. The draft force demanded by the paraplough shows a reduction of 16% with respect to mouldboard. Larger clods of soil characterized conventional tillage, while a soil fragmentation pattern was found during non-inversion tillage simulation.

The simulated draft force is modified by the differences in the shape of the subsoiler. The draft force demanded by the frontal knife subsoilers remains small compared to the simple tool, despite the bigger rake angle of the chisel. By adding lateral blades to the subsoiler wedge, the disrupted area is increased almost twice whereas the horizontal force increases only 25%.

Soil hard-pan disruption can be modelled using two sections in the same virtual block of soil with different soil strength and dry bulk density. The prediction of draft forces, measured on the main tool body and the lateral blades, independently, allows evaluating the geometrical changes in the tool design in contrast with the desired expansion of soil disruption.

Chapter 7

Conclusions

7.1 General Conclusions

In the present study, a frictional-cohesive model was implemented in a DEM model to simulate the soil-tool interaction based on the Mohr-Coulomb criterion of failure. To modelling the soil behaviour, the mechanical properties of a clay Oxisol soil were determined by standard mechanical tests as a function of water content and dry bulk density. As a result, a set of regression equations was obtained to calculate the soil macro-properties according to moisture content and compaction. Friction and cohesion were the parameters used to calibrate the model through the micro-macro relationship. These parameters were used as a core of the inter-particles bond. The model validation was made with the results of the tillage operation performed in soil-bin tests at different soil condition. Finally, several simulations of tillage application were carried out using different designs of tillage tool. According to the objectives presented in section 1.3 the following conclusions are attained:

The macroscopic mechanical properties of an Oxisol Cuban soil, obtained by a triaxial compression test and direct shear test were sufficiently accurate to be used as parameters for the calibration of the model micro-parameters of a phenomenological DEM model for modelling the soil-tool interaction. Statistical regression equations for Young's modulus, Poisson's ratio, cohesion, adhesion, internal friction, and soil-metal friction, as a function of water content and dry bulk density, allowed predicting their magnitudes according to the real soil physical state. In a general sense, increases in dry bulk density, increased the soil strength too. Inversely, the soil strength was reduced as the water content increases.

To model the soil mechanical response during soil-tool interaction of the Oxisol soil, a three dimensional frictional cohesive model was implemented in the software DEMeter++ using the Discrete Element Method. The soil mechanical properties obtained from experimental tests were used in the model to calculate the inter-particle contact forces which were defined by normal, shear, friction, cohesion and gravity forces. Inter-particle bonds resulted as effective methods to achieve the reinforcement of the virtual soil structure.

Using the frictional-cohesive model to simulate the soil deformation under direct shear test and biaxial compression test the micro-friction and micro-cohesion parameters of the model could be calibrated according to the real values of soil internal friction and cohesion. Particle sizes and radius distribution were found related to soil force fluctuation. The particle sizes were selected according to the computational capacity and the acceptable parameters of force standard deviation. The model was verified with the results obtained for soil and narrow-tool interaction using an empirical Perumpral-Grisso-Desai model showing the potential of Mohr-Coulomb criterion of soil failure.

The draft force and vertical force reactions, as well soil loosening indicators measured during tillage tests in a soil-bin condition, were found to depend on soil water content and soil compaction level. In the indoor experiment, the Oxisol soil was tested during a cultivation operation at nine experimental conditions. The forces in both directions increased with soil compaction and decreased as the soil moisture became lower. However maximum values of degrees of loosening, soil profile and density variation were found in an intermediate soil condition ($w = 15.4$ %, $\rho_d = 1.12 g/cm^3$) as the soil reached a friable condition defined by the optimum water content.

Modifying the soil macro-parameters by means of the aforementioned statistical regression analysis, the friction cohesive DEM model was able to predict the variation of the soil condition in accordance with the experimental points defined in the soil-bin test. The draft forces obtained during the simulation of soil-tool interaction were in agreement with those obtained from the soil-bin test with an error ranging between 3 and 11%. The pattern found in the simulated daft force showed a tendency towards an overestimate of the predicted force with respect to the

measured one in compacted and dry soil condition. The vertical force, however, tended to be lower than the measured one for all simulated points.

Modelling soil tillage operations as cultivation, primary tillage and decompaction, the reaction forces on the tillage tool could be predicted in accordance with the predefined soil conditions. The model also provided information about the effect of the tool shape over the soil bottom surface and particle loosening during tillage. The simulated draft forces obtained corresponded with the variation of soil general strength in the model. The performance of the tool geometrical design for primary tillage and decompaction could be evaluated according to the disruption area and force requirements. Combining particle layers with different bulk densities, it was possible to simulate the operation of hard pan disruption.

7.2 Future work

From the results of this work, considerable improvement of the soil-tool interaction could still be made by the introduction of contact models that include mineral, organic and biological elements as rocks, plants and organic matter to modeling the effect of tillage on a real soil ecosystem. At the same time, experimental procedures should be developed to collect the data of macro properties for these kinds of contacts.

To obtain accurate soil macro-parameters according to the natural soil condition to feed the particle model, an investigation of in situ soil strength instead of the laborious mechanical tests should be appropriate to reduce the differences between natural and remoulded soil. The soil penetration or undisturbed compression tests taken before tillage should be used to correlate the variation of soil mechanical properties taking places during sample consolidation.

The influence of parameters as cementation degree, porosity, micro-density, and particle shape can be studied and incorporated into the model for more complete calibration. Besides, an inter-particle bond that considers the soil water suction will better clarify the effect of moisture at the particle level.

Further studies for real soil should consider the introduction of several kinds of particles which represent clay, silt and sand, each one characterized from its mineralogical composition and mechanical behaviour, also considering the shape of the different components.

An important suggestion would be the introduction of an alternative model adopting the criterion of soil failure according to Tresca and Drucker-Prager, being suitable for predicting the soil deformation in non-cohesive and hypo-plastic soil conditions, respectively.

An experimental replication of a soil bin test could be carried out under field conditions to evaluate the variation of the mechanical state of a real soil in controlled field conditions and the effect of the tool parameters on draft and vertical force prediction. In addition, the setup of experiments of hardpan tillage operation would be appropriate for model validation and improvement.

Bibliography

ABBAS, E.-Z., JOHN, P. C. & DAVID, W. A. (2006) Three-dimensional finite elements for the analysis of soil contamination using a multiple-porosity approach. *International Journal for Numerical and Analytical Methods in Geomechanics,* 30**,** 577-597.

ABO-ELNOR, M., HAMILTON, R. & BOYLE, J. T. (2004) Simulation of soil-blade interaction for sandy soil using advanced 3D finite element analysis. *Soil and Tillage Research,* 75**,** 61-73.

ADAMCHUK, V. I., HUMMEL, J. W., MORGAN, M. T. & UPADHYAYA, S. K. (2004) On-the-go soil sensors for precision agriculture. *Computers and Electronics in Agriculture,* 44**,** 71-91.

AL-JANOBI, A. A., WAHBY, M. F., ABOUKARIMA, A. M. & AL-HAMED, S. A. (2002) Influence of shank shape of three common chisel ploughs on horizontal and vertical force requirements. *Agricultural Sciences,* 7(1)**,** 13-19.

ALUKO, O. B. (2008) Finite element aided brittle fracture force estimation during two-dimensional soil cutting. *International Agrophysics,* 22**,** 5-15.

ALUKO, O. B. & CHANDLER, H. W. (2006) A Fracture Strength Parameter for Brittle Agricultural Soils. *Biosystems Engineering,* 93**,** 245-252.

ARCHER, J. R. & MARKS, M. J. (1985) Techniques for Measuring Soil Physical Properties. *ADAS Reference Book***,** 22,130.

ARVIDSSON, J., KELLER, T. & GUSTAFSSON, K. (2004) Specific draught for mouldboard plough, chisel plough and disc harrow at different water contents. *Soil and Tillage Research,* 79**,** 221-231.

ASAF, Z., RUBINSTEIN, D. & SHMULEVICH, I. (2006) Evaluation of link-track performances using DEM. *Journal of Terramechanics,* 43**,** 141-161.

ASAF, Z., RUBINSTEIN, D. & SHMULEVICH, I. (2007) Determination of discrete element model parameters required for soil tillage. *Soil and Tillage Research,* 92**,** 227-242.

ASTM D2216 Standard Test Methods for Laboratory Determination of Water (Moisture) Content of Soil and Rock by Mass. *Book of Standards. Committee D-18.*

ASTM D2487 Test Method for Classification of Soils for Engineering Purposes. *Annual Book of ASTM Standards, Vol 04.08.*

ASTM D2850 Standard Test Method for Confined Compressive Strength of Soil. *Book of Standards. Committee D-18.*

ASTM D3080 Standard Test Method for Direct Shear Test of Soils Under Consolidated Drained Conditions. *Book of Standards. Committee D-18.*

AYERS, P. D. (1987a) Moisture and bulk density effects on soil shear strength parameters for coarse grained soils. *Transactions of the ASAE,* 31**,** 1282-7.

AYERS, P. D. (1987b) Utilizing the torsional shear test to determine soil strength-properties relationships. *Soil and Tillage Research,* 10**,** 373-380.

BARBER, R. G., ORELLANA, M., NAVARRO, F., DIAZ, O. & SORUCO, M. A. (1996) Effects of conservation and conventional tillage systems after land clearing on soil properties and crop yield in Santa Cruz, Bolivia. *Soil and Tillage Research,* 38**,** 133-152.

BARZEGAR, A., HASHEMI, A. M., HERBERT, S. J. & ASOODAR, M. A. (2004) Interactive effects of tillage system and soil water content on aggregate size distribution for seedbed preparation in Fluvisols in southwest Iran. . *Soil & Tillage Research,* 78.

BAYHAN, Y. (2006) Reduction of wear vía hardfacing of chiesel plougshare. *Tribology International,* 39**,** 570-574.

BIERWISCH C, KRAFT T, RIEDEL H & M, M. (2009) Three-dimensional discrete element models for the granular statics and dynamics of powders in cavity filling. *Journal of Mech and Phys Solids,* 57**,** 10-31.

CAIRO, P. (1995) *Segunda clasificación genética de los suelos de Cuba. La Habana. 38p. . ,* La Habana, Ciencias Agrícolas.

CARTER, M. R. & DANIEL, H. (2005) CONSERVATION TILLAGE. *Encyclopedia of Soils in the Environment.* Oxford, Elsevier.

CHANCELLOR, W. J. (1994) Soil physical properties Capítulo 2. IN VOL. 1, M. A., ST JOSEPH, MICHIGAN, USA. (Ed.) *Advances in soil dynamic.*

CHIVENGE, P. P., MURWIRA, H. K., GILLER, K. E., MAPFUMO, P. & SIX, J. (2007) Long-term impact of reduced tillage and residue management on soil carbon stabilization: Implications for conservation agriculture on contrasting soils. *Soil and Tillage Research,* 94**,** 328-337.

COETZEE, C. J. & ELS, D. N. J. (2009a) Calibration of discrete element parameters and the modelling of silo discharge and bucket filling. *Computers and Electronics in Agriculture,* 65**,** 198-212.

COETZEE, C. J. & ELS, D. N. J. (2009b) Calibration of granular material parameters for DEM modelling and numerical verification by blade–granular material interaction. *Journal of Terramechanics,* in press.

COULOMB, C. A. (1776) Essai sur une application des regles des maximis et minimis a quelues problemes de statique relatifs a l'architecture. *Mem. Acad. Roy. des Sciences, Paris, 3, p.38.*

CUETO, O. G. (2011) Modelación de la Compactación Provocada por el Tráfico de Neumáticos de los Vehículos Agrícolas en Suelos en Condiciones de Laboratorio. *Centro de Mecanizacion Agropecuaria.* La Habana, Universidad Fructuoso Rodriguez.

CUI, K., DE´FOSSEZ, P. & GUY, R. (2007) A new approach for modelling vertical stress distribution at the soil/tyre interface to predict the compaction of cultivated soils by using the PAXIS code. *Soil & Tillage Research* 95**,** 277-2.

CUNDALL, P. A. (1971) A computer model for simulating progressive, large-scale movements in blocky rock systems *Pro. Symp. Int. Soc. Rock Mech,* Nancy 2.

CUNDALL, P. A. (1988) Formulation of a three-dimensional distinct element model--Part I. A scheme to detect and represent contacts in a system composed of many polyhedral blocks. *International Journal of Rock Mechanics and Mining Sciences & Geomechanics Abstracts,* 25**,** 107-116.

CUNDALL, P. A. & STRACK, O. D. L. (1979) A discrete numerical model for granular assemblies. *Geotechnique* 29

DA SILVA, A. P. & KAY, B. D. (1997.) Estimating the least limiting water range of soils from properties and management. *Soil Sci,* 61**,** 877-883.

DAVOUDI, S., ALIMARDANI, R., KEYHANI, A. & ATARNEJAD, R. (2008) A Two Dimensional Finite Element Analysis of a Plane Tillage Tool in Soil Using a Non-linear Elasto-Plastic Model. *American-Eurasian J. Agric. & Environ. Sci.,* 3**,** 498-505.

DESBIOLLES J.M.A., GODWIN R.J., KILGOUR J., J., B. B. S. & 295-309. (1997) An approach for prediction of draft required by primary tillage implements operating in field conditions. *Agric. Eng,* 66.

DEXTER, A. R. (2004) Soil physical quality: Part II. Friability, tillage, tilth and hard-setting. *Geoderma,* 120**,** 215-225.

DEXTER, A. R., CZYZ, E. A. & GATE, O. P. (2007) A method for prediction of soil penetration resistance. *Soil and Tillage Research,* 93**,** 412-419.

DOLINAR, B. (2010) Predicting the normalized, undrained shear strength of saturated fine-grained soils using plasticity-value correlations. *Applied Clay Science,* 47**,** 428-432.

DUNCAN, J. M. & CHANG, C. Y. (1970) Nonlinear analysis of stress and strain in soils. *Journal of Soil Mechanics and Foundation Division,* 96**,** 53.

EL-SAYED, G. H. (1991) The relationship between the design of the shank and blade angle of chisel plough and the draft requirement. *Agricultural Engineering Department.* Egypt, Cairo University.

FENG, C., DRUMM, E. C. & GUIOCHON, G. (2007) Prediction/Verification of Particle Motion in One Dimension with the Discrete-Element Method. *International Journal of Geomechanics,* 7**,** 344-352.

FERVERS, C. W. (2004) Improved FEM simulation model for tire-soil interaction. *Journal of Terramechanics,* 41**,** 87-100.

GARCÍA DE LA FIGAL, A. (1978) Estudio de las propiedades tecnológicas mas importantes de los suelos cubanos. *Revista Ciencias Técnicas Agropecuarias,* 3(2)**,** 61-77.

GEBREGZIABHER, S., MOUAZEN, A. M., VAN BRUSSEL, H., RAMON, H., MERESA, F., VERPLANCKE, H., NYSSEN, J., BEHAILU, M., DECKERS, J. & DE BAERDEMAEKER, J. (2007) Design of the Ethiopian ard plough using structural analysis validated with finite element analysis. *Biosystems Engineering,* 97**,** 27-39.

GODWIN, R. J. (2007) A review of the effect of implement geometry on soil failure and implement forces. *Soil and Tillage Research,* 97**,** 331-340.

GONZÁLEZ CUETO, O., IGLESIAS CORONEL, C., HERRERA SUÁREZ, M., LÓPEZ BRAVO, E. & SÁNCHEZ IZNAGA, A. L. (2009) Influencia de la densidad de volumen en parámetros elastoplásticos empleados para la modelación de la compactación del suelo. *Revista Ciencias Técnicas Agropecuarias,* 18.

GRAFF, L. J., ROBERGE, R. C. & CROWE, T. G. (2007) Wear of Ripper Point Hardsurfacing. IN PRESENTATION, A. A. S. M. (Ed. *2007 ASABE/CSBE North Central Intersectional Conference.* North Dakota State University. Fargo, North Dakota, USA.

GRIM, R. E. (1988) THE HISTORY OF THE DEVELOPMENT OF CLAY MINERALOGY. *Clays and Clay Minerals,* 36**,** 97-101.

GUEÂRIF, J. & SOANE, B. D. (1994) Effects of compaction on soil strength parameters. *Soil Eng. Series 11. Elsevier, Amsterdam, The Netherlands,* Compaction in Crop Production, Development in Agric**,** 191-214.

GUPTA, C. P. & RAJPUT, D. S. (1993) Effect of amplitude and frequency on soil break-up by an oscillating tillage tool in a soil bin experiment. *Soil and Tillage Research,* 25**,** 329-338.

GUPTA P.D (1985) Influence of tool design and tillage system parameters on performance of wide cutting blades for dry land farming. *Agricultural Engineering* Kharagpur, IIT, Kharagpur.

HENTZ, S. B., DAUDEVILLE, L. & DONZE, F. D. R. V. (2004) Identification and Validation of a Discrete Element Model for Concrete. *Journal of Engineering Mechanics,* 130**,** 709-719.

HERRERA SUÁREZ, M., IGLESIAS CORONEL, C., GONZALEZ CUETO, O., LÓPEZ BRAVO, E. & SÁNCHEZ IZNAGA, A. L. (2008) Propiedades mecánicas de un Rhodic Ferralsol requeridas para la simulación de la interacción suelo implemento de labranza mediante el Método de Elementos Finitos: Parte I. *Revista Ciencias Técnicas Agropecuarias,* 17**,** 31-37.

HETTARATCHI, D. R. P. & REECE, A. R. (1967) Simetrical three-dimensional soil failure. *Journal of Terramechanics,* 4**,** 45-67.

HETTARATCHI, D. R. P., WITNEY, B. D. & REECE, A. R. (1966) The calculation of passive pressure in two dimensional soil failure. *J. Agric. Eng.,* Res.11 (2)**,** 89-107.

HORN, R. & FLEIGE, H. (2003) A method for assessing the impact of load on mechanical stability and on physical properties of soils. *Soil and Tillage Research,* 73**,** 89-99.

HUANG, W., SHENG, D., SLOAN, S. W. & YU, H. S. (2004) Finite element analysis of cone penetration in cohesionless soil. *Computers and Geotechnics,* 31**,** 517-528.

IBARRA, S. Y., MCKYES, E. & BROUGHTON, R. S. (2005) Measurement of tensile strength of unsaturated sandy loam soil. *Soil and Tillage Research,* 81**,** 15-23.

IBUKI T, O. A. (2000) Simulation to analyze the interaction between soil and a tire lug by distinct element method. *Proc 8th Eur ISTVS Conf.* Umea.

JEAN-YVES DELENNE, M. S. E. Y. F. C. J.-C. B. (2004) Mechanical behaviour and failure of cohesive granular materials. *International Journal for Numerical and Analytical Methods in Geomechanics,* 28**,** 1577-1594.

JIANG, M. J., LEROUEIL, S. & KONRAD, J. M. (2005) Yielding of microstructured geomaterial by distinct element method analysis. *Journal of Engineering Mechanics-Asce,* 131**,** 1209-1213.

KARMAKAR, S. (2005) Numerical modeling of soil flow and presure distribution on a simple tillage tool using computational fluid dynamics. *Deparment of Agricultural and Bioresource Engineering.* Saskatoon. Canada, Saskatchewan.

KARMAKAR, S. & KUSHWAHA, R. L. (2006) Dynamic modeling of soil-tool interaction: An overview from a fluid flow perspective. *Journal of Terramechanics,* 43**,** 411-425.

KELLER, T., DÉFOSSEZ, P., WEISSKOPF, P., ARVIDSSON, J. & RICHARD, G. (2007) SoilFlex: A model for prediction of soil stresses and soil compaction due to agricultural field traffic including a synthesis of analytical approaches. *Soil and Tillage Research,* 93**,** 391-411.

KÉZDI, Á. (1980) *Handbook of soil mechanics, Vol. 2 Soil Testing,* Amsterdam.

KOMÁNDI, G. (1992) On the mechanical properties of soil as they affect traction. *Journal of Terramechanics,* 29**,** 7.

KUSHWAHA, R. L. & LINKE, C. (1996) Draft-speed relationship of simple tillage tools at high operating speeds. *Soil & Tillage Research,* 39**,** 61-73.

LAMBE, T. W. & WHITMAN, R. V. (1969) *Soil Mechanics,* Massachusetts Institute of Technology, New Yorks, JOHN WILLEY & SONS.

LAMEI, M. & MIRGHASEMI, A. A. (2011) A discrete element model for simulating saturated granular soil. *Particuology* 9 650- 658.

LEYS, A., GOVERS, G., GILLIJNS, K., BERCKMOES, E. & TAKKEN, I. (2010) Scale effects on runoff and erosion losses from arable land under conservation and conventional tillage: The role of residue cover. *Journal of Hydrology* 390**,** 143-154.

LIAO, C.-L., CHANG, T.-P., YOUNG, D.-H. & CHANG, C. S. (1997) Stress-strain relationship for granular materials based on the hypothesis of best fit. *International Journal of Solids and Structures,* 34**,** 4087-4100.

LIU, M. D. & CARTER, J. P. (2002) A structured Cam Clay model. *Canadian Geotechnical Journal,* 39**,** 1313-1332.

LIU, S. H., SUN, D. A. & WANG, Y. (2003) Numerical study of soil collapse behavior by discrete element modelling. *Computers and Geotechnics,* 30 399-408.

LIYANAPATHIRANA, D. S. (2009) Arbitrary Lagrangian Eulerian based finite element analysis of cone penetration in soft clay. *Computers and Geotechnics,* 36**,** 851-860.

MAK, J., CHEN, Y. & SADEK, M. A. (2012) Determining parameters of a discrete element model for soil–tool interaction. *Soil & Tillage Research,* 118**,** 117-122.

MAKANGA, J. T., SALOKHE, V. M. & GEE-CLOUGH, D. (1997) Effects of tine rake angle and aspect ratio on soil reactions in dry loam soil. . *Journal of Terramechanics,* 34(4).

MARTIN OBERMAYR, K. D., CHRISTOS VRETTOS, PETER EBERHARD (2011) Prediction of draft forces in cohesionless soil with the Discrete Element Method. *Journal of Terramechanics,* 48**,** 47-58.

MCKYES, E. (Ed.) (1989) *Agricultural Engineering Soil Mechanics,* Amsterdam, ElsevierSciences.

MCKYES, E. & ALI, O. S. (1977) The cutting of soil by narrow blades. *Journal of Terramechanics,* 14**,** 43-58.

MCKYES, E. & MASWAURE, J. (1997) Effect of design parameters of flat tillage tools on loosening of a clay soil. *Soil and Tillage Research,* 43**,** 195-204.

MCKYES, E., NYAMUGAFATA, P. & NYAMAPFENE, K. W. (1994) Characterization of cohesion, friction and sensitivity of two hardsetting soils from Zimbabwe. *Soil and Tillage Research,* 29**,** 357-366.

MIGUEL HERRERA SUÁREZ , C. I. C., DARINA LARA COBA, OMAR GONZÁLEZ CUETO, ELVIS LÓPEZ BRAVO (2011) Desarrollo de un sensor para la medición continúa de la compactación del suelo. *Ciencias Técnicas Agropecuarias* 20.

MOOTAZ, A. E., R., H. & BOYLE, J. T. (2003) 3D Dynamic analysis of soil–tool interaction using the finite element method. *Soil & Tillage Research,* 40**,** 51-62.

MORGAN, J. K. (1999) Numerical simulation of granular shear zones using the distinct element method *Journal of Geophysical Research,* 104**,** 03-19.

MORRIS, N. L., MILLER, P. C. H., J.H.ORSON & FROUD-WILLIAMS, R. J. (2010) The adoption of non-inversion tillage systems in the United Kingdom and the agronomic impact on soil, crops and the environment--A review. *Soil and Tillage Research,* 108**,** 1-15.

MOSADDEGHI, M. R., MORSHEDIZAD, M., MAHBOUBI, A. A., DEXTER, A. R. & SCHULIN, R. (2009) Laboratory evaluation of a model for soil crumbling for prediction of the optimum soil water content for tillage. *Soil and Tillage Research,* 105**,** 242-250.

MOUAZEN, A. M. (2002) Mechanical behaviour of the upper layers of a sandy loam soil under shear loading. *Journal of Terramechanics,* 39**,** 115-126.

MOUAZEN, A. M. & NEMENYI, M. (1996) A finite element model of soil loosening by a subsoiler with respect to soil conservation. IN BLUME, H. P., EGER, H., FLEISCHHAUER, E., HEBEL, A., REIJ, C. & STEINER, K. G. (Eds.) *9th Conference of the International-Soil-Conservation-Organisation.* Bonn, Germany, Catena Verlag.

MOUAZEN, A. M. & NEMÉNYI, M. (1999) Finite element analysis of subsoiler cutting in non-homogeneous sandy loam soil. *Soil and Tillage Research,* 51**,** 1-15.

MOUAZEN, A. M. & RAMON, H. (2002) A numerical-statistical hybrid modelling scheme for evaluation of draught requirements of a subsoiler cutting a sandy loam soil, as affected by moisture content, bulk density and depth. *Soil and Tillage Research,* 63**,** 155-165.

MOUAZEN, A. M., RAMON, H. & BAERDEMAEKER, J. D. (2002) Effects of Bulk Density and Moisture Content on Selected Mechanical Properties of Sandy Loam Soil. *Biosystems Engineering* 83**,** 217-224.

MOUAZEN, A. M., SMOLDERS, S., MERESA, F., GEBREGZIABHER, S., NYSSEN, J., VERPLANCKE, H., DECKERS, J., RAMON, H. & DE BAERDEMAEKER, J. (2007) Improving animal drawn tillage system in Ethiopian highlands. *Soil and Tillage Research,* 95**,** 218-230.

MUELLER, L., SCHINDLER, U., FAUSEY, N. R. & LAL, R. (2003) Comparison of methods for estimating maximum soil water content for optimum workability. *Soil and Tillage Research,* 72**,** 9-20.

OBERMAYR, M., DRESSLER, K., VRETTOS, C. & EBERHARD, P. (2011) Prediction of draft forces in cohesionless soil with the Discrete Element Method. *Journal of Terramechanics,* 48**,** 47-58.

ODA, M., KONISHI, J. & NEMAT-NASSER, S. (1982) Experimental micromechanical evaluation of strength of granular materials: effects of particle rolling. *Mech Mater,* 1**,** 15.

OIDA A, S. H., OHAKUBO S, YAMAZAKI M. (1997) Simulation of soil deformation under a track shoe by DEM. *Proc 7th Eur ISTVS Conf.* Ferrara.

OÑATE, E. & ROJEK, J. (2004) Combination of discrete element and finite element methods for dynamic analysis of geomechanics problems. *Comput. Methods Appl. Mech. Engrg. ,* 193 3087-3128.

PAYNE, P. C. J. (1956) The relationship between the mechanical properties of soil and the performance of simple cultivation implements. *Journal of Agricultural Engineering Research,* 4**,** 312-325.

PERDOK, U. D. & KOUWENHOVEN, J. K. (1994) Soil-tool interactions and field performance of implements. *Soil and Tillage Research,* 30**,** 283-326.

PERON, H., DELENNE, J. Y., LALOUI, L. & EL YOUSSOUFI, M. S. (2009) Discrete element modelling of drying shrinkage and cracking of soils. *Computers and Geotechnics,* 36**,** 61-69.

PERUMPRAL, J. V., GRISSO, R. D. & DESAI, C. S. (1983) A soil-tool model based on limit equilibrium analysis. *Transactions of the ASABE,* 26**,** 991-996.

PINHEIRO-DICK, D. & SCHWERTMANN, U. (1996) Microaggregates from Oxisols and Inceptisols: dispersion through selective dissolutions and physicochemical treatments. *Geoderma,* 74**,** 49-63.

PLOUFFE, C., RICHARD, M. J., TESSIER, S. & LAGUE, C. (1999) Validations of moldboard plow simulations with FEM on a clay soil. *Transactions of the Asae,* 42**,** 1523-1529.

PORTER, M. A. & MCMAHON, T. A. (1987) Simulation of change in bulk density of the cultivated layer in a swelling clay soil. *Soil and Tillage Research,* 10**,** 147-166.

PORTER, M. A. & MCMAHON, T. A. (1990) The Melbourne University tilled soil model. *Transactions of the ASAE,* 30**,** 5.

PUTTEA, A. V. D., GOVERS, G., DIELSA, J., GILLIJNS, K. & DEMUZEREA, M. (2010) Assessing the effect of soil tillage on crop growth: A meta-regression analysis on European crop yields under conservation agriculture. *Europ. J. Agronomy,* 33**,** 231-241.

R. JAFARI, T. T. H., S. MINAEE, M.H. RAOUFAT (2004) Large deformation modeling in soil-tillage tool interaction

using advanced 3D nonlinear finite element approach. *Proceedings of the 6th WSEAS International Conference on Simulation, Modelling and Optimization, Lisbon, Portugal, September 22-24, 2006.*

RAPER, R. L. & ERBACH, D. C. (1990) Effect of variable linear elastic parameters on finite element predictions of soil compaction *Transaction of ASAE,* 33**,** 731-736.

RAPER, R. L. & HALL, E. H. (2003) SOIL STRENGTH MEASUREMENT FOR SITE-SPECIFIC AGRICULTURE. IN PATENT, U. S. (Ed. *US Patent.* USA.

RICKMAN, R. W. (1971) Sonic radiation for soil mechanical property measurement. *Transactions of the ASAE,* 14**,** 5.

RODRÍGUEZ, M. (1999) Fundamentación de un sistema de rodajes por semiesteras en las cosechadoras cubanas de caña de azúcar para trabajar en suelos de mal drenaje. *Departamento de Mecanizacion Agropecuaria.* Santa Clara, Cuba, Doctorado en Ciencias Técnicas, Phd, Universidad Central "Marta Abreu".

ROSA, U. A. & WULFSOHN, D. (1999) Constitutive model for high speed tillage using narrow tools. *Journal of Terramechanics,* 36**,** 221-234.

ROSA, U. A. & WULFSOHN, D. (2008) Soil bin monorail for high-speed testing of narrow tillage tools. *Biosystems Engineering,* 99**,** 444-454.

ROUL, A. K., RAHEMAN, H., PANSARE, M. S. & MACHAVARAM, R. (2009) Predicting the draught requirement of tillage implements in sandy clay loam soil using an artificial neural network. *Biosystems Engineering,* 104**,** 476-485.

S. H. LIU, D. A. S. (2002) Simulating the collapse of unsaturated soil by DEM. *International Journal for Numerical and Analytical Methods in Geomechanics,* 26**,** 633-646.

SAFFIH-HDADI, K., DÉFOSSEZ, P., RICHARD, G., CUI, Y. J., TANG, A. M. & CHAPLAIN, V. (2009) A method for predicting soil susceptibility to the compaction of surface layers as a function of water content and bulk density. *Soil and Tillage Research,* 105**,** 96-103.

SAHU, R. K. & RAHEMAN, H. (2006a) An approach for draft prediction of combination tillage implements in sandy clay loam soil. *Soil and Tillage Research,* 90**,** 145-155.

SAHU, R. K. & RAHEMAN, H. (2006b) Draught Prediction of Agricultural Implements using Reference Tillage Tools in Sandy Clay Loam Soil. *Biosystems Engineering,* 94**,** 275-284.

SÁNCHEZ-GIRÓN RENEDO, V. (1999) *Dinamica y mecánica de suelos: Ensayo de cortante directo del suelo* España, Ediciones Agrotécnicas, S.L.

SÁNCHEZ-GIRÓN, V., ANDREU, E. & HERNANZ, J. L. (2001) Stress relaxation of five different soil samples when uniaxially compacted at different water contents. *Soil and Tillage Research,* 62**,** 85-99.

SHARMA, V. K., SINGH, G. & GEE-CLOUGH, D. (1992) Soil failure caused by flat tines in sand. Part I: Rake angles 15 deg. to 90 deg. . *Agricultural Engineering Journal,* 1 (2) 71-91.

SHEN, J. & KUSHWAHA, R. L. (Eds.) (1998) *Soil-Machine interactions: A finite element perspective.,* New York, Marcel Dekker, Inc.

SHMULEVICH, I., ASAF, Z. & RUBINSTEIN, D. (2007) Interaction between soil and a wide cutting blade using the discrete element method. *Soil and Tillage Research,* 97**,** 37-50.

SHMULEVICH., ASAF, Z. & RUBINSTEIN, D. (2006) Interaction between Soil and a Wide Cutting Blade Using the Discrete Element Method. *Faculty of Civil and Environmental Engineering, Agricultural Engineering Department.* Haifa 32000, Israel, Technion - Israel Institute of Technology.

SHRESTHA, D. S., SINGH, G. & GEBRESENBET, G. (2001) PM--Power and Machinery: Optimizing Design Parameters of a Mouldboard Plough. *Journal of Agricultural Engineering Research,* 78**,** 377-389.

SONI, P., SALOKHE, V. M. & NAKASHIMA, H. (2007) Modification of a mouldboard plough surface using arrays of polyethylene protuberances. *Journal of Terramechanics,* 44**,** 411-422.

SPOOR, G., TIJINK, F. G. J. & WEISSKOPF, P. (2003) Subsoil compaction: risk, avoidance, identification and alleviation. *Soil and Tillage Research,* 73**,** 175-182.

SUAREZ, M. H. (2006) Simulación del comportamiento mecánico de los suelos ferralíticos rojos mediante el método de elementos finitos *Centro de Mecanizacion Agropecuaria.* La Habana, Universidad Agraria, Tesis de doctorado Phd.

SUÁREZ, M. H., CORONEL, C. I., CUETO, O. G., BRAVO, E. L. & IZNAGA, Á. S. (2008) Propiedades mecánicas de un Rhodic Ferralsol requeridas para la simulación de la interacción suelo implemento de labranza mediante el Método de Elementos Finitos: Parte I. *Ciencias Técnicas Agropecuarias,* 17**,** 31-37.

SUÁREZ, M. H., CORONEL, C. I. & OROZCO, M. R. (2001) Propiedades Dinámicas de los vertisuelos que intervienen en el diseño de organos escarificadores *Ciencias Técnicas Agropecuarias,* 10**,** 29-36.

SWICK, W. C. & PERUMPRAL, J. V. (1988) A model for predicting soil-tool interaction. *Journal of Terramechanics,* 25**,** 43-56.

TADESSE, D. (2004) Evaluating DEM with FEM perspectives of load soil-interaction. Wageningen University.

TANAKA, H., MOMOZU, M., OIDA, A. & YAMAZAKI, M. (2000) Simulation of soil deformation and resistance at bar penetration by the Distinct Element Method. *Journal of Terramechanics,* 37**,** 41-56.

TANAKA, H., OIDA, A., DAIKOKU, M., INOOKU, K., SUMIKAWA, O., NAGASAKI, Y. & MIYAZAKI, M. (2007) DEM Simulation of Soil Loosening Process Caused by a Vibrating Subsoiler. IN CIGR (Ed. *Agricultural Engineering International: the CIGR Ejournal.*

THALLAK. G. SITHARAM, S. V. D. N. S. (2002) Micromechanical modelling of monotonic drained and undrained shear behaviour of granular media using three-dimensional DEM. *International Journal for Numerical and Analytical Methods in Geomechanics,* 26**,** 1167-1189.

TIJSKENS, E., RAMON, H. & BAERDEMAEKER, J. D. (2003) Discrete element modelling for process simulation in agriculture. *Journal of Sound and Vibration* 266 493-514.

TORMENA, C. A., DA SILVA, A. P. & LIBARDI, P. L. (1999) Soil physical quality of a Brazilian Oxisol under two tillage systems using the least limiting water range approach. *Soil and Tillage Research,* 52**,** 223-232.

TROUSE, A. C. (1985) Development of the controlled traffic concept. *Proceedings of International Conference on Soil Dynamics*, 1112 -1119.

UPADHYAYA, S. K., ROSA, U. A. & WULFSOHN, D. (2002) Application of the Finite Element Method in Agricultural Soil Mechanics. *Advances in Soil Dynamics, ASAE. St. Joseph, MI,* vol. 2, 117-153.

UTILI, S. & NOVA, R. (2008) DEM analysis of bonded granular geomaterials. *International Journal for Numerical and Analytical Methods in Geomechanics,* 32, 1997-2031.

VAN OOST, K., GOVERS, G., VAN MUYSEN, W. & QUINE, T. A. (2000) Modeling Translocation and Dispersion of Soil Constituents by Tillage on Sloping Land. *Soil Sci. Soc. Am. J. ,* 64, 1733-1739.

VILLARD, P., CHEVALIER, B., HELLO, B. L. & COMBE, G. (2009) Coupling between finite and discrete element methods for the modelling of earth structures reinforced by geosynthetic. *Computers and Geotechnics* 36 709-717.

YAO, Y. & ZENG, D. (1988) Investigation on the relationship between sliding speed and soil-metal friction. *Trans. Chinese Soc. Agric.Math.,* 19, 33-40.

ZADEH, S. R. A. (2006) MODELLING OF ENERGY REQUIREMENTS BY A NARROW TILLAGE TOOL. *Department of Agricultural and Bioresource Engineering.* Saskatoon, University of Saskatchewan.

ZHANG, J. X., SANG, Z. Z. & L.R.GAO (1986) Adhesion and friction between soils and solids. *Trans. Chinese Soc. Agric.Math.,* 17, 32-40.

Curriculum Vitae

Personal data	
First name	Elvis López Bravo
Address	Crucero Carmita, Camajaní, Villa Clara, Cuba
Telephone	43 52 281692
E-mail	evislb@uclv.edu.cu
Nationality	Cuban
Date of birth	1971-11-20
Gender	Male
Mother tongue	Spanish
Occupation field	Engineering research and education.
Experience and place	2000-2013 Lecturer in agricultural engineering topics. Central University of Las Villas, Santa Clara, Cuba.
	1999-1995 Researcher in soil mechanics, Pedagogical Institute Félix Varela, Santa Clara, Cuba.
Position	Lecturer
Main activities	Training of pre-graduate students in agricultural and technology and Research in the field of soil sustainable management.
Employer address	Central University "Marta Abreu" of las Villas, Santa Clara City, Cuba. 54 500.
Business	Education
Titles	Master Science in Mechanical Engineering. 2003. UCLV, Cuba Mechanical and Pedagogical graduate. ISPFV, Cuba
Principal skills	Soil mechanics and agricultural tests. Modelling and simulation agricultural process. Design and manufacturing tools and agricultural machinery. Software programming for engineering calculus.

Congress	V International Conference on Agricultural Development and Sustainability, Agrocentro 2012. Cuba, 15-19 May, 2012. Oral presentation. Simulation of soil-tool interaction by Discrete Element Model.
	II International Conference on Particles base methods. Barcelona, Spain 26-28 October 2011. Oral presentation. Numerical tillage models application in compacted Cuban soil
	I Scientific Congress in Agricultural Engineering. University of Informatics and biosciences of Havana. Cuba. 23-25 Mar 2009. Oral presentation. Physic and mechanical properties of Ferralitics soils.
	X International Congress of Metallurgic and Agro-forest Industry. Convention Palace, Havana, Cuba 2007. Oral presentation. Simulation of tillage soil-tool interaction by FEM model in sandy soils.
Publications	Non-inversion tillage simulations implemented on Discrete Element Method. Journal of Terramechanics. 2013. Manuscript D-11-00059R1, Editing process.
	Simulation of Soil-tool Interaction under Non-inversion Tillage. Proceedings. V International Conference on Agricultural Development 2012. ISBN: 978-950-250-775-3.
	Simulation of Clay Soil De-compaction by Subsoiling process using Discrete Element Methods. Proceedings of the II international Conference on Particle Methods. ISBN: 978-84-89925-69-4. 2011.
	Development of a Sensor for Soil Continuous Compaction Measurement, J. Agrop. Tech. Scince, 20(1): 6-11, 2011.
	Analysis of wear impact on the work parts of the tillage tool, *J. Agrop. Tech. Scince*, 19(2): 1-9, 2010.
	Mechanical properties of a Rhodic Ferralsol required for the simulation of soil-tool interaction by Finite Elements Method, *J. Agrop. Tech. Scince*, 17(4): 50-54, 2008.
	The influence of soil moisture in elastic-plastic parameters used during compaction modelling, *J. Agrop. Tech. Scince*, 17(3): 26-30.